THE
PHYSICAL REVIEW

A journal of experimental and theoretical physics established by E. L. Nichols in 1893

SECOND SERIES, VOL. 71, No. 3 FEBRUARY 1, 1947

On the Scattering and Absorption of Particles by Atomic Nuclei

H. FESHBACH, D. C. PEASLEE, AND V. F. WEISSKOPF
Physics Department, Massachusetts Institute of Technology, Cambridge, Massachusetts

(Received August 5, 1946)

Expressions very similar to the "Breit-Wigner" formulas are derived for the scattering and absorption cross section of nuclear particles, e.g. neutrons, protons, etc. The resonance energies, particle widths and other characteristic features can be expressed in terms of the logarithmic derivative of the particle wave function at the nuclear surface. Simple assumptions about the behavior of the incident particle inside the nucleus are used to find approximate expressions for (1) the particle widths in terms of the level spacing; (2) the neutron scattering cross section near and between resonances; (3) the total cross section and the absorption cross section averaged over neighboring levels for neutron energies up to 1 Mev. These results are then compared with the experimental data and are found to be in qualitative agreement.

1. INTRODUCTION

THE scattering and absorption of neutrons, protons, or other particles by nuclei is currently described by a picture that makes use of the existence of certain resonance states of the compound nucleus. The cross section of these processes, and its dependence on the energy of the incident particles is given by the so-called "Breit-Wigner" formula[1,2] which is built in close analogy to the corresponding expressions in optical dispersion. It has the following form for an incident particle of an angular momentum $l\hbar$, if the spins of the particle and of the nucleus are disregarded:[3]

$$\sigma_{sc}=\frac{4\pi}{k^2}(2l+1)\left|\sum_r \frac{\frac{1}{2}\Gamma_n^{(r)}}{E-E_r+i\Gamma^{(r)}/2}+p_{sc}\right|^2, \quad (1)$$

$$\sigma_{abs}=\frac{\pi}{k^2}(2l+1)\left|\sum_r \frac{(\Gamma_n^{(r)}\Gamma_a^{(r)})^{\frac{1}{2}}e^{i\varphi_r}}{E-E_r+i\Gamma^{(r)}/2}\right|^2. \quad (2)$$

σ_{sc} is the cross section for elastic scattering, σ_{abs} is the cross section for absorption or any other process that changes the initial state of the bombarded nucleus. It includes radiative capture, fission, and inelastic scattering. Here k is the wave number of the incident particle, E is its energy, E_r are the resonance energy values for the compound nucleus, $\Gamma^{(r)}$ is the total width of the resonance, $\Gamma_n^{(r)}$ is the neutron width, corresponding to the reemission of the neutron with its original energy, $\Gamma_a^{(r)}$ is the absorption width and φ_r is a phase. $\Gamma_a^{(r)}$ contains the radiation width and also the width for any other process that does not lead to the elastic reemission of the incident particles, such as fission or inelastic scattering. The sum is taken over all resonance states of the compound nucleus. The

[1] G. Breit and E. Wigner, Phys. Rev. 49, 519 (1936).
[2] H. Bethe and G. Placzek, Phys. Rev. 51, 450 (1937).
[3] Consideration of the spins of the nucleus and the particle introduces a factor $(2J+1)/[(2i+1)(2s+1)(2l+1)]=\xi(J,i,s,l)$ to the expressions (1) and (2), where i is the spin of the bombarded nucleus, s of the particle and J of the compound nucleus; J can take on the values $J=|i+j|$, $|i+j-1|$, $\cdots|i-j|$, and j the values $|l+s|$, $|l+s-1|$, $\cdots|l-s|$. It can be shown that $\Sigma_J\,\xi(J,i,s,l)=1$, if the sum taken over all possible values of J. All expressions, in which averages are taken over many resonance levels, are therefore identical for the case $s=0$, $i=0$ and for the general case.

amplitude p_{sc}, contained in the formula for σ_{sc}, describes the so-called "potential scattering" which is not caused by resonance effects.

The derivation of these expressions and the theoretical determination of the constants appearing in them have been given by several authors.[2,4-6] The difficulty lies in the fact that the strong interaction between the impinging particles and the nucleus prevents a perturbation calculation in analogy with the dispersion theory of light. Especially the definition and the properties of the levels far off resonance have led to great complications and the theories were not able to give an unambiguous result. These levels contribute, mainly, to the background between resonances and are of special importance for the scattering cross section, since they are responsible, partly or fully, for the potential scattering.

We propose in this paper a different way of approach to a derivation of expressions for the absorption and scattering cross sections. The result is, of course, very similar to (1) and (2), but it does not contain a summation over far away levels. The cross sections are determined by a function $f(E)$, which is equal to the ratio of the derivative to the value of the eigenfunction of the incoming particle at the surface of the nucleus. It is possible to express some characteristic quantities, as the neutron width $\Gamma_n^{(r)}$ and the resonance energies E_r, in terms of some general properties of this function f. In order to obtain numerical values for the cross sections, certain simple assumptions will be made as to the general behavior of the function $f(E)$. These assumptions cannot be exact and the results derived from it must be interpreted as qualitative indications only.

The fundamental idea of this derivation can be expressed in qualitative terms in the following way. Let us consider an incident beam of neutrons of low energy. It is represented outside the nucleus by a wave of a wave number k. Near the nuclear surface this wave is joined smoothly with equal value and derivative to the wave function inside the nucleus, which is the solution of a complicated many-body problem. We expect that the neutron will have, in the average, a very high kinetic energy inside the nucleus. The dependence of the wave function inside on the coordinate of the incoming neutron will therefore be qualitatively represented by a wave with a high wave number $K \gg k$. We thus have to join, at the nuclear surface, a wave of low wave number k with a wave of high wave number K. In general, this can only be done if the amplitude A inside is very much smaller than the amplitude outside which we conveniently normalize to unity. A is of the order k/K. In the exceptional cases, however, when the derivative of the inside wave function is near zero at the surface, the two waves can be joined with about equal amplitude: $A \sim 1$. (See Fig. 1.) There are certain narrow intervals in the energy for which the wave function inside will have this exceptional property. These are the excitation energies of the compound nucleus for which the neutron can get into the nucleus, since, for these values, the amplitude is large inside. These energies are the observed resonances, and the widths of the intervals are the resonance widths. If we assume that the phase of the inside wave function at the nuclear surface changes smoothly with the energy, we will expect that the energy intervals, in which the derivative is small enough to give rise to large A, are proportional to the distance D between resonances: $\Gamma = \alpha D$ where α is a small number of the order k/K. Thus the width of the resonance is expected to be proportional to D. (This consideration does not consider any absorption inside the nucleus so that this conclusion applies to the neutron width only.) This simple picture also gives some indication of the scattering cross section. The outside wave function assumes a very small value for all energies

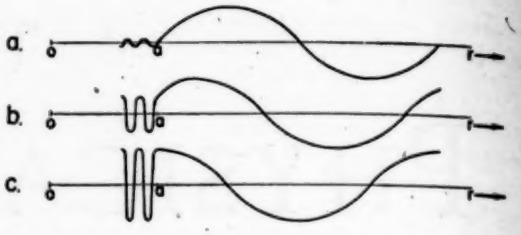

FIG. 1. Schematic representation of neutron wave functions at the nuclear surface. The wave functions are indicated as functions of the distance r from the center of the nucleus. $r=a$ is the nuclear radius. Case a corresponds to a neutron energy between resonances, Case b is near resonance, Case c is in resonance.

[4] P. L. Kapur and R. Peierls, Proc. Roy. Soc. A166, 277 (1938).
[5] A. J. Siegert, Phys. Rev. 56, 750 (1939).
[6] G. Breit, Phys. Rev. 69, 472 (1946).

at the nuclear surface except the ones near the resonances. Therefore, the situation is similar to the scattering of an impenetrable sphere of the same size as the nucleus, since in the latter case the wave function vanishes at the surface. We thus expect, in addition to a resonance scattering, a potential scattering between resonances whose cross section is similar to the one of an impenetrable sphere.

2. THE CASE OF NEUTRONS WITH $l=0$

(a) Derivation of the General Expressions

The wave function ψ of the incident particle outside the nucleus is a linear combination of an incoming and an outgoing wave:

$$\varphi = r\psi = e^{-ikr} + \eta e^{ikr}, \tag{3}$$

where k is the wave number of the incoming neutron. If there is no absorption, the absolute square of η is unity; in case of absorption, $|\eta|^2<1$. The absorption cross section is given by

$$\sigma_{abs} = (\pi/k^2)(1-|\eta|^2), \tag{4}$$

which is easily understood, if one remembers that π/k^2 is the maximum possible absorption cross section which is reached when there is no outgoing wave e^{+ikr} at all.

The scattering cross section is given by

$$\sigma_{sc} = (\pi/k^2)|1+\eta|^2. \tag{5}$$

This can be seen by observing that, in a plane wave the $l=0$ part of the wave function has the form $r\psi = e^{-ikr} - e^{+ikr}$; this differs from (3) by $(1+\eta)e^{+ikr}$ which, therefore is the scattered wave.

We now express the two cross sections in terms of the logarithmic derivative of φ at the nuclear radius a. We define a function $f(E)$ by

$$f(E) = a[(d\varphi/dr)/\varphi]_{r=a}. \tag{6}$$

The value of η is connected with f by

$$\eta = e^{-2ix}\left[\frac{x-if}{x+if}\right], \tag{7}$$

where $x=ka$. The nuclear radius a is the smallest distance from the center of the nucleus at which the incoming particle is no longer under the influence of the nuclear forces.

We obtain an expression for the cross sections by inserting (7) into (4) and (5) and by putting $f=f_0-ih$, where f_0 and h are real functions; we note that h is necessarily non-negative in order to insure $|\eta|^2\leqslant 1$.

$$\sigma_{abs} = \frac{4\pi x h}{k^2}\left|\frac{1}{x+if}\right|^2 = \frac{4\pi}{k^2}\frac{xh}{(x+h)^2+f_0^2}, \tag{8}$$

$$\sigma_{sc} = \frac{4\pi}{k^2}\left|\frac{x\cos x - f\sin x}{x+if}\right|^2 = \frac{4\pi}{k^2}\left|\frac{x}{i(x+h)-f_0} + e^{ix}\sin x\right|^2. \tag{9}$$

It is seen that resonances occur always when $f_0=0$. We therefore call the values E for which $f_0(E)=0$, the resonance energies E_r of the nucleus. In the neighborhood of the resonances we put

$$f_0(E) = (E-E_r)(df_0/dE)_{E=E_r} \tag{10}$$

and introduce the following abbreviations (the negative sign in (11) and (12) will be explained later and is caused by the fact that df_0/dE can be shown to be negative):

$$\Gamma_n^{(r)} = -2x/(df_0/dE)_{E=E_r}, \tag{11}$$

$$\Gamma_a^{(r)} = -2h/(df_0/dE)_{E=E_r}. \tag{12}$$

Then

$$\sigma_{abs} = \frac{\pi}{k^2}\frac{\Gamma_a^{(r)}\Gamma_n^{(r)}}{(E-E_r)^2+(\Gamma_n^{(r)}+\Gamma_a^{(r)})^2/4}, \quad E \text{ near } E_r, \tag{13}$$

$$\sigma_{sc} = \frac{4\pi}{k^2}\left|\frac{\frac{1}{2}\Gamma_n^{(r)}}{E-E_r+(i/2)(\Gamma_n^{(r)}+\Gamma_a^{(r)})} + e^{ix}\sin x\right|^2, \quad E \text{ near } E_r. \tag{14}$$

These expressions show the familiar forms (1) and (2) although they contain only contributions from one level. They are valid only as long as (10) is a good approximation for $f_0(E)$. Formulae (9) and (14) contain the characteristic "potential scattering" term which, if it were present without the other term, would give rise to a scattering cross section:

$$\sigma_{sc} = (4\pi/k^2)\sin^2 ka.$$

This is equivalent to the scattering of an impene-

trable sphere of radius a. It must be said, however, that the split of the scattering amplitude into a "potential scattering" term: $e^{ix}\sin x$ and a "resonance term":

$$\tfrac{1}{2}\Gamma_n^{(r)}/(E-E_r+i(\Gamma_n^{(r)}+\Gamma_a^{(r)})/2)$$

is so far purely formal since no use was made of the fact that a is the nuclear radius. Actually a could have been any radius r for which the wave function of the incoming particle is given by (3); this means a could assume any value larger than or equal to the nuclear radius. It is evident that any change in value of a entails a corresponding change in $f(E)$ which makes the values (8) and (9) of the cross sections invariant to the choice of a. It will be shown in the next section, however, that $f(E)$ is expected to have certain simple properties which depend only on the nuclear structure inside the nucleus, in case a is chosen to be the nuclear radius. Specifically, relation (10) is then supposed to be valid over an energy region much larger than the line width $\Gamma_n^{(r)}+\Gamma_a^{(r)}$. In this case expression (14) is valid also for energies at which the resonance term becomes smaller than the potential scattering term, so that the potential scattering assumes real significance.

(b) Definition and Determination of the Function $f(E)$

It is possible to make qualitative statements as to the behavior of the function $f(E)$, if the wave-length λ of the wave function outside of the nucleus is much longer than the average distance d between particles inside the nucleus:

$$\lambda=1/k\gg d. \tag{15}$$

The actual value of λ is then of no importance for the shape of the wave functions inside since λ is very much longer than the wave-lengths inside which are of the order d. The value of $f(E)$ will depend on the energy E of the incoming particle, only by being an explicit function $f(W)$ of the excitation energy W of the compound nucleus: $W=E+B$, where B is the binding energy of the neutron to the nucleus. Expression (11) shows therefore the characteristic proportionality of $\Gamma_n^{(r)}$ with k, since f_0 or its derivative should not depend explicitly on k.

The actual determination of $f(W)$ itself can be done only by finding the solution of the Schrödinger equation for the compound nucleus corresponding to the energy W, and by calculating the logarithmic derivative of this solution with respect to r at the nuclear surface. Because of condition (15), the value of this derivative does not change appreciably outside the nucleus in distances of the order d. The function $f(W)$ is therefore well defined, in spite of the fact that the actual position of the nuclear surface is not sharply determined. The Schrödinger equation for the compound nucleus can be written in the form:

$$H_0\Psi(r_1\cdots r_A)=W\Psi(r_1\cdots r_A), \tag{16}$$

where $r_1\cdots r_A$ are the coordinates of all constituents. Since W is the energy of the compound nucleus after the neutron has entered from outside, it belongs, strictly speaking, to the continuous spectrum of the Hamiltonian H_0. We assume, for the sake of simplicity, that no other particle but the incoming neutron can be emitted at the energy W. The wave function Ψ is then completely defined by the boundary conditions

$$\Psi(r_1\cdots r_A)=0 \quad \text{for} \quad r_i=\infty, \quad i=2\cdots A,$$

if r_1 are the coordinates of the incoming neutron. We then obtain a definite value for

$$f_0(W)=a\left(\frac{\partial r_1\Psi}{\partial r_1}\Big/(r_1\Psi)\right)_{r_1=a}$$

$$=a\left(\frac{dr_1\psi}{dr_1}\Big/(r_1\psi)\right)_{r_1=a} \tag{17}$$

since, for $r_1=a$, Ψ has assumed the form of a product $\psi(r_1)\chi(r_2\cdots r_A)$, where χ is the eigenfunction of the initial (or residual) nucleus.

This function $f_0(W)$ is not yet the function $f(W)$ in which we are interested, since the damping effect of the radiative absorption has not been considered yet. It is possible to express the effect of the radiative absorption by an imaginary addition to the Hamiltonian H_0:

$$H\Psi=(H_0+H^1)\Psi, \quad H^1=-i\Gamma_a/2.$$

The term H^1 would add to the eigenvalues of H_0 an imaginary term $-i\Gamma_a/2$, which describes the

characteristic exponential time dependence:

$$|\Psi|^2 \sim |e^{-i(W-i\Gamma_a/2)t}|^2 = e^{-\Gamma_a t}.$$

The solution of H which is needed to determine $f(E)$ is given by

$$H\Psi = W\Psi$$

which also can be written in the form

$$H_0\Psi = (W+i\Gamma_a/2)\Psi.$$

Hence, if $f_0(W)$ was determined according to (17) from Eq. (16), the actual $f(W)$ will be given by

$$f(W) = f_0(W+i\Gamma_a/2) \simeq f_0(W)+i(\Gamma_a/2)(df_0/dW), \quad (17a)$$

if $\Gamma_a/2$ is very small compared to W. The imaginary part $-h$ of $f(W)$ is thus

$$h = -(\Gamma_a/2)(df_0/dW),$$

which agrees with our definition (12) of Γ_a.

The resonance value $W_r = B+E_r$ and the neutron widths $\Gamma_n^{(r)}$ are defined by:

$$f_0(W_r) = 0, \quad \Gamma_n^{(r)} = -2x/(df_0/dW)_{W=W_r}. \quad (18)$$

Since the imaginary part of $f(W)$ is necessarily non-positive in order to fulfill in (7) the condition $|\eta|^2 \leqslant 1$, we conclude from (17a)

$$df_0/dW \leqslant 0.$$

In view of the fact that the derivative of f_0 is never positive and that f_0 has zero points at $W = W_r$, it is convenient to write it in the form

$$f_0(W) = -Ka \tan z(W), \quad (19)$$

where K is a constant of the dimension of a wave number and $z(W)$ is a monotonically increasing function, which is equal to multiples of π for the resonance values W_r:

$$z(W_r) = n\pi, \quad n \text{ an integer}. \quad (20)$$

The value of K can be estimated in the following way: the wave function Ψ inside the nucleus depends on the coordinates of all constituents. We make the qualitative assumption that Ψ, in its dependence on r, has the character of a periodic function with a high wave number:

$$r\Psi \sim \cos(Kr+\delta) \quad (21)$$

from which one obtains (see (6))

$$f = -Ka \tan(Ka+\delta).$$

If this is compared to (19), it seems plausible to assume that K is a wave number corresponding to the kinetic energy of a particle in the nucleus. We would like to emphasize that this procedure is not equivalent to the use of a one-particle model as the form of (21) may perhaps suggest. Expression (19) uses only the fact that Ψ has a periodic dependence on r with a period given by K. The function z is left, so far, completely undetermined. It would have the form $z = (2mW/\hbar^2)^{\frac{1}{2}}a$ in the one-particle model.

The order of magnitude of K can be obtained in the following way: the maximum momentum P of N equal free Fermi-Dirac particles in their lowest states, if kept within a volume V, is given by

$$P = 2\pi\hbar(3N/4\pi V)^{\frac{1}{3}}.$$

If A is the number of constituents in a nucleus, we put $N = A/4$, because of the 4 types of particles in the nucleus and get:

$$P/\hbar = (2\pi/r_0)(9/64\pi^2)^{\frac{1}{3}},$$

where r_0 is the elementary radius which determines nuclear radii by $a = r_0A^{\frac{1}{3}}$. If $r_0 = 1.5\times10^{-13}$, we obtain $P/\hbar \simeq 1.0\times10^{13}$ cm^{-1} which corresponds to an energy of 20 Mev. The average kinetic energy of a neutron entering the nucleus will be of the order of this energy plus the binding energy B. The wave number K should therefore correspond to an energy of about 28 Mev which would be:

$$K \approx 1.2\times10^{13} \text{ cm}^{-1}. \quad (22)$$

The function $f(W)$ would be qualitatively determined if some assumption could be made as to the behavior of $f(W)$ between the values $n\pi$ which it reaches at W_r. It seems natural to assume that $z(W)$ increases smoothly from $n\pi$ to $(n+1)\pi$ if the energy W goes from one resonance to the next. This assumption can be expressed by

$$(dz/dW)_{W_r} = \pi/D^* \quad (23)$$

where D^* is an energy of the order of the average level distance D. D itself is, of course, a function of W. The function f_0 can then be written as function of E by means of (19) in the form:

$$f_0(E) = -Ka \tan[(\pi/D^*)(E-E_r)]. \quad (24)$$

It is evident that this expression has only very approximate validity.

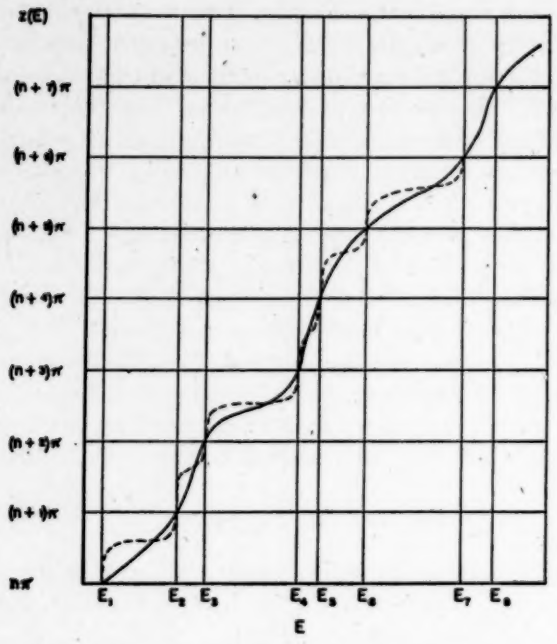

FIG. 2. Function $z(E)$ (Eq. (19)) plotted *vs.* the energy E, E_1 to E_8 are resonance energies. The solid curve gives a smooth dependence as assumed in this paper. The broken line gives an example of an anomalous dependence which would lead to low absorption cross sections.

The relation between D^* and the average level distance D depends on the detailed properties of the function $z(W)$ which, so far, is only defined by (20). If $z(W)$ is laid as smoothly as possible through its values given by (20), we obtain $D^*=D$ in case of equidistant levels. It is seen in Fig. 2 that fluctuations in the level distance tend to decrease D^*/D, since the slope of z at resonances will be closer to the slope of the straight connection with the neighbor resonance which lies closest. It seems to be a good definition of a "smooth curve" to assume that D^*, as defined in (23), is the smaller of the two distances between the resonance W_r and the two adjacent resonance values. If this definition is adopted, one can show that a random level distribution gives

$$D^*/D=\tfrac{1}{2}. \tag{25}$$

The assumption of a "smooth" function $z(W)$ is somewhat arbitrary, and may not be justified in every case. One may argue, however, that the many-body problem of the nucleus is in some way equivalent to a one-body problem with a coordinate r which has a much larger interval at its disposal than $0<r<a$, because of internal reflections and exchanges. The eigenfunction inside the nucleus has then the form $C\cos[K(r+s)]$, where s is a length much larger than a, and K the average wave number for the excitation energy W. One then expects a smooth dependence on W of the function $z=K(W)\cdot(a+s)$. One can, of course, explain any value for D^*/D by a suitable function $z(W)$. The dotted curve in Fig. 2 gives an example, which would lead to an abnormally small value.

3. THE ABSORPTION AND SCATTERING CROSS SECTION OF s-NEUTRONS

The assumptions made in the preceding section give rise to a simple expression for the neutron width Γ_n, which becomes according to (18), (19), and (23):[7]

$$\Gamma_n^{(r)}=\frac{2k}{K}\frac{D^*}{\pi}. \tag{26}$$

The neutron width for s-neutrons can be determined experimentally from an analysis of the neutron absorption resonances. The material available indicates that the values of Γ_n are all of the order of $10^{-3}\sqrt{E_r}$ ev where E_r is the resonance energy in electron volts. This value would give rise to $D^*\sim 10$ ev which seems to be a reasonable order of magnitude for the resonance level distance.

Let us consider the average of σ_{abs} over an energy interval ΔE which contains many levels:

$$\langle\sigma_{abs}\rangle_{Av}=\frac{1}{D}\int\frac{\pi}{k^2}\frac{\Gamma_n\Gamma_a dE}{(E-E_r)^2+(\Gamma_n+\Gamma_a)^2/4}$$
$$=\frac{2\pi}{k^2}\frac{\Gamma_n}{D}\frac{\Gamma_a}{\Gamma_n+\Gamma_a}=\frac{4\pi}{kK}\frac{D^*}{D}\frac{\Gamma_a}{\Gamma_n+\Gamma_a}. \tag{28}$$

Here the integral is taken over the neighborhood of a typical resonance E_r within the interval. It can be shown from the more general expression (8) that only the immediate neighborhood of the resonances contributes to the integral. Γ_n and Γ_a are the average values of $\Gamma_n^{(r)}$ and $\Gamma_a^{(r)}$ over the resonances included within ΔE. Expression (26) was used to eliminate Γ_n in the final expression.

For very low energies the following inequality

[7] N. Bohr and J. A. Wheeler, Phys. Rev. **56**, 426 (1939).

holds: $\Gamma_a \gg \Gamma_n$. Since, for heavy nuclei ($A>100$) $\Gamma_a \sim 0.1$ ev and D^* is of the order of 10 ev, we find $\Gamma_a = \Gamma_n$ according to (26) for $E \sim 7000$ ev. We thus expect the following expression to hold:

$$\langle \sigma_{abs} \rangle_{Av} = \frac{4\pi}{kK}\frac{D^*}{D} \simeq \frac{250}{(E_{ev})^{\frac{1}{2}}} 10^{-24}\,\text{cm}^2, \quad \begin{matrix} E \ll 7000\,\text{ev} \\ A>100 \end{matrix} \quad (29)$$

if E_{ev} is the incident energy in ev and (25) is used. No measurement of $\langle \sigma_{abs} \rangle_{Av}$ in this energy region is available at present for heavy nuclei ($A>100$). It is not possible to derive a similar expression for lighter nuclei because of the larger D which would restrict the limit of validity to even lower energies. The larger D will then make it impossible to take an average over many levels within the validity of the expression. It should be noticed that the cross section (29) is an average over an energy region containing many levels and it should therefore not be applied to the thermal absorption cross section.

We now turn to the scattering cross section as a function of energy. The value of σ_{sc} for any energy E can be calculated from (9) and (24). The evaluation gives rise to a line shape of the characteristic form given in Fig. 3. This figure is calculated for the indium resonance, and a value $D^*=25$ ev was used which would give the observed neutron width[8] of 3×10^{-3} ev in expression (26). The depression at the low energy side and the high shoulder at the high energy side can also be understood as destructive and constructive interference of the "potential scattering" amplitude with the resonance term as shown in (9). This phenomenon has been also described by Bethe.[9] The extensions of these features in the energy scale are much larger than the width $(\Gamma_a+\Gamma_n)$ of the line. It is of the order $2D/(Ka)$, which is about $\frac{1}{8}$ of the level distance in case of heavy nuclei.

No measurements of σ_{sc} as a function of energy have been made so far, but the value of σ_{sc} for thermal energies or for energies near the thermal value are known for several elements. We expect these values to be near $4\pi a^2$. However, they may be above or below this value if there is a level nearby below or above the energy at which the scattering was measured. The distance of this level must be at most of the order of about a fifth of the average level distance, in order to influence the scattering cross section. The nuclear radius a which determines the potential scattering is roughly defined as the distance at which the wave number of the incoming neutron assumes values of the order K. It is thus defined with an inherent inaccuracy of $\pm 1/K$. We therefore expect the scattering cross section away from resonance to be near to $4\pi R^2$, where R is the nuclear radius determined from other sources. The deviation from $4\pi R^2$ should be of the order $8\pi R/K$ which is about 37 percent of the total for elements near Fe and 25 percent of the total at the upper end of the periodic table.

Table I shows a number of scattering cross sections measured, together with the values of $4\pi R^2$ based upon the assumption $R=1.5\times10^{-13}A^{\frac{1}{3}}$ cm. Of course, there will be fluctuations away from this average value. This table contains scattering cross sections mostly of elements which show small absorption at low energies.

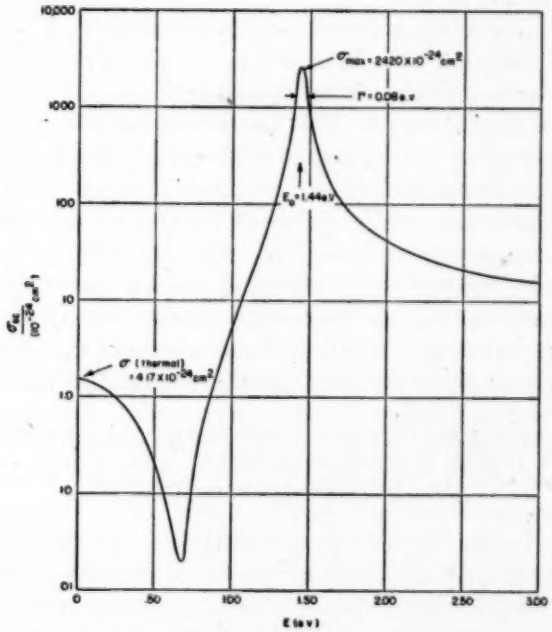

FIG. 3. The scattering cross section for neutrons as a function of neutron energy in the neighborhood of a resonance. The numerical values used for Γ and E_r are those for the indium resonance. Because of a typographical error the value of σ_{sc} for thermal energy is given wrongly in this figure. It should read: $\sigma(\text{thermal}) = 1.47\times10^{-24}$ cm^2.

[8] J. Hornbostel, H. H. Goldsmith, J. H. Manley, Phys. Rev. 58, 18 (1940); J. Rainwater and W. Havens, unpublished; we are grateful to these authors for communicating their results before publication.

[9] H. A. Bethe, Rev. Mod. Phys. 9, 95 (1937).

This selection is attributed to experimental reasons. It follows therefore that in the case of heavier elements ($A>100$) there is no resonance nearby to interfere with the potential scattering. The cross section should therefore be $4\pi a^2$, which should not differ from $4\pi R^2$ by more than about 30 percent. The values of Table I bear out this expectation with the possible exception of Sb and Hg. In these cases, the actual value of R may be considerably different from the assumed value $R=1.5\times10^{-13}A^{1/3}$. In the case of the lighter elements ($A<100$), however, the neutron width is probably much larger than the absorption width because of the larger D, so that resonance scattering may occur in spite of weak absorption. We expect then, in some cases, to find an interference effect of resonance and potential scattering which may account for the abnormally high cross sections in Fe, Ni, Cu, Ge, Se, and Sr, and for the low value in Mn.

Finally, measurements[10] of the change in phase of the scattered wave with respect to the incident wave has been measured for several heavy nuclei for energies in or near to the thermal region. In most cases this phase change was 180°. This result is in agreement with the assumption that the potential scattering p_{sc} is the scattering by an impenetrable sphere for, in this case, the outgoing wave must be exactly out of phase with the incident wave. This phase relation will hold as long as the potential scattering term is the most important term in σ_{sc}. In the resonance region, this phase relation holds for neutron energies greater than the resonance energy. It does not hold for energies smaller than the resonance energy. This is, of course, just a very small portion of the neutron spectrum so that for most energies the phase change will be near 180°.

TABLE I. Elastic scattering cross sections σ_{sc} for thermal and epithermal neutrons.

Element	$4\pi R^2$	σ_{sc}	Energy (ev)	Reference
Ti	3.6	6	C	*A*
Mn	3.8	2.4	1	*B*
Cr	3.8	4	1	*B*
Fe	4.0	11.5	1	*B*
		11.1	1.44	*E*
Co	4.2	5	*C*	*C*
Ni	4.4	18	1	*B*
Cu	4.5	8	1	*B*
		8.3	1.44	*E*
Zn	4.6	4.2	1	*B*
		4.2	1.44	*E*
Ge	5.0	22	1	*B*
Se	5.3	10	*C*	*A*
Sr	5.5	10	*C*	*A*
Br	5.4	7	*C*	*A*
Cb	5.9	5	*C*	*A*
Mo	6.0	6.5	*C*	*A*
Ru	6.1	6	*C*	*A*
Pd	6.3	4.5	*C*	*A*
Ag	6.4	6.6	0–0.5	*B*
Cd	6.5	5.3	1	*B*
Sn	6.6	5.0	1	*B*
Sb	6.9	4.2	1	*B*
Te	7.0	5	*C*	*A*
Ba	7.5	8	*C*	*A*
Ta	9.0	7.2	1	*B*
Os	9.2	10	1	*B*
W	9.3	5.7	0.5	*B*
Pt	9.4	12	1	*B*
Tl	9.8	9.7	1	*B*
Hg	9.8	15	0–1	*B*
Pb	9.9	12.5	1	*B*
Bi	10.0	9.2	1	*B*

A M. Goldhaber and G. H. Briggs, Proc. Roy. Soc. **A162**, 127 (1937).
B J. Rainwater and W. Havens, unpublished. We thank Rainwater and Havens for communicating these results.
C N. E. Bradbury, F. Bloch, H. Tatel, and P. A. Ross, Phys. Rev. **52**, 1023 (1937).
E H. B. Hanstein, Phys. Rev. **59**, 489 (1941).
Remarks:
The fourth column gives the energy at which σ_{sc} was determined. In all references but reference *A*, the value measured is always the total cross section $\sigma_{sc}+\sigma_a$. In these cases, σ_a was either known to be much smaller than σ_{sc} or it was possible to subtract unambiguously a term proportional to $1/v$ which was considered to be σ_a. *C* means neutron energies absorbable in Cd. The velocity selector measurements were taken mostly in the neighborhood of 1 ev (~1) except where other energies are quoted. In the latter cases, the nearest level was already influencing the value at 1 ev, so that it was advisable to choose a lower value.
The scattering cross section of Cd was determined as an additive term to the best fitting Breit-Wigner expression covering the resonance.

4. GENERALIZATION TO NEUTRONS $l>0$ AND TO OTHER KINDS OF INCIDENT PARTICLES (E.G., CHARGED PARTICLES)

So far, we have considered only neutrons in the s state, i.e., $l=0$. When neutrons with $l>0$, or charged particles, protons, deuterons, α-particles, etc., are considered, the radial equation for the particle for $r>a$ now will contain potential energy terms. In the case of charged particles, $l=0$, the potential energy term is Zze^2/r where Z is the nuclear charge and z is the particle charge. When $l\neq0$, then for both cases, neutron or charged particles, one must introduce an additional effective potential energy equal to $\hbar^2l(l+1)/2mr^2$. In any of these cases, the particle may be considered to be moving in the region $r>a$, in a potential $V(r)$. It is then possible to generalize the discussion of Sections 2 and 3 as follows.

Let $u(r)$ equal the product of r and the wave function of the incident particle moving in the potential $V(r)$, which asymptotically for large r

[10] E. Fermi and L. Marshall, Phys. Rev. **70**, 103 (1946).

behaves as e^{-ikr}:

$$u(r)\underset{r\to\infty}{\longrightarrow}e^{-i(kr-l\pi/2)} \quad \text{and similarly} \quad v(r)\underset{r\to\infty}{\longrightarrow}e^{i(kr-l\pi/2)}.$$

The wave function φ for the particle can then be written as in (3) as:

$$\varphi=r\psi=u+\eta v, \quad |\eta|\leqslant 1. \tag{31}$$

The absorption cross section is given by

$$\sigma_{\text{abs}}=(2l+1)(\pi/k^2)[1-|\eta|^2] \tag{32}$$

and the scattering cross section by

$$\sigma_{\text{sc}}=(2l+1)(\pi/k^2)|1+\eta|^2. \tag{33}$$

A function $f(E)$ may be defined in analogy to (7) as:

$$f(E)=a(\varphi'/\varphi)=x\frac{u'+\eta v'}{u+\eta v}, \tag{34}$$

where u' and v' denote derivatives with respect to kr at $r=a$. Solving (34) for η we obtain

$$\eta=-\frac{xu'-fu}{xv'-fv}. \tag{35}$$

It is convenient to express u and v and their derivatives in terms of their absolute value and phase:

$$\begin{aligned} u&=|v|e^{-i\delta}, \quad & v&=|v|e^{i\delta}, \\ u'&=|v'|e^{-i\delta'}, \quad & v'&=|v'|e^{i\delta'}. \end{aligned} \tag{36}$$

Note δ' and $|v'|$ are not the derivatives of δ and $|v|$. If one uses the relation

$$|vv'|\sin(\delta'-\delta)=1 \text{ for all } r \tag{37}$$

one may transform (32) and (33) into

$$\sigma_{\text{abs}}=\frac{4\pi}{k^2}(2l+1)\frac{xh/|v|^2}{(x/|v|^2+h)^2+[f_0-x|v'/v|\cos(\delta'-\delta)]^2}, \tag{38}$$

$$\sigma_{\text{sc}}=\frac{\pi}{k^2}(2l+1)\left|\frac{x/|v|^2}{i(x/|v|^2+h)-[f_0-x|v'/v|\cos(\delta'-\delta)]}+\sin\delta e^{i\delta}\right|^2. \tag{39}$$

Here $f=f_0-ih$, $|v|$, $|v'|$, δ and δ' are evaluated at $x=ka$. The resonances occur when

$$f_0=x|v'/v|\cos(\delta'-\delta). \tag{40}$$

In the neighborhood of the resonances, we expand $f_0(E)$ as in (10) and introduce the following abbreviations

$$\Gamma_n^{(r)}=-\frac{2x}{|v|^2}\left(\frac{df_0}{dE}\right)^{-1}_{E=E_r}, \tag{41}$$

$$\Gamma_a^{(r)}=-2h\left(\frac{df_0}{dE}\right)^{-1}_{E=E_r}. \tag{12}$$

We obtain

$$\sigma_{\text{abs}}=\frac{\pi}{k^2}(2l+1)\frac{\Gamma_n^{(r)}\Gamma_a^{(r)}}{(E-E_r)^2+[(\Gamma_n^{(r)}+\Gamma_a^{(r)})/2]^2}, \tag{42}$$

$$\sigma_{\text{sc}}=\frac{4\pi}{k^2}(2l+1)\times\left|\frac{\frac{1}{2}\Gamma_n^{(r)}}{(E-E_r)+i/2(\Gamma_n^{(r)}+\Gamma_a^{(r)})}+p_{\text{sc}}\right|^2, \tag{43}$$

with

$$p_{\text{sc}}=e^{i\delta}\sin\delta.$$

These expressions are almost identical with the ones obtained for neutrons with $l=0$. The term in σ_{sc}, which represents the potential scattering is changed, and the expression (41) for the neutron width contains the characteristic factor $|v|^{-2}$ which expresses the effect of the potential field outside the nucleus. This factor is the ratio $|v(\infty)/v(x)|^2$ of the intensities of an outgoing wave at infinity and at the nuclear surface. It is a small number for repulsive fields. Its appearance in the expression of the neutron width is expected, since the nuclear eigenfunction adjusts its form to the wave function of the particle at the nuclear surface, whereas the width is connected with the current of outgoing particles through a sphere around the nucleus with a very large radius. The factor $|v|^{-2}$ has also been used in earlier papers by Kapur and Peierls,[4] Weisskopf and Ewing,[11] and Bethe.[9]

There is a limitation to the validity of these considerations, which corresponds to the condition (15) of the case without barrier. Here the

[11] V. F. Weisskopf and D. H. Ewing, Phys. Rev. 57, 472 (1940).

condition is:

$$1/\kappa \gg d, \quad \kappa = k|v'/v|_{r=a},$$

where κ is the instantaneous wave number at the nuclear surface. This condition is necessary, in analogy to (15), to insure small variations of the wave function outside, in intervals of the order d. It puts a limit of about several Mev's to the height of the barrier to which our expressions are applicable.

5. APPLICATION TO NEUTRON CROSS SECTIONS FOR HIGHER ENERGIES

When different l values are involved, the function v will depend upon l. This dependence will be indicated by a subscript l. In the case of neutrons v_l is given by:

$$v_l = i(\pi x/2)^{\frac{1}{2}} H_{l+\frac{1}{2}}^{(1)}(x). \tag{44}$$

The value[12] $|v_l|^2$ is then

$$\begin{aligned} |v_l|^2 &= \tfrac{1}{2}\pi x |H_{l+\frac{1}{2}}^{(1)}(x)|^2, \\ |v_0|^2 &= 1, \\ |v_1|^2 &= (1+x^2)/x^2, \\ |v_2|^2 &= (9+3x^2+x^4)/x^4, \\ |v_3|^2 &= (225+45x^3+6x^4+x^6)/x^6. \end{aligned} \tag{45a}$$

The function $\delta_l(x)$ is:

$$\delta_l(x) = -\tan^{-1}\frac{J_{l+\frac{1}{2}}(x)}{N_{l+\frac{1}{2}}(x)}, \tag{45b}$$

$$\begin{aligned} \delta_0 &= x, \\ \delta_1 &= x - \pi/2 + \cot^{-1} x, \\ \delta_2 &= x - \pi + \cot^{-1} \tfrac{1}{3}(x^2-3), \\ \delta_3 &= x - 3\pi/2 + \cot^{-1}[x(x^2-15)/(6x^2-15)]. \end{aligned}$$

The width Γ_{nl} for the emission of a neutron of angular momentum l is therefore given by

$$\Gamma_{nl} = \frac{2k}{K}\frac{1}{|v_l|^2}\frac{D_l^*}{\pi} \tag{46}$$

if the same assumptions about $f_0(E)$ are made as in (24). This is the generalization of (26).

These expressions can be applied to the absorption cross section of neutrons. Let us consider the average cross section over a small energy integral ΔE containing many resonances. This is the cross section observed, if the neutron beam is not sufficiently monochromatic to distinguish resonances. The average over (42) for a given l gives:

$$\langle \sigma_{abs} \rangle_{Av}^{(l)} = \frac{\pi}{k^2}(2l+1)\frac{2\pi\langle \Gamma_{nl}\Gamma_{al}\rangle_{Av}}{D_l(\langle \Gamma_{nl}\rangle_{Av} + \langle \Gamma_{al}\rangle_{Av})}.$$

Here D_l is the level distance of resonance levels excited by particles with an angular momentum $l\hbar$; $\langle \Gamma_{nl}\rangle_{Av}$ and $\langle \Gamma_{al}\rangle_{Av}$ are the average neutron width and absorption width, respectively, for neutrons of angular momentum $l\hbar$ in the energy region E. This can be transformed by means of (41) and (23) and (46) into:

$$\langle \sigma_{abs} \rangle_{Av}^{(l)} = \frac{4\pi}{kK}(2l+1)\frac{D_l^*}{D_l}\frac{1}{(1+\langle \Gamma_{nl}\rangle_{Av}/\langle \Gamma_{al}\rangle_{Av})|v_l|^2} \tag{47}$$

where $|v_l|^2$ is given in (45). We now assume that the ratio $\langle \Gamma_{al}\rangle_{Av}/D_l^*$ and the wave number K is independent of l and of the energy. One then can write:

$$\frac{\langle \Gamma_{nl}\rangle_{Av}}{\langle \Gamma_{al}\rangle_{Av}} = \frac{\langle \Gamma_{n0}\rangle_{Av}}{\langle \Gamma_{a0}\rangle_{Av}|v_l|^2} = \frac{x}{x_0|v_l|^2},$$

where x_0 is the value of $x=ka$ for which

$$\langle \Gamma_{n0}\rangle_{Av} = \langle \Gamma_{a0}\rangle_{Av}, \quad x_0 = \frac{\pi}{2}\frac{Ka}{D}\langle \Gamma_{a0}\rangle_{Av}.$$

The total absorption cross section can be obtained by summing (47) over all l's:

$$\langle \sigma_{abs} \rangle_{Av} = \frac{4\pi}{kK}\sum_{l=0}^{\infty}\frac{D_l^*}{D_l}(2l+1)\frac{1}{|v_l|^2 + x/x_0}. \tag{48}$$

The assumption that $\langle \Gamma_{al}\rangle_{Av}/D_l^*$ is independent of the energy will break down when inelastic scattering or fission sets in which, in this treatment, are included in $\langle \Gamma_{al}\rangle_{Av}$. This increase in $\langle \Gamma_{al}\rangle_{Av}$ will make x_0 increase sharply at higher energies. We may assume that the inelastic scattering is unimportant for energies less than 0.4 Mev.

The value of $x_0 = \frac{1}{2}\pi Ka\Gamma_a/D$ will vary from element to element but it is expected to be much

[12] The functions $|v_l(x)/x|^2$, $|v_l'(x)/x|^2$, $\delta(x)$, $\delta'(x)$ have been tabulated for $l=0(1)20$ and $x=0(.1)10$ in "Scattering and Radiation from Circular Cylinders and Spheres," Morse, Lowan, Feshbach, and Lax, a report issued by the N.D.R.C. Division (6).

smaller for lighter elements than for heavier ones. This comes mainly from its dependence on the level distance D. We expect that D is substantially larger for light elements. The ratio Γ_a/D for any width Γ_a corresponding to an individual transition is usually considered to be independent of D. However, Γ_{al} is the sum of all individual transition widths to lower states of the compound nucleus. The number of possible end states is roughly inversely proportional to D, so that Γ_{al}/D is expected to decrease considerably with increasing D.

The variation of D seems to occur, however, only at values of $A \leq 100$. The fact that the neutron widths in known nuclear resonance levels show approximately the same proportionality factor of $\sqrt{E}$ in elements different as indium ($A=115$) rhodium ($A=103$) and Au ($A=187$) indicates, according to (26), that the level distance D at the neutron resonances does not change appreciably for these values of A. This is probably the effect of two opposing trends: (a) The level distance D decreases with increasing A for a given excitation energy of the compound nucleus. (b) The excitation energy at which D is measured is the binding energy of the neutron, which decreases with increasing A for $A>100$ and which is roughly constant for $A<100$. For $A>100$ the two effects a and b operate in opposite directions, giving rise to D and consequently to an x_0 which is comparatively constant. In the region $A<100$, only the trend given in (a) remains, which will give rise to an increase in D and thus to a decrease in x_0 for decreasing A. This probably explains the marked decrease of the absorption cross section, σ_{abs}, for elements for which $A<100$ as observed by Hughes.[13]

Expression (48) is, strictly speaking, valid only for nuclei with spin zero. If the spin is not zero, reemission of the neutron is possible with an l different from the incoming one, without exciting the nucleus. The partial widths corresponding to these processes should be included in $\langle\Gamma_{al}\rangle_{Av}$ since they represent an "inelastic" scattering inasmuch as the state of the nucleus has changed during the process. Thus $\langle\Gamma_{al}\rangle_{Av}$ would be made larger than the pure radiation width, by an amount which depends on the neutron energy. Closer investigation and application of selection rules reveals, however, that this effect is not very important. It decreases σ_{abs} by less than 10 percent if $x \lesssim 1$.

Expression (48) for the absorption cross section of neutrons can be compared with experiments performed by Greisen, Linenberger, Miskel, and Segrè,[14] on the elements Ag, In, I, and Au, with neutrons of energies between 5 and 400 kev. Figure 4 shows these results plotted as a function of $x^2=k^2a^2$, which is proportional to the energy. An energy scale is given for In and Au. The solid curves are plots of expression (48) with different values of x_0. It is hard to predict the actual value of x_0, even in elements like In and Au, where one resonance level is analyzed, since the properties of this level are probably not typical. The best values[8] for the In resonance are:

$$\Gamma_n \simeq 3\times10^{-3}(E_r)^{\frac{1}{2}}\text{ ev}, \quad \Gamma_a \sim 0.08\text{ ev}$$

and for Au:

$$\Gamma_n \simeq 6\times10^{-3}(E_r)^{\frac{1}{2}}\text{ ev}, \quad \Gamma_a \sim 0.15\text{ ev}.$$

This gives $x_0 \sim 0.05$ for both elements. The actual value of x_0 is probably somewhat higher since these two resonances are unusually strong which points to an abnormally large Γ_n. Moreover, there is an additional uncertainty due to the fluctuations in the nuclear radius from the assumed average value. Figure 4 shows that the theoretical curves give a fair representation of the experimental material.

The rather sharp decrease of σ_{abs}/σ_0 for Ag and Au for energies greater than a few hundred kev is caused by the onset of inelastic scattering of the neutrons. The cross section for this competing process is not included in the measured absorption cross section. Bismuth and lead,[14] however, seem to represent notable exceptions since they have shown no observable absorption in this energy region. These five nuclei (lead has four isotopes) fall completely out of the rules observed with so many other heavy nuclei. Within the framework of this theory, this would only be explained by an unusually large level distance D for these elements, which would point to an unusually low binding energy of the last neutron.

[13] Hughes, Phys. Rev. **70**, 106 (1946).

[14] We are grateful to these authors for communicating their results before publication.

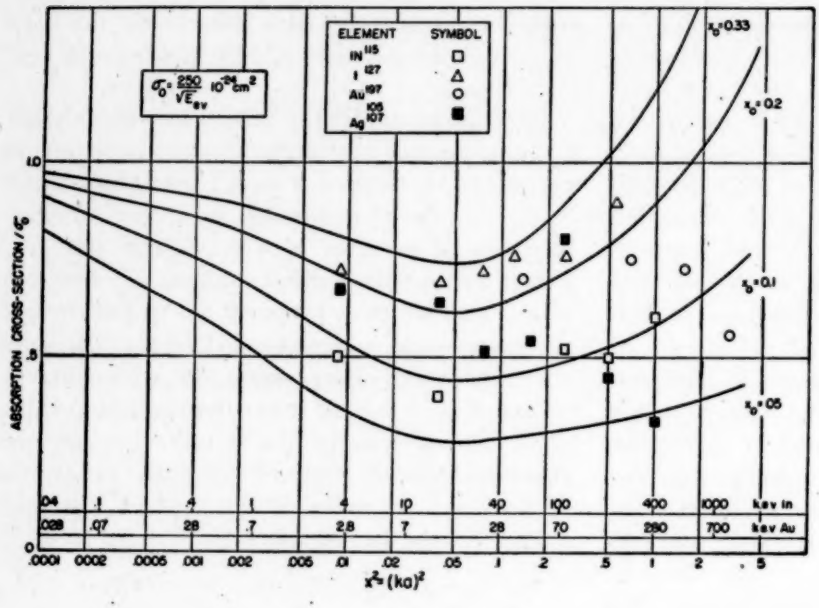

FIG. 4. The absorption cross section for neutrons as a function of $(ka)^2$. The experimental points were obtained by Greisen, Linenberger, Miskel, and Segrè. We are grateful to these authors for communicating their results prior to publication.

The elastic cross section of neutrons can be calculated with the help of (43). We consider again the average $\langle\sigma_{sc}\rangle_{Av}^{(l)}$ over many resonances, since this is the magnitude which can be measured most readily. We obtain

$$\langle\sigma_{sc}\rangle_{Av}^{(l)}=\frac{1}{D}\int_{E_r-D/2}^{E_r+D/2}\frac{4\pi}{k^2}(2l+1)\times\left|\frac{\frac{1}{2}\langle\Gamma_{nl}\rangle_{Av}}{(E-E_r)+\frac{1}{2}(\langle\Gamma_{nl}\rangle_{Av}+\langle\Gamma_{al}\rangle_{Av})}+p_{sc}\right|^2 dE$$

$$=\frac{4\pi}{k^2}(2l+1)\left[\left(1-\frac{\pi\langle\Gamma_{nl}\rangle_{Av}}{D}\right)\sin^2\delta_l+\frac{\pi}{2}\frac{\Gamma_{nl}^2}{D(\Gamma_{nl}+\Gamma_{al})}\right].$$

With the aid of approximations (46) and (47), we may now write

$$\langle\sigma_{sc}\rangle_{Av}=\sum_l\langle\sigma_{sc}\rangle_{Av}^{(l)}=\sigma_0+\frac{4\pi}{k^2}\frac{D^*}{D}\frac{x}{X}\times\sum_l\frac{2l+1}{|v_l|^2}\left[\frac{1}{1+(x_0|v_l|^2/x)}-2\sin^2\delta_l\right],\quad(49)$$

where $X=Ka$, δ_l is defined by Eqs. (36), (45b) and σ_0 is:

$$\sigma_0=\frac{4\pi}{k^2}\sum_l(2l+1)\sin^2\delta_l.$$

This is the scattering cross section of an impenetrable sphere of radius a, σ_0 is $4\pi a^2$ for small energies ($ka\ll1$) and approaches $2\pi a^2$ asymptotically for large energies ($ka\gg1$).

The quantity usually measured is not $\langle\sigma_{sc}\rangle_{Av}$ but rather the total scattering cross section

$$\langle\sigma_t\rangle_{Av}=\langle\sigma_{sc}\rangle_{Av}+\langle\sigma_{abs}\rangle_{Av}.$$

The theoretical formula for $\langle\sigma_t\rangle_{Av}$ is obtained by adding (49) and (48)

$$\langle\sigma_t\rangle_{Av}=\sigma_0+\frac{4\pi}{k^2}\frac{D^*}{D}\frac{x}{X}\sum_l\frac{2l+1}{|v_l|^2}\cos2\delta_l.\quad(50)$$

Note that $\langle\sigma_t\rangle_{Av}$ is independent of x_0.

The total nuclear cross section is, according to (50) always greater than σ_0. For low energies, one need only use the $l=0$ term in (50).

$$\langle\sigma_t\rangle_{Av}=4\pi a^2[1+D^*/DXx].$$

The excess of $\langle\sigma_t\rangle_{Av}$ over $4\pi a^2$ for small x will be large since the $1/x$ term ($1/v$ law of absorption) becomes very large for small x. For larger energies, several values of l contribute to the cross section. In the limit the positive and negative terms cancel so that $\langle\sigma_t\rangle_{Av}\to\sigma_0$.

Measurements of the total cross section of several elements of neutrons in the energy region between 20 kev and 800 kev are made by

Leipunsky[15] and Wattenberg.[16] Figure 5 shows these experimental results in units of πa^2, together with curves for σ_0 and $\langle\sigma_t\rangle_{Av}$ for indium, and $D^*/D=\frac{1}{2}$. Curves for other nuclei may be calculated quite easily from this one by making use of the fact that $\langle\sigma_t\rangle_{Av}-\sigma_0$, from (50), depends inversely on the nuclear radius. In comparing the theoretical and experimental values, one must keep in mind that a was assumed to be $1.5\times10^{-13}A^{\frac{1}{3}}$ cm. The actual value of the nuclear radius will probably deviate from this average value. In Fig. 5, representative elements from among the middle and heavy elements have been included. It is seen that the qualitative features of $\langle\sigma_t\rangle_{Av}$ are in substantial agreement with the theory for the elements Fe, Ni, W, Pb. Although the cadmium points are of the right order of magnitude, they do not show the characteristic decrease with increasing ka. This behavior is exhibited by other elements with $A\sim100$ such as Sn, I, Sb, all of which have about the same $\langle\sigma_t\rangle_{Av}$ as Cd.

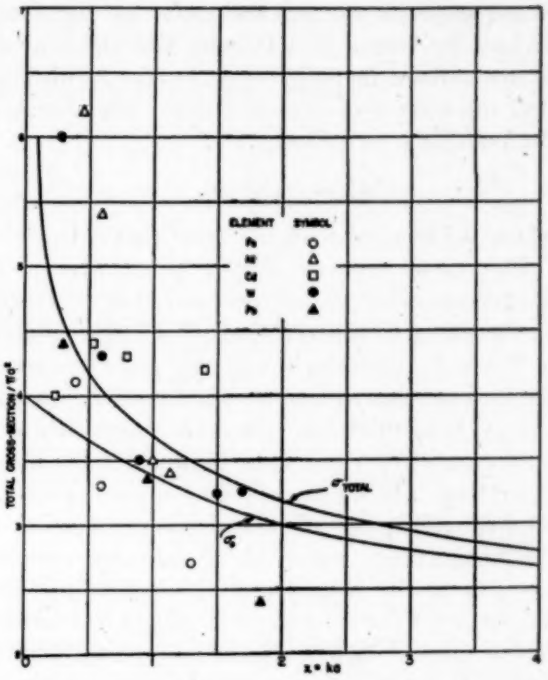

FIG. 5. The total cross section for neutrons as a function of ka. σ_{TOTAL} is the total cross section curve for $A=115$. The σ_0 curve is the cross section for scattering by an "impenetrable sphere." The experimental points are typical examples taken from Wattenberg (reference 17). Similar results have also been obtained by Leipunski (reference 16).

6. RELATION TO OTHER METHODS

The derivation of the resonance formulas presented here is in many respects similar to the method employed by Kapur and Peierls.[4] It may be useful for the understanding of the situation to point out the similarities.

It is possible to write the expressions (8) and (9) in a form in which the familiar sum over resonance levels appears, if the following relation is used:

$$g(E)=\frac{1}{f(E)-ix}=\sum_r\frac{C_r}{S_r-E}, \tag{50a}$$

where S_r are the poles of the function $g(E)$, which are defined by

$$f(S_r)=ix. \tag{51}$$

The C_r are the residues: $C_r=(1/(df/dE))_{E=S_r}$. Here x is considered as a constant parameter independent of E. It follows from (17a) and (18) that

$$S_r=E_r-i\Gamma_a^{(r)}/2-i\Gamma_n^{(r)}/2 \tag{52}$$

where E_r is the solution of $f_0(E)=0$. If the imaginary parts of S_r are small compared to the real ones, the relation $C_r=-\Gamma_n^{(r)}/2x$ holds because of (18), and we can write (8) in the form

$$\sigma_{abs}=\frac{\pi}{k^2}\left|\sum_r\frac{(\Gamma_n^{(r)}\Gamma_a^{(r)})^{\frac{1}{2}}}{E-E_r+i(\Gamma_n^{(r)}+\Gamma_a^{(r)})/2}\right|^2 \tag{53}$$

after using the relation

$$h=-\tfrac{1}{2}\Gamma_a^{(r)}(df/dE)_{E=S_r}.$$

Expression (9) can similarly be written in the form:

$$\sigma_{sc}=\frac{4\pi}{k^2}\left|\tfrac{1}{2}\sum_r\frac{\Gamma_n^{(r)}}{E-E_r+i(\Gamma_n^{(r)}+\Gamma_a^{(r)})/2}+e^{ix}\sin x\right|^2. \tag{54}$$

[15] A. I. Leipunsky, J. Phys. Academy of Science, U.S.S.R. **3**, 231 (1940).
[16] J. Wattenberg, unpublished. We are grateful to the author for communicating his results before publication.

These expressions are the same as the ones derived by Kapur and Peierls. The eigenvalues S_r are defined in their paper by the condition, that the wave ψ of the emitted particles satisfies the boundary condition

$$\partial\psi/\partial r - ik\psi = 0,$$

which is identical with our condition (51).

The cross sections for a given energy E between resonances are represented in this form as the effect of contributions of a large number of levels E_r, whereas in our case the same cross sections are determined by the function f at the energy E in question. The two approaches are mathematically equivalent because of the identity (50a). The method presented here seems to offer the advantage of an easier interpretation of the magnitudes involved. Qualitative conclusions as to the behavior of the logarithmic derivatives $f(E)$ of the wave function at the surface of the nucleus can be drawn more readily than conclusions concerning a whole series of eigensolutions of a complicated eigenvalue problem at energies far off the value E. Especially the levels far off resonance and their contribution to scattering offer some difficulties of interpretation. It was pointed out by Siegert,[5] that they do not correspond to any physical state since the boundary condition contains the k of the incident particle and not the k which would correspond to the emission of the particle by the resonance level itself. Siegert's method avoids this difficulty by using a different boundary condition for the definition of the compound states. However, the physical meaning of compound states of high energy is questionable, when their width becomes larger than their distances, which is bound to happen at higher energies.

Bethe[17] has derived expressions similar to ours for the average cross sections and particle widths by ascribing to the nucleus a strong absorption coefficient in form of an imaginary potential energy. This absorption was supposed to describe the "amalgamation" of the incident particle with the nucleus. It therefore was assumed to be so strong that the wave function of the incoming particle decreases by a factor e^{-1} at a distance b of the order of the reciprocal of our K. Bethe's expression for the average neutron capture cross section for $l=0$ $\langle\sigma_{abs}\rangle_{Av}=2\pi^2\lambda b$ [his formula (27a)] is identical with ours (28) if

$$b=(1/K)(D^*/D)(2/\pi).$$

Bethe's model does not exhibit any resonances because of the strong absorption assumed. This absorption is very much larger than the actual one due to radiative capture, and the corresponding breadth is so large that it would broaden any levels until they merge. The similarity of Bethe's results with ours comes from the fact that his fictitious absorption causes the wave function of the incoming particle to assume a high logarithmic derivative after entering the nucleus of the order $K\sim 1/b$. This fact alone determines the average cross sections, whereas the special form (24) of the logarithmic derivative is important only for the finer details relating to resonance phenomena. Bethe's assumption of an absorption coefficient of the order b^{-1} appears to be equivalent to our assumption (21) about the average wave numbers inside of the nucleus. Our way of introducing high wave numbers inside the nucleus seems to be more general since it also permits the description of resonance phenomena.

The authors express their appreciation to Dr. H. H. Goldsmith for his invaluable help in analyzing the unpublished experimental material obtained from the recently declassified work of the Manhattan Project. They also wish to thank Dr. G. Placzek for many enlightening discussions.[18]

[17] H. A. Bethe, Phys. Rev. **57**, 1125 (1940).

[18] The research described in this paper was supported in part by contract N5ori, U. S. Navy Department.

Formation of Radium E and Polonium by Deuteron Bombardment of Bismuth

H. E. TATEL
Applied Physics Laboratory, Johns Hopkins University, Silver Sping, Maryland

AND

J. M. CORK
Department of Physics, University of Michigan, Ann Arbor, Michigan

(Received November 4, 1946)

The direct production of RaE and Po by deuteron bombardment of bismuth has been reinvestigated. Present results indicate that as the deuteron energy is lowered from 8.8 to 7.3 Mev, the production ratio of RaE/Po increases 25 percent but as the deuteron energy is dropped from 7.3 Mev to 5.5 Mev, the ratio more than doubles. The trend is in agreement with the Oppenheimer-Phillips reaction in which RaE is produced by a d, p reaction and Po is produced by a d, n reaction. Assuming these reaction cross sections to be respectively proportional to Bethe's OP penetration factor and to the Gamow-Condon-Guerney penetration factor, best agreement of the variation with energy of the ratios of these cross sections is obtained with a nuclear radius of $2.0A^{\frac{1}{3}}\times10^{-13}$ cm for bismuth.

INTRODUCTION

THE disintegration products of bismuth under bombardment by deuterons with energy in the region of 5 to 9 million electron volts has been studied experimentally and two different results were found.[1,2] Since bismuth with its single isotope and high atomic number affords an excellent opportunity for the comparison of two competing processes under deuteron bombardment—proton emission and neutron emission—the problem was reinvestigated experimentally at the University of Michigan Physics Department in 1940. Because of the war, the results have only just now been interpreted and are herewith reported.

THE NUCLEAR REACTIONS

The nuclear reactions have been previously reported and there is a d, p and a d, n reaction which may be described by means of three processes:

I. $_1d^2+{}_{83}\mathrm{Bi}^{209}\rightarrow{}_{83}\mathrm{RaE}^{210}+{}_1p^1$,

II. $_1d^2+{}_{83}\mathrm{Bi}^{209}\rightarrow{}_{84}{}^*\mathrm{Po}^{211}\rightarrow{}_{83}\mathrm{RaE}^{210}+{}_1p^1$,

III. $_1d^2+{}_{83}\mathrm{Bi}^{209}\rightarrow{}_{84}{}^*\mathrm{Po}^{211}\rightarrow{}_{84}\mathrm{Po}^{210}+{}_0n^1$.

The first two reactions have the same end products and so may not be distinguished by measurement of only the end products. Process I is an Oppenheimer-Phillips reaction[3] in which the deuteron splits up outside the nucleus with the neutron being absorbed in the final nucleus which is identical with the compound nucleus. Formally, reaction II appears the same as I but here an intermediate compound nucleus is formed and the proton emission must compete with the more probable neutron emission as in III. If III is more probable than II, only I and III will occur and these two are distinguishable by a fortunate set of circumstances. The RaE formed in I decays by β-ray emission with a half-life of 5.0 days into polonium and the Po thus formed, as well as the Po produced in III, decays with a lifetime of 136 days by the emission of α-particles. Thus, by the measuring of the α-particle activity as it changes, the amounts of each product may be determined. The number of Po nucleii N_2 present at any time is given by

$$N_2=[\lambda_1N_1{}^0/(\lambda_1-\lambda_2)][\exp(-\lambda_2t)-\exp(-\lambda_1t)]+N_2{}^0\exp(-\lambda_2t). \quad (1)$$

$N_1{}^0$ is the number of RaE nucleii formed by the bombardment in reaction I (and II) while $N_2{}^0$ is the amount of Po nucleii present at $t=0$ (at the instant of bombardment) in reaction III. λ_1 and λ_2 are, respectively, the decay constant of RaE

[1] Hurst, Lantham, and Lewis, Proc. Roy. Soc. **174**, 126 (1940).
[2] Cork, Halpern, and Tatel, Phys. Rev. **57**, 348 (1940); **57**, 371 (1940).
[3] H. A. Bethe, Phys. Rev. **53**, 39 (1938).

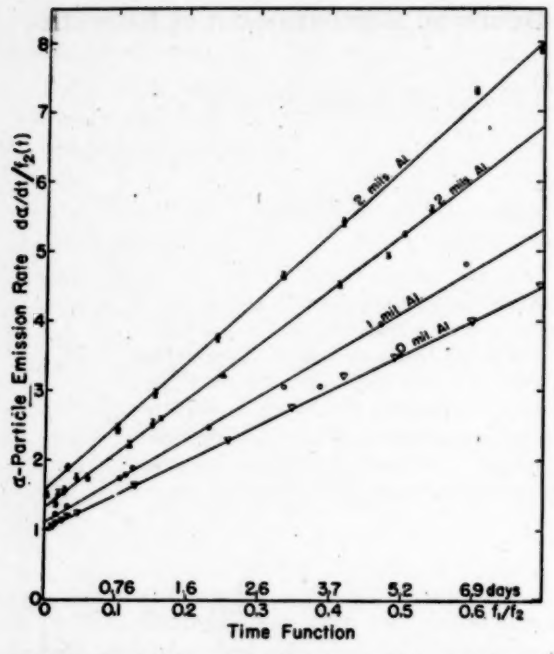

FIG. 1. Straight-line plot of alpha-particle emission as a function of time for the various targets with deuteron bombarding energy. Ordinates should be multiplied by 1.10×10^{8}, 1.60×10^{8}, 10.0×10^{8}, and 3.06×10^{8} for the 0, 1, 2, 2 mil curves, respectively.

$(1.60\times10^{-6}$ second$^{-1})$ and Po $(5.89\times10^{-8}$ second$^{-1})$. N_1^0 and N_2^0 may be found from the experiment by integration or by differentiation of (1). For the latter method, the alpha-particle emission rate at any time is given by $d\alpha/dt = -\lambda_2 N_2$ which can be combined with (1) to give

$$-\frac{d\alpha}{dt}\Big/ f_2(t) = N_1^0[f_1(t)/f_2(t)]+N_2^0; \qquad (2)$$

$$f_1(t) = [\lambda_1\lambda_2/(\lambda_1-\lambda_2)] \times[\exp(-\lambda_2 t)-\exp(-\lambda_1 t)],$$

$$f_2(t) = \lambda_2 \exp(-\lambda_2 t).$$

Expression (2) is the equation of a straight line and so if the α-particle rate divided by f_2 is plotted as ordinate against f_1/f_2 as abscissa, the intercept N_2^0 gives the yield in III and the slope N_1^0 is a measure of the yield in I (and II). Figures 1 and 2 show plots of the data in this form. The vertical lines through each point are a measure of the statistical fluctuation of the number of counts. This fluctuation is taken as $N^{\frac{1}{2}}$ where N is the total number of alpha-particles measured in a given interval.

THE OBJECT OF THE EXPERIMENT AND GENERAL PROCEDURE

For a given target of bismuth, it is possible to compare the cross sections for deuteron bombardment of the two types of reactions, emission of a proton and emission of a neutron. Generally, when a compound nucleus is formed at excitations below the barrier height, it is considerably more probable that a neutron is emitted than a proton because, for one thing, the neutron does not have to penetrate the potential barrier. However, if the mechanism proposed by Oppenheimer and Phillips prevails, it is possible for the d, p reaction to be more probable. A test of whether or not the OP process occurs is to compare its cross section with an ordinary reaction as the deuteron bombarding energy is varied, the OP process diminishing relatively as the top of the deuteron barrier is approached. In this experiment, the energy of the deuterons was varied by interposing aluminum foils between

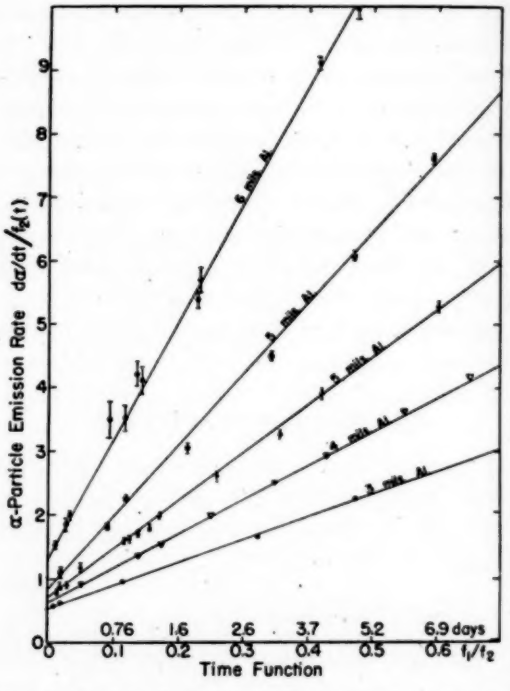

FIG. 2. Straight-line plot of alpha-particle emission as a function of time for the various targets with lower bombarding energy. The ordinates should be multiplied by 2.00×10^{8}, 2.00×10^{8}, 10.0×10^{8}, 10.0×10^{8}, 263×10^{8} for the 3, 4, 5, and 6 mil curves, respectively. In comparing Fig. 2 to Fig. 1, it is seen that there is greater slope divergence in Fig. 2 although the intercept spread is over the same range. This increase in slope indicates relatively more N_1(RaE) with lower energy.

TABLE I. Experimental results.

Mils of Al	Deuteron energy Mev	N_1^0 $\times 10^{-7}$	N_2^0 $\times 10^{-7}$	Numbers of deuterons in coulombs	Bombardment time-hr.	$N=N_1^0/N_2^0$	R	$\sigma_{dp}\times 10^{28}$ cm²	$\sigma_{dn}\times 10^{28}$ cm²	R_{HLL}	R_{CHT}
0	8.7	55.2	11.3	0.012	0.58	4.9	5.0	34	6.8	4.3	4.9
1	8.2	36.9	7.3	0.015_6	0.5	5.1	5.2	18	3.4	5.0	5.0
2	7.8	20.9	3.7	0.016_8	1.0	5.6	5.7	$9._2$	1.6	4.9	6.0
2	7.8	29.9	5.3	0.015_0	0.5	5.6	5.7	15	2.6		
2*	7.8	7.8	1.3_1	0.027_7	1.5	5.8	6.0	$6._3$	1.0_8	6.3	
3	7.3	17.8	2.7_8	0.016_6	0.83	6.2	6.3	8	1.3_0		8
4	6.8	27.2	3.2	0.040_4(?)	1.8	8.1	9.5	5	0.5		17
5	6.3	7.5	0.72	0.036_7	2.0	$10._2$	$10._9$	1.5	0.14	6.5	
6	6.3	11.3	0.83	0.056_5	2.0	13	14	1.4	0.10		
6	5.8	0.52	0.033	0.07_2	4.0	$13._6$	16	0.5_4	0.03_4	—	

* Target of approximately 3.2 mg/cm² of Bi on Al.

the beam and the bismuth target. Hence, for a given energy, a bismuth target was bombarded and the rate of emission of alpha-particles was measured from the time the bombardment stopped and plotted as already explained. Then N_1^0 and N_2^0 which are the end products of the d, p and d, n reaction, respectively, may be found and so their ratio for each energy. Since for each target the deuteron energy and distribution is identical, an excellent value of the ratio of these two quantities $N=N_1^0/N_2^0$ may be found. This ratio must be corrected for the time of bombardment especially for the weak samples which have both a long bombardment time and a large ratio. The reason is that the radium E is always decaying into polonium and so at the end of a bombardment there will, in general, be less radium E and more polonium thereby giving a smaller ratio. The true ratio of cross sections is to a first and sufficient approximation:

$$R=\frac{N}{1-\frac{1}{2}\lambda_1 T(N+1)} \qquad (3)$$

where λ_1 is the decay constant of radium E and T is the bombardment time. This correction amounts to 1 percent for an N of 5.6 and a bombardment of 0.5 hour; and to 9 percent for a bombardment of 2 hours with an N of 13. These values with N and R and T are shown in Table I.

There are two types of targets which have been used in this experiment and both are "thin." HLL[1] used evaporated layers of bismuth on thin aluminum foils with a total thickness of about 1 air-cm. The second procedure[2]—used here—employs a physically thick piece of bismuth for the target but makes use of the short range 3.8 air-cm polonium alpha-particles compared to the long range deuterons to secure an essentially thin target. Since the alpha-particles had to travel one centimeter before entering the ionization chamber grid to be registered, the only ones counted must originate within 2.8 air-cm of the surface of the bismuth target. At the deuteron energy limits of 6 and 9 Mev used in this experiment, the deuterons lose, respectively, 0.07 and 0.05 Mev/cm or 0.20 and 0.14 Mev in the effective thickness (2.8 air-cm) of the target. Hence no correction need be made here for the target thickness. There is a disadvantage in using this thick target scheme, for the alpha-particles coming into the chamber have residual ranges extending from zero to 2.8 air-cm and so fluctuations in over-all counter sensitivity give variations in counting rates. However, a change in counter sensitivity of 1 percent gave a change of less than 1 percent in the counting rate. Before each count, the amplifier sensitivity was set to within 1 percent of a fixed value and generally the statistical fluctuations in counts was about 1 percent so that this error does not affect the readings more than the statistical fluctuations of the counting. The advantage in this type of thick target is that the target is simple to prepare and there is little danger in burning it out during bombardment or breaking it during the subsequent measurements.

Each bombardment was monitored with a current integrator to obtain absolute cross section. However, since the cyclotron was never considered to give an identical bombardment for different runs, the absolute cross section is not

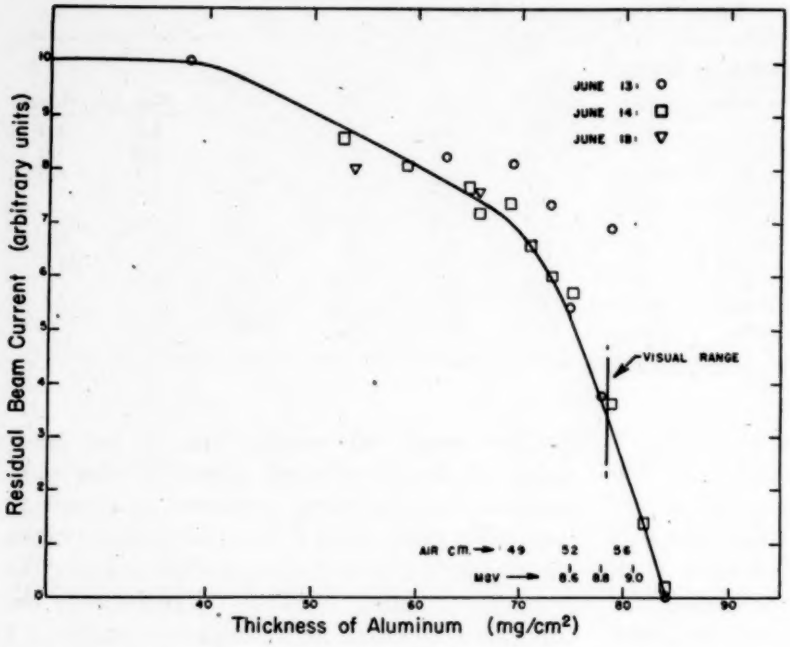

FIG. 3. Plot of residual current of deuteron beam of cyclotron through different thicknesses of aluminum foil.

considered to be a reliable result although the trend should be fairly consistent.

The energy of the deuteron beam was estimated visually by measuring the range in air of the beam, the mean range being taken as the point along the beam at which the brilliancy of an irradiated fluorescent screen started to diminish rapidly. This measurement was made as a check on a residual range determination in which the residual beam current to a Faraday cup was measured as the beam passed through aluminum foils of various thickness, Fig. 3. The air equivalent of aluminum was taken as 1.52 milligrams per cm² per air-cm and corrected according to Livingston and Bethe. The effective maximum deuteron range is taken as 54 air-cm or 8.8 Mev. Although, the beam is not monoenergetic, the trend of the results should not be seriously affected as the cross section is changing so rapidly that for any experiment only the high energy tail is efficacious in making the transmutation. The straggling in energy for a 5- and 9-Mev deuteron beam is about 0.1 and 0.16 Mev, respectively, while the approximate straggling of the beam in the cyclotron was 0.5 Mev.

RESULTS

Bismuth targets were bombarded with deuterons from zero to 0.006 inch of aluminum in steps of 0.001 inch (6.6 mg/cm²). These steps decreased the mean energy of the beam by approximately 0.5 Mev per step from a maximum of 8.8 Mev. During bombardment, the beam current was kept to within 70 percent of a norm and the total quantity of deuterons and the time of bombardment recorded. After bombardment, the targets were mounted in front of a parallel plate ionization chamber and linear pulse amplifier arrangement. Counting rates of the emitted alpha-particles were measured at intervals for from five to ten days. All targets showed an initial rate, an increase, and then (if followed long enough) a decrease. The graphs in Figs. 1 and 2 show that each target accurately follows the assumed pattern of formation of RaE and Po. The quantities of these end products, their ratios, and the ratios corrected for finite bombardment time are all shown in Table I. The absolute cross section is roughly computed assuming that all the Bi nucleii in 2.8 air cm (10.6 mg/cm²) are effective as targets and that the effective solid angle is defined by the circular 1.5-cm opening of the ionization chamber 1 cm from the target under observation. For comparison, the ratios from the two previous measurements are also tabulated R_{HLL}[1] and R_{CHT}[3]. These results are plotted as follows: cross section for formation of Po (σ_{dn}) in Fig. 4 and the

corrected ratio R for finite bombardment time, of RaE/Po or σ_{dp}/σ_{dn} in Fig. 5.

SOURCES OF ERROR

A major source of uncertainty in the measurements is the deuteron energy. There are two difficulties. First, the beam had a considerable spread as shown in Fig. 3 and second, the energy varied from time to time. This may be the reason for the disagreement of the two measurements of R with 5 mils of Al. Because so many measurements were taken on each sample, it is thought that the measurement of R on any particular sample has an over-all accuracy of 10 percent at 6 mils to 3 percent at zero mils of Al absorber in the beam.

DISCUSSION

As has been pointed out, the d, p reaction may formally be described by either an OP process, I, or by the formation of a compound nucleus with subsequent proton mission, II. The reaction III is clearly of the latter type. In order to compare the OP process, I, with an "ordinary" process as III, it would be necessary for reaction II to be extremely improbable. However, there are no experimental data by which reaction II may be ruled out compared to reaction III.

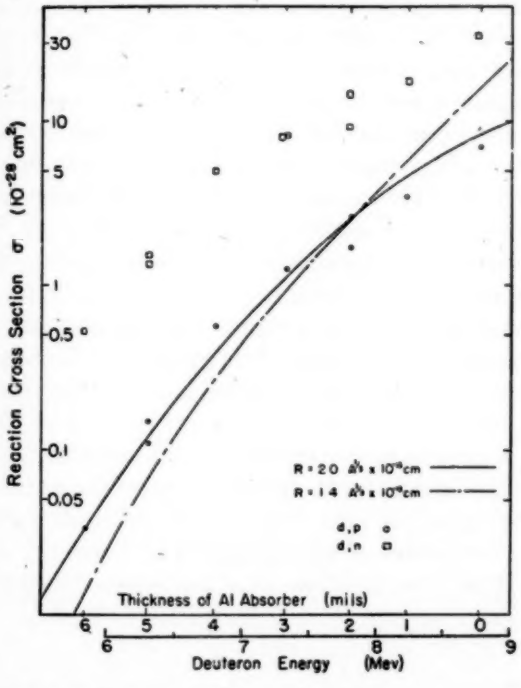

FIG. 4. Plot of cross section of d, n reaction as a function of the energy. The two curves are plotted for the Gamow-Condon-Guerney penetration function for small and large nuclear radius. Both curves arbitrarily fit at about 8 Mev.

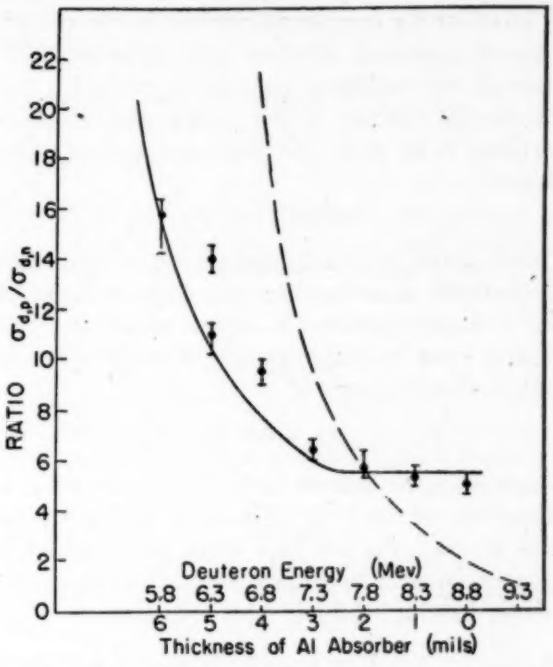

FIG. 5. Plot of ratio of cross sections of d, p and d, n reaction as a function of the deuteron bombarding energy. The curves are the ratio of Bethe's Oppenheimer-Phillips penetration factor to the Gamow-Condon-Guerney penetration factor. The best fit is with the larger nuclear radius of $2.0A^{\frac{1}{3}}\times10^{-13}$ cm.

It is usually considered that when a heavy compound nucleus is formed, the competition of the various processes is such that the emission of a neutron is considerably more probable than emission of a proton and so reaction III would be more probable than reaction II. This is deduced by Bethe,[4] paragraph 79, in the following manner: For the ordinary type of reaction in which a compound nucleus is formed by deuteron bombardment with subsequent emission of neutrons and protons:

$$\sigma_{dn}=\pi\lambda^2\xi_d P_d l_e^2\Gamma_n/\Gamma$$

and

$$\sigma_{dp}=\pi\lambda^2\xi_d P_d l_e^2\Gamma_p/\Gamma \qquad (4)$$

where ξ_d is the deuteron "sticking function," P_d is the deuteron penetrability, l_e is the "effective orbital momentum," and Γ is the total width of

[4] H. A. Bethe, Rev. Mod. Phys. 9, 69 (1937).

all levels of the compound nucleus in the energy region in question. All these quantities are functions of the incoming particles leaving Γ_n, Γ_p, the partial widths of the states with emitted particles n or p in the final residual nucleus. Hence,

$$\sigma_{dn}/\sigma_{dp}=\Gamma_n/\Gamma_p. \quad (3)$$

These partial widths depend on the total number of available states and on the penetrabilities of the emitted particles both of which in turn depend upon available energy. The difference in this available energy is

$$U_n-U_p=\epsilon_--0.8 \text{ Mev}+B_p,$$

which is expression 40 from Bethe,[3] where ϵ_- is the energy of the β-ray of RaE (in this particular case 2 Mev), the 0.8 Mev is the mass difference of neutron and hydrogen atom, and B_p is the proton barrier height (5 Mev) whence

$$U_n-U_p\sim 6 \text{ Mev}.$$

Hence, there is considerably more energy available for the neutron emission than for the proton emission and since the partial widths depend upon the energy available, it is seen that Γ_n should be greater than Γ_p and, therefore, from (3) the cross section for emission of the neutron should be greater than the cross section for the emission of the proton. While there is not enough knowledge on the details of these nucleii available, a probable estimate of this ratio may be obtained from statistical considerations. Bethe (41)[3] shows that the ratio of the neutron and proton partial widths is given by

$$\Gamma_n/\Gamma_p=\exp(U_n-U_p)/T.$$

The nuclear temperature T for bismuth for this type of excitation will be approximately 1.3 Mev and so the ratio of the cross sections would be a rather large number e^4 which would indicate that reaction III is considerably more probable than reaction II and thus the experiment is measuring only reaction I and III. Assuming then that this is true, it should be noted that Bethe's critiques[3] for observing the OP process are fulfilled in this reaction, i.e., the deuteron bombarding energy is below the barrier height minus the deuteron binding energy (2.2 Mev). The barrier height of bismuth for deuterons is 9.8 and 14.3 Mev for the large and small nuclear radius, respectively.

The only factor used here in the theoretical treatment of the comparison of the Oppenheimer-Phillips type of reaction to the ordinary type of reaction are the penetrability factor. These are also the most rapidly varying factors with respect to energy and it is usually considered that the ratio of the cross sections (γ) is given by the ratio of the penetrabilities. Hence

$$\gamma=\sigma_{OP}/\sigma_{GCG}\sim P_{OP}/P_{GCG},$$

where the subscript OP refers to the Oppenheimer-Phillips penetrability function and GCG refers to the Gamow-Condon-Guerney type of penetrability for the deuteron.

In fitting the theoretical γ to the experiment, the most important parameter is the nuclear radius. Near the barrier height, this is especially important as the theory predicts that $\gamma=1$ at the barrier height minus the binding energy of the deuteron. For a radius of $2.0A^{\frac{1}{3}}\times10^{-13}$ cm and $1.4A^{\frac{1}{3}}\times10^{-13}$ cm, this occurs for $Z=83$ at 7.6 and 12.1 Mev, respectively. In Fig. 5, the data have a more slowly varying region in the neighborhood of 7.6 Mev which is what the theory predicts for the larger nuclear radius. The γ's for these two values are plotted also in Fig. 5. The values for the smaller radius are taken from Volkoff's[5] discussion of Bethe's OP theory. The theoretical curves are fitted to the experimental values at 7.6 Mev. The trend of the results are in general agreement with an OP process of finite nuclear radius and the radius best matching these results is the larger $2.0A^{\frac{1}{3}}\times10^{-13}$ cm. Of further interest, it is seen that d, n follows rather closely the P_{GCG} function and so the effect of the other factors which enter in the cross sections other than the penetration factors varies slowly compared to them.

This investigation was made possible by a grant from the Horace H. Rackham Fund.

[5] G. M. Volkoff, Phys. Rev. 57, 866 (1940).

Slow Neutron Velocity Spectrometer Studies. II. Au, In, Ta, W, Pt, Zr*

W. W. HAVENS, JR., C. S. WU, L. J. RAINWATER, AND C. L. MEAKER
Columbia University, New York, New York

(Received November 4, 1946)

The slow neutron velocity spectrum of Au, In, Ta, W, Pt, and Zr have been investigated. The results for Au and In check the values previously obtained using the "old" system. The results for the gold level at (4.8±0.1)ev with $\sigma_0\Gamma^2=600$, and for the main indium level at (1.44±0.02) ev with $\sigma_0\Gamma^2=210$ agree with the earlier results. Additional indium levels were found at (3.8±0.2) ev with $\sigma_0\Gamma\sim120$ and at (8.6±0.4) ev with $\sigma_0\Gamma\sim300$. The cross-section curve for Ta below 1 ev is well matched by $\sigma=[(7.2\pm0.4)+(3.0\pm0.1)E^{-\frac{1}{2}}]$. Tantalum has levels at (4.1±0.1) ev with $\sigma_0\Gamma^2\sim44$, at (10.0±0.3) ev with $\sigma_0\Gamma^2\sim25$, at (13±0.5) ev with $\sigma_0\Gamma^2\sim3$, at (22±2) ev with $\sigma_0\Gamma^2\sim18$, at (37±3) ev with $\sigma_0\Gamma^2\sim400$, and other dips probably indicating multiple strong levels near 100 ev, 300 ev, and at higher energies. The cross section curve for W below 1 ev is well matched by $\sigma=[(5.7\pm0.2)+(2.72\pm0.05)E^{-\frac{1}{2}}]$. There are levels at (4.0±0.1) ev with $\sigma_0\Gamma^2\sim13$, at (7.4±0.2) ev with $\sigma_0\Gamma^2\sim5$, at (18.0±0.5) ev with $\sigma_0\Gamma^2\sim3000$ (perhaps multiple), at (45±2) ev with $\sigma_0\Gamma^2\sim400$ (perhaps multiple), at (180±20) ev with $\sigma_0\Gamma^2\sim10{,}000$ if single (probably multiple), and a dip at 1100 ev which is probably multiple. The results for Pt show pronounced crystal interference effects in the thermal region. The $1/v$ line is probably $\sigma=[(12.0\pm0.3)+(1.03\pm0.06)E^{-\frac{1}{2}}]$. There are levels at (11.5±0.4) ev with $\sigma_0\Gamma^2\sim55$, at (18.2±1) ev with $\sigma_0\Gamma^2\sim30$, and broad dips near 100 ev and near 1000 ev indicating the presence of several strong unresolved levels. The results for Zr below 0.6 ev are well matched by $\sigma=[(6.8\pm0.3)+(0.74\pm0.10)E^{-\frac{1}{2}}]$. There are weak levels at (1.09±0.03) ev with $\sigma_0\Gamma\sim5$ and at (2.30±0.07) ev with $\sigma_0\Gamma\sim8$. A complex dip near 7 ev probably consists of two levels at $E_0=(5.7\pm0.5)$ ev with $\sigma_0\Gamma\sim10$ and at (7.6±0.4) ev with $\sigma_0\Gamma^2\sim40$.

INTRODUCTION

THIS is the second of a series of papers in which the results of measurements using the new Columbia University Slow Neutron Velocity Spectrometer are presented. A description of the first system and a detailed analysis of operational factors is given in two previous papers.[1,2] The description of the new system and the results for Cd, Ag, Sb, Mn, and Ir are given in the first paper of this series.[3]

For convenience in interpreting these results a few of the factors involved in the operation of the apparatus and in the analyses applied to the data are listed below. A complete discussion of these factors is given in the three previous papers.

OPERATION

1. A burst of neutrons is produced at the source between $t=0$ and $t=\tau$, and these neutrons are detected 6.2 meters from the source between $t=t$, and $t=t+\tau$ to define the neutron energy in terms of its time of flight t, over the measured path length.

2. Sixteen adjacent timing intervals are measured simultaneously for each of two independent detectors, thus 32 measurements are made simultaneously.

3. The detection intervals are spaced in time an amount τ equal to the width of the individual intervals. The resolution function of the instrument may be considered as triangular in shape with a base of approximate width 2τ or twice the spacing between adjacent points. Actually the width of the resolution triangle includes other factors such as a term due to the counter length, and, below 0.3 ev, a term due to the diffusion time of the thermal neutrons leaving the source. In almost all cases, the resolution width may be taken as 2 to 3 times the spacing between adjacent points.

4. The results of the measurements are presented as plots of the slow neutron transmission

* This document is based on work performed under Contract W-7405-Eng-50 with the Manhattan Project and Columbia University. It will also be published in the Manhattan Project Technical Series, Division III, as part of the contribution of the Physics Department, Columbia University. Publication assisted by the Ernest Kempton Adams Fund for Physical Research of Columbia University.

[1] L. J. Rainwater and W. W. Havens, Jr., Phys. Rev. 70, 136 (1946).

[2] W. W. Havens, Jr. and L. J. Rainwater, Phys. Rev. 70, 154 (1946).

[3] L. J. Rainwater, W. W. Havens, Jr., C. S. Wu and J. R. Dunning, Phys. Rev. 71, 65 (1947).

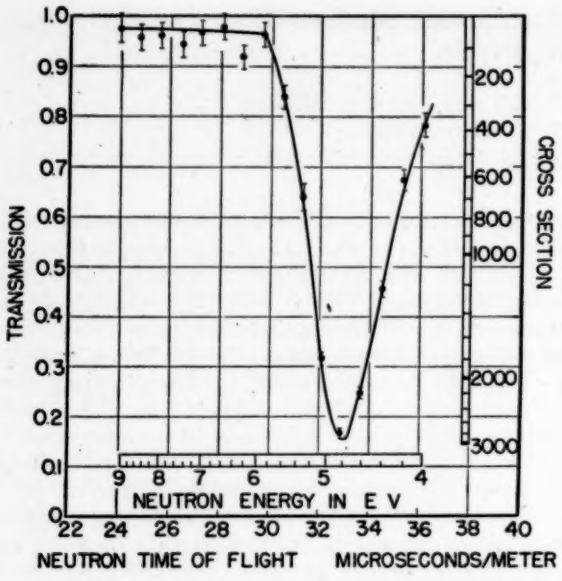

FIG. 1. The slow neutron transmission of 0.210 g/cm² of gold. This curve shows the resonance dip in transmission at 4.8 ev.

of the sample *vs.* the slow neutron time of flight in μsec./meter. Scales of energy are provided for convenience. The relation $E=(72.3/t)^2$ ev gives the neutron energy for a timing t μsec./meter.

5. The cross section, σ, is related to the transmission, T, by the relation $T=e^{-n\sigma}$ where n =atoms/cm² of the element studied (if only the element is present). From this equation a cross section scale indicated on each curve is computed, and if σ is a slowly varying function of t, the measured value of σ will correspond to the true value within the accuracy of each measurement. Near a resonance the effect of the resolution width will affect the measured cross section appreciably, and for resonances above 1 ev, the value of σ calculated from the transmission curve is usually very much smaller than the true value of σ. In particular the true value of σ_0 at exact resonance may be from 2 to 1000 times larger than the directly measured value σ max., from the transmission dip.

The quantity $\sigma_0\Gamma^2$ can usually be determined to within a factor of two by a method previously described.[2,3] This value is usually given in addition to the position (energy) of the resonance level. In some cases where the condition $n\sigma_0 \gg 1$ is not satisfied, a rough value of $\sigma_0\Gamma$ may be given. Although these values are only roughly quantitative, any information concerning the "strength" of the levels, was thought to be of value.

6. For many elements the cross section curve for energies lower than the first resonance may be closely matched by the sum of a $1/v$ term and a constant term. The equation for the cross section in this form is given where possible.

7. The units of energy E, cross section σ and the $\sigma_0\Gamma$ and $\sigma_0\Gamma^2$ values will usually not be stated specifically. It is to be understood that energy is expressed in units of electron volts, ev, and cross sections in units of $\times 10^{-24}$ cm²/atoms. Γ is the full level width (in ev) at half-maximum in the Breit-Wigner formula.

Unless otherwise specified all cross sections are averages for the natural element and are not assigned to particular isotopes.

GOLD

The resonance in gold near 4.8 ev has previously been studied with the first Columbia Neutron Spectrometer.[2] The earlier measurements in gold have been checked with the new system. In Fig. 1, the transmission curve is shown for a 0.210 g/cm² gold foil. The position of the resonance at (4.8±0.1) ev is in agreement with the previous measurement. The earlier value $\sigma_0\Gamma^2$ =600 is also in good agreement with Fig. 1.

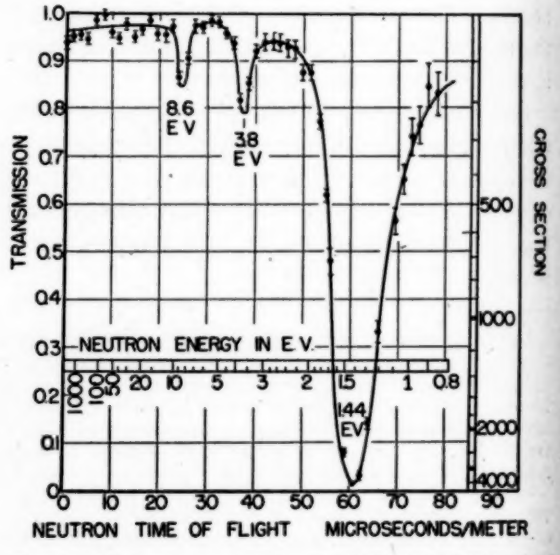

FIG. 2. The slow neutron transmission of 0.193 g/cm² of indium. This curve illustrates the three resonances at 8.6 ev, 3.8 ev, and 1.44 ev.

This level must be assigned to the Au^{197} for gold has only one isotope. The half-life of Au^{198} resulting from the capture of a neutron by Au^{197} is 2.7 days.[4,5] If $\Gamma \sim 0.1$ ev, then $\sigma_0 \sim 60{,}000$, which is 20 times larger than the measured σ max.

INDIUM

The indium resonance was also investigated with the previous system.[2] The main level was located at 1.44 ev with $\sigma_0\Gamma^2 = 210$. The same sample has been remeasured over a wider range with better resolution using the new system with the results shown in Fig. 2. Two additional resonances at 3.8 ev and 8.6 ev have been located with $\sigma_0\Gamma \sim 120$ for the 3.8 ev level and $\sigma_0\Gamma \sim 300$ for the 8.6 ev level. For $\Gamma \sim 0.1$ ev this corresponds to $\sigma_0 \sim 1200$ and 3000 respectively. There is no indication of other strong levels. (Since the sample is thin, only strong levels would be observed.)

The results $E_0 = 1.44$ ev and $\sigma_0\Gamma^2 = 210$, for the main level, agree with the results of Fig. 2. The 1.44 ev level was also studied using a 38.65 mg/cm² sample with the results shown in Fig.3, where the resonance is more nearly resolved since σ max. = 11,000. If $\Gamma = 0.09$ ev, then $\sigma_0 = 26{,}000$ which is within a factor of $2\frac{1}{2}$ of the measured value of σ max.

Indium has two isotopes In^{113} (4.5 percent) and In^{115} (95.5 percent). In^{114} results from the capture of a neutron by In^{113}, which has a half-life of 48 days.[6] The 13-sec. and 54-min. In^{116} are isomers.[4,7] The level strengths for the responsible isotopes must be correspondingly corrected. The final results may be expressed:

1. The first resonance has $E_0 = (1.44 \pm 0.02)$ ev $\sigma_0\Gamma^2 \sim 210$. (If $\Gamma = 0.09$ ev, then $\sigma_0 \sim 26{,}000$.) Value $\sigma_{max} = 11{,}000$ was obtained.
2. The second resonance has $E_0 = (3.8 \pm 0.2)$ ev $\sigma_0\Gamma \sim 120$. (If $\Gamma \sim 0.1$ ev, then $\sigma_0 \sim 1200$.)
3. The third resonance has $E_0 = (8.6 \pm 0.4)$ ev with $\sigma_0\Gamma \sim 300$. (If $\Gamma \sim 0.1$ ev, then $\sigma_0 \sim 3000$.)

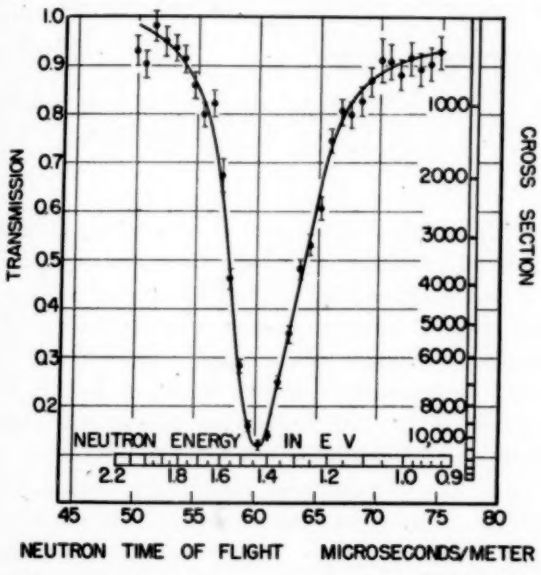

FIG. 3. The slow neutron transmission of 0.03865 g/cm² of indium near the 1.44 ev resonance. The solid line is a theoretical Breit-Wigner curve with $E_0 = 1.44$ ev, $\sigma_0\Gamma^2 = 210$, and $\Gamma = 0.09$ ev, corrected for the resolution width of the apparatus.

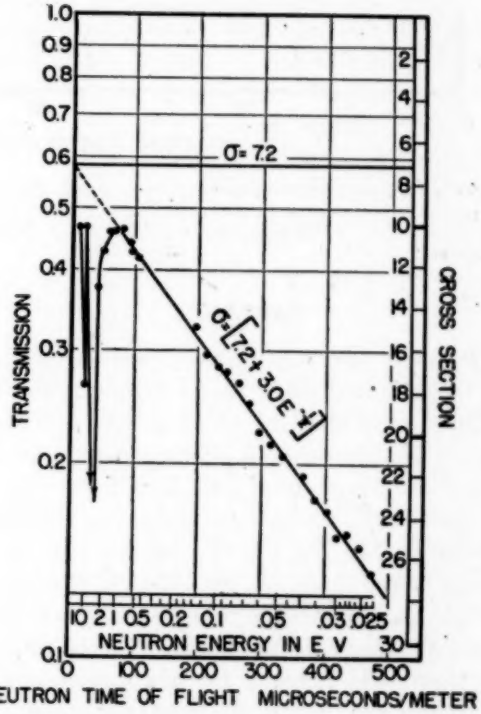

FIG. 4. The slow neutron transmission of 22.4 g/cm² of tantalum. This curve illustrates the $1/v$ type cross section in the thermal region with $(\sigma = 7.2 + 3.0E^{-\frac{1}{2}})$ and also shows the resonance levels at the higher energies.

[4] Amaldi, D'Agostino, Fermi, Ponticorvo, Rasetti, and Segrè, Proc. Roy. Soc. London **A149**, 522 (1935).
[5] McMillan, Kaman, and Ruben, Phys. Rev. **52**, 375 (1937); Pool, Cork, and Thornton, Phys. Rev. **52**, 239 (1937); Dzelepow and Constantinov, Comptes Rendus U.S.S.R. **30**, 701 (1941).
[6] Lawson and Cork, Phys. Rev. **52**, 531 (1937); Mitchell, Phys. Rev. **53**, 269 (1938).
[7] Lawson and Cork, Phys. Rev. **52**, 531 (1937); Mitchell and Langer, Phys. Rev. **53**, 505 (1938).

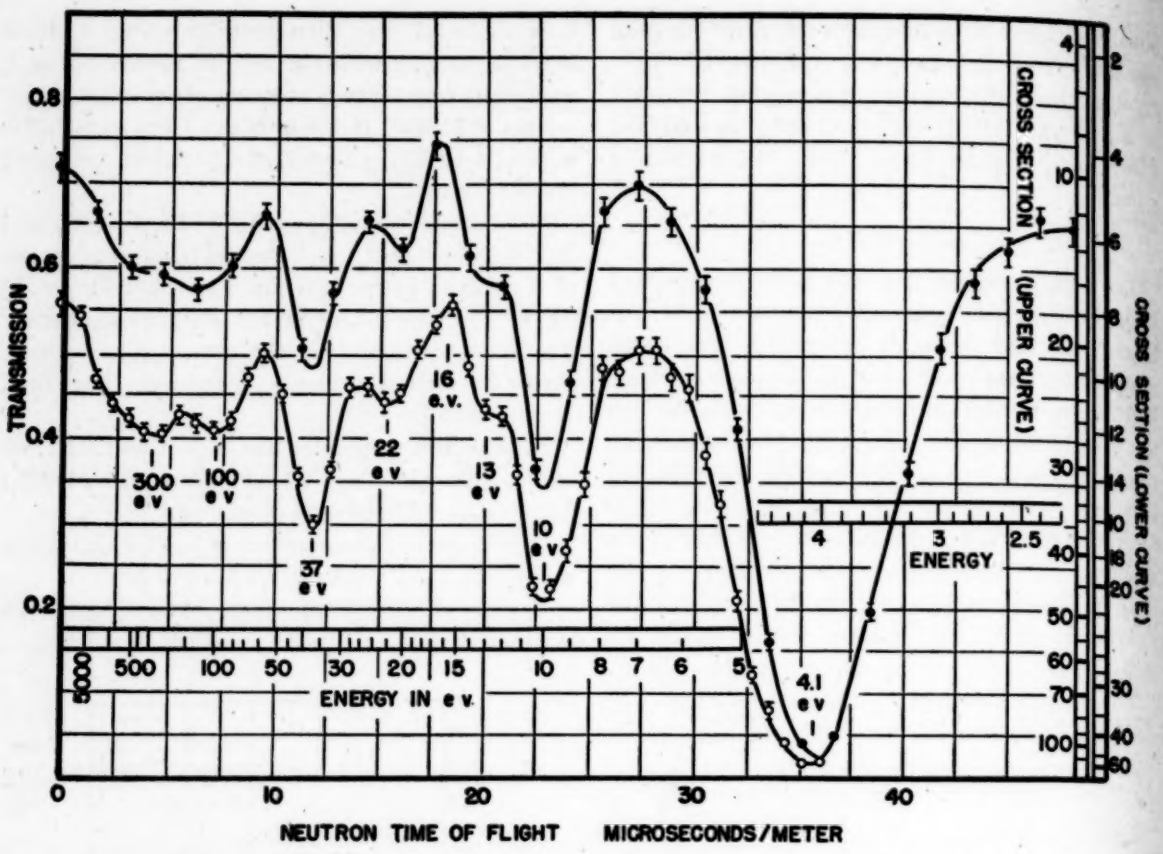

FIG. 5. The slow neutron transmission of tantalum. The upper curve shows the transmission for a 9.98 g/cm² sample with a resolution width of 3.6 μsec./meter. The lower curve shows the transmission for a 22.44 g/cm² sample with a resolution width of 1.8 μsec./meter. The use of the thicker sample with higher resolution increases the detail that can be obtained.

TANTALUM

The slow neutron transmission of tantalum was investigated using plates of tantalum metal obtained from the University of Chicago Metallurgical Laboratories. A spectrographic analysis of the samples showed less than 5 percent Cb; less than 0.05 percent Zr and Al; less than 0.005 percent Ti, Mo, Fe, Co, Os, Ag, Zn, Cd, Sn, Pb, Sb and traces of Cr, Ni, Ru, Rh, Pd, Pt, and Hg. For all other metals the prominent lines were not apparent, therefore the impurity was probably less than 0.05 percent for arc insensitive materials and less than 10^{-5} percent for arc sensitive materials. Samples of 9.98 g/cm² and 22.44 g/cm² thickness were studied. The results of these measurements are shown in Figs. 4 and 5.

The general features of the curve over a wide energy range are shown in Fig. 4. The results for $E<1$ ev are well matched by the relation $\sigma=(7.2+3.0E^{-\frac{1}{2}})$ and several levels are shown at higher energies. The high energy region was first investigated using a 9.98 g/cm² sample with about 3.2 μsec./meter resolution width. The results shown in the upper curve of Fig. 5 show the presence of strong levels at 4.1 ev, 10 ev, and 37 ev with indication of several other levels near 13 ev, 22 ev, and above 100 ev.

In view of the complex structure revealed, the portion of the curve above 4 ev was remeasured using a 22.44 g/cm² sample with twice the resolution. The results are shown in the lower curve of Fig. 5. All of the structure in the upper curve is repeated with better resolution in the lower curve, thus conclusively demonstrating the reality of the effects obtained.

An analysis of Fig. 5 can be made by using the position of the $1/v$ line and the constant term for the thick sample as determined in Fig. 4. If the

curve is assumed to consist of a series of resonance dips there are strong levels at 4.1 ev, 10 ev, and 37 ev, weaker levels at 13 ev, 22 ev, and probably multiple levels near 100 ev and 300 ev, and in the higher energy region. Even though the levels below 100 ev may be multiple, an analysis to determine $\sigma_0\Gamma^2$ has been made assuming them to be single. The curve cannot be divided into a series of separate dips with any degree of accuracy near 13 ev and 22 ev. Therefore, the values of $\sigma_0\Gamma^2$ for these levels may be uncertain by more than the customary factor of 2.

The results for tantalum are of particular importance since all of the levels must be ascribed to the single Ta^{181} isotope. This is the first time in the knowledge of the authors that so many closely spaced levels have been experimentally demonstrated to belong to a single nucleus, although such effects are expected from the theory of level spacing.[8] The strength of the levels makes it unlikely that slight sample impurities can be responsible for any of the levels observed. The activity induced in tantalum by the (n, γ) reaction has a half-life of 97 days.[9]

The results for tantalum may be summarized:

1. Below 1 ev the data are well matched by the $1/v$ relation
   $\sigma=[(7.2\pm0.4)+(3.0\pm0.1)E^{-\frac{1}{2}}]$.
2. The first and main level occurs at $E_0=(4.1\pm0.1)$ ev
   $\sigma_0\Gamma^2\sim44$.
   (If the $1/v$ slope were entirely attributed to a level at 4.1 ev then $\sigma_0\Gamma^2=96$ is required.)
3. The second strong level is at $E_0=(10.0\pm0.3)$ ev
   $\sigma_0\Gamma^2\sim25$.
4. The third level is at $E_0=(13\pm0.5)$ ev
   $\sigma_0\Gamma^2\sim3$.
5. The fourth level is at $E_0=(22\pm2)$ ev
   $\sigma_0\Gamma^2\sim18$.
6. The fifth level is at $E_0=(37\pm3)$ ev
   $\sigma_0\Gamma^2\sim400$.
7. There are indications of probably more than one strong level near 100 ev, near 300 ev and at higher energies.

[8] H. A. Bethe, Phys. Rev. **50**, 332 (1936).
[9] Oldenberg, Phys. Rev. **53**, 35 (1938); Fomin and Houtermans, Physik. Zeits. Sowjetunion **9**, 273 (1936); Houtermans, Naturwiss. **28**, 578 (1940).

TUNGSTEN

The slow neutron transmission of tungsten was studied using rolled tungsten plates supplied by the General Electric Company, Cleveland Wire Works. Six plates were used for the 29.2 g/cm² sample (Fig. 6) and single plates of 5.06 and 4.90 g/cm² for the high energy region (Figs. 7 and 8). A spectrographic analysis of the sample showed less than 1 percent As; 0.5 percent Bi; 0.05 percent Zr, V, Zn, Cd, and Si; 0.005 percent Be, Fe, Pd, Au, Ge; traces of La, Ru, Rh, Cu, Hg, Al, Tl, Sn, Pb. For all other metals the prominent lines were not apparent.

The entire region was first investigated with low resolution using the thick sample as shown in Fig. 6. Below 1 ev the data are well matched by the relation $\sigma=(5.7+2.72E^{-\frac{1}{2}})$, and a dip is obtained showing the presence of one or more levels above 3 ev.

The region above 2 ev was next investigated using the 4.90 g/cm² sample and about 3.2 μsec./meter resolution width as shown in Fig. 7. This shows the presence of a strong level at 18 ev, a strong level at 4.0 ev, and weaker levels near 7.4 ev, 45 ev, 180 ev, and 1100 ev. Since the curve was so complex, it was considered of interest to investigate the region above 4 ev with higher resolution. A 5.1-g/cm² sample was

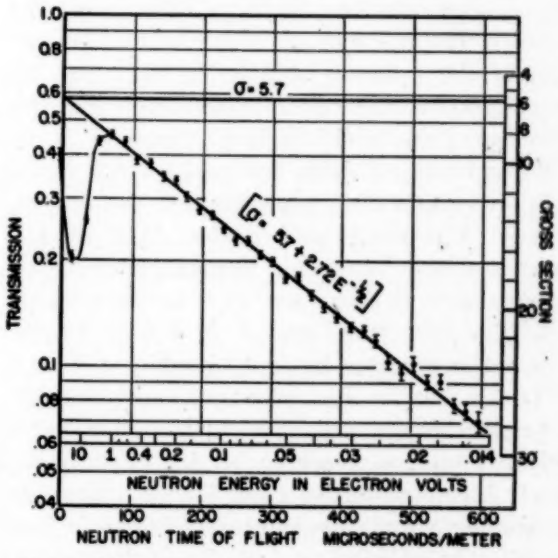
TRANSMISSION
CROSS SECTION
σ = 5.7
[σ = 5.7 + 2.72E^-½]
10 1 0.4 0.2 0.1 .05 .03 .02 .014
NEUTRON ENERGY IN ELECTRON VOLTS
0 100 200 300 400 500 600
NEUTRON TIME OF FLIGHT MICROSECONDS/METER

FIG. 6. The slow neutron transmission of 29.2 g/cm² of tungsten. This curve shows the $1/v$ type cross section for tungsten in the thermal region with $\sigma=(5.7+2.72E^{-\frac{1}{2}})$ and also illustrates the effect of resonances in the high energy region when broad resolution is used.

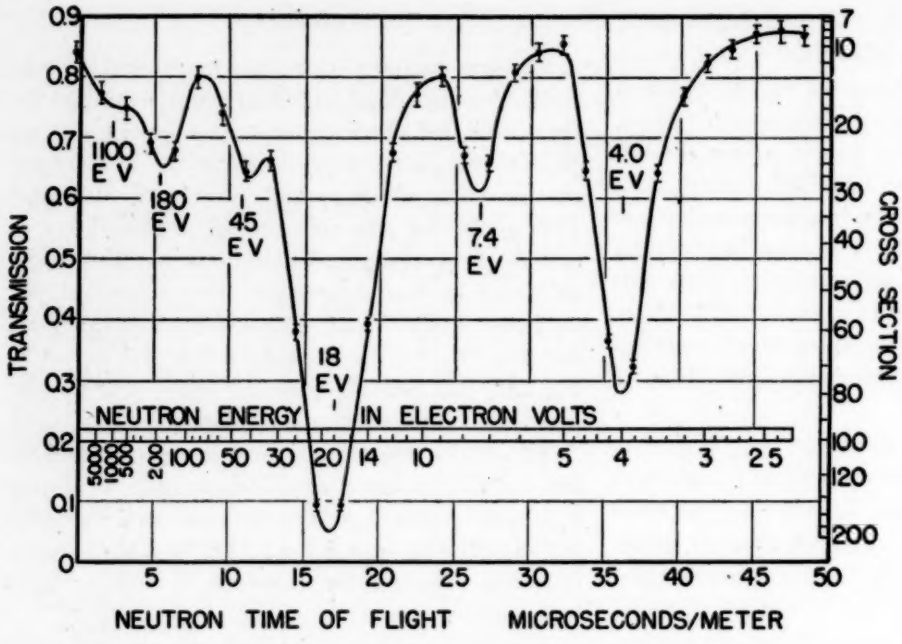

FIG. 7. The slow neutron transmission of 4.90 g/cm² of tungsten. This curve illustrates the complex neutron spectrum of tungsten showing transmission dips at 4.0 ev, 7.4 ev, 18 ev, 180 ev, and possible dips at 45 ev and 1100 ev.

used for this purpose with the results shown in Fig. 8. As in the case of tantalum all of the effects observed with the thicker sample and higher resolution are repeated with greater detail thus giving an excellent check on the measurements. The level at 7.4 ev appears again as a sharp dip, a more definite dip is now obtained at 45 ev; the level (or levels) near 180 ev is more pronounced; and the dip near 1100 ev is more definite. The shape of the curve near 10 ev may suggest the presence of a weak level, but the magnitude of the effect is so small that the presence of the level here is questionable.

Tungsten has 5 stable isotopes of which 4 have (within a factor of 2) approximately equal abundances. The single odd isotope W^{183} of 17.3 percent abundance should be responsible for the strong levels.[8] There are two well-established activities with half-lives of 77-d and 24.1-hr. induced in tungsten by (n, γ) reactions.[4,10]

The possibility has been suggested that the 4.0 ev level in Fig. 7 is caused by a small tantalum impurity and represents the 4.1 ev tantalum level. A comparison of Figs. 5 and 7, however, indicates a small but definite difference in level position. In addition a calculation of the strength $\sigma_0\Gamma^2\sim13$ for the level would require that the sample be about 30 percent tantalum by weight.

The results for tungsten may be summarized as follows:

1. Below 1 ev the data are well matched by the $1/v$ relation
   $\sigma=[(5.7\pm0.2)+(2.72\pm0.05)E^{-\frac{1}{2}}]$.
2. The first strong level is at $E_0=(4.0\pm0.1)$ ev
   $\sigma_0\Gamma^2\sim13$.

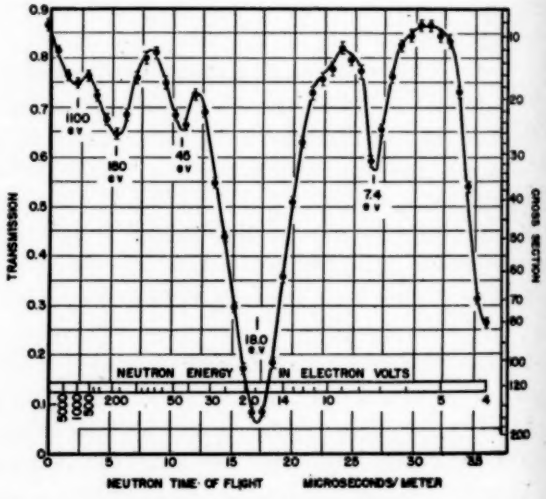

FIG. 8. The slow neutron transmission of 5.06 g/cm² of tungsten. The resolution used in this curve is twice as high as that used for Fig. 7 and confirms dips at 45 ev and 1100 ev. This data also gives greater detail for the levels at 7.4 ev and 180 ev.

[10] Minakawa, Phys. Rev. **57**, 1189 (1940); Fajans and Sullivan, Phys. Rev. **58**, 276 (1940); McLennan, Grimmet, and Read, Nature **135**, 147 (1935).

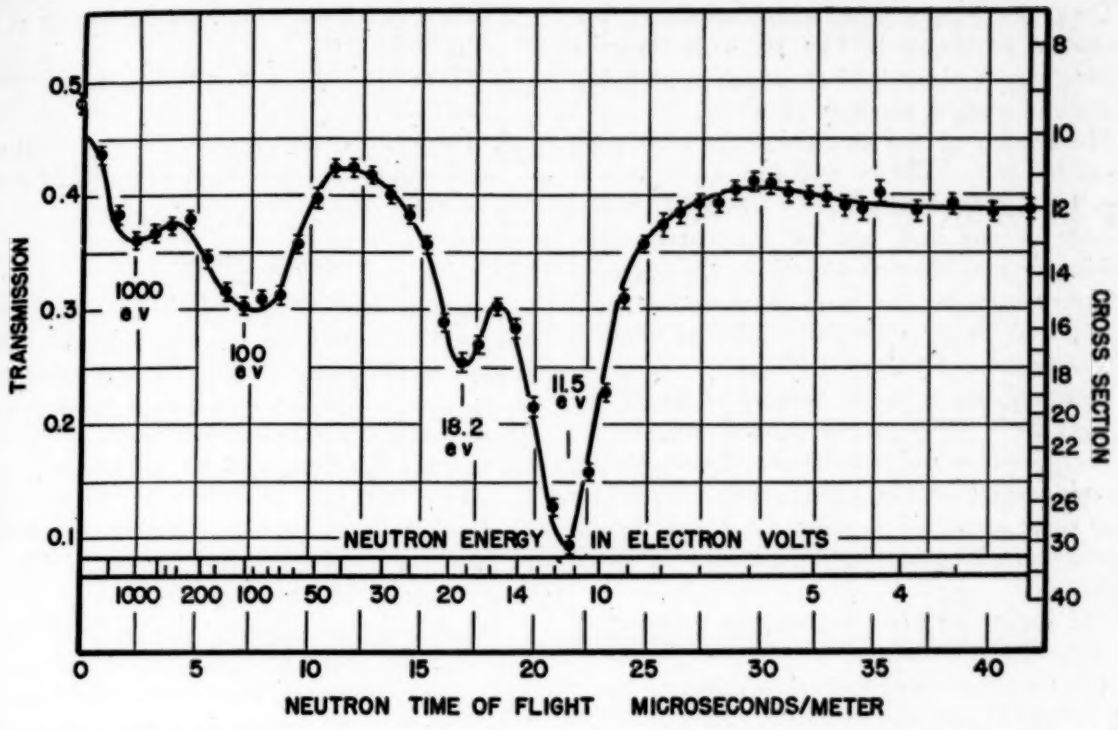

FIG. 9. The slow neutron transmission of 25.8 g/cm² of platinum above 2.2 ev. This curve shows transmission dips for platinum at 11.5 ev, 18.2 ev, 100 ev, and 1000 ev with the upper transmission dips not completely resolved.

If the W^{183} isotope is responsible, then $\sigma_0\Gamma^2\sim 75$ for this isotope.

3. The second (weaker) level is at $E_0=(7.4\pm 0.2)$ ev
   $\sigma_0\Gamma^2\sim 5$.
4. The third and strongest level is at $E_0=(18.0\pm 0.5)$ ev
   $\sigma_0\Gamma^2\sim 3000$.
   This may be multiple as the curve in Fig. 8 recovers more slowly on the high energy side of the resonance than would be expected for a single level.
5. The fourth level is at $E_0=(45\pm 2)$ ev
   $\sigma_0\Gamma^2\sim 400$. (Perhaps multiple.)
6. The fifth dip is at $E_0=(180\pm 20)$ ev
   $\sigma_0\Gamma^2\sim 10{,}000$ if it is due to a single level.
7. Another dip near 1100 ev is probably multiple.

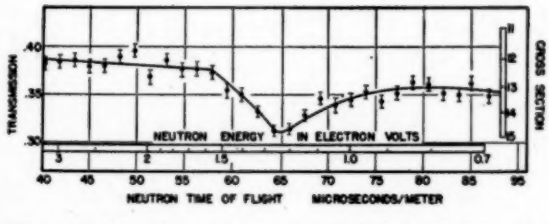

FIG. 10. The slow neutron transmission of 25.8 g/cm² of platinum from 0.7 ev to 3 ev. This curve shows a transmission dip at about 1.25 ev which is probably caused by a rhodium impurity.

PLATINUM

A sample containing 25.8 g/cm² of metallic platinum was used for the slow neutron transmission measurements. A spectrographic analysis of the sample showed less than 0.5 percent Ca, Al; 0.05 percent Fe, Rh, Pd, Cu, Au; 0.005 percent Ag and Si; traces of Cr, Ru, and In. For all other metals the prominent lines were not apparent.

The results of the measurements with the highest resolution for energies above 2.2 ev are shown in Fig. 9. This shows that there is a moderately strong level at 11.5 ev, a weaker level at 18.2 ev, a broad dip probably indicating several strong levels from 70 ev to 200 ev, and another broad dip near 1000 ev again suggesting several levels.

The region was extended with somewhat lower resolution as shown in Fig. 10. This shows a shallow dip at about 1.25 ev which is probably because of a slight rhodium impurity.

The results of the measurements with wide resolution from 0.009 ev to 0.4 ev are shown in Fig. 11. A $1/v$ slope $\sigma=(12.0+1.03E^{-\frac{1}{2}})$ is obtained for the first part of the curve while definite crystal interference effects are obtained for lower energies. The main discontinuities correspond to Bragg reflection limits at neutron wave-lengths of 1.6A and 2.4A.

Platinum has 5 stable isotopes of which the isotope Pt^{195} (35.3 percent abundance) is the only odd isotope and, according to theory, should be responsible for the strong levels.[8] There are only three activities of 18-hr. 3.3-d and 31-min. associated with the (n, γ) reactions in platinum.[11]

The results for platinum may be summarized as follows:

1. The $1/v$ slope (0.04 to 0.8 ev) is $\sigma=[(12.0\pm0.3)+(1.03\pm0.06)E^{-\frac{1}{2}}]$.
2. There are definite crystal effects for $E<0.035$ ev with transmission discontinuities for the neutron wave-lengths $\lambda=1.6$A and 2.4A.
3. There is a level at $E_0=(11.5\pm0.4)$ ev $\sigma_0\Gamma^2\sim55$.
4. There is a level at $E_0=(18.2\pm1)$ ev $\sigma_0\Gamma^2\sim30$.
5. There are broad dips at 100 and 1000 ev indicating the presence of strong unresolved levels.

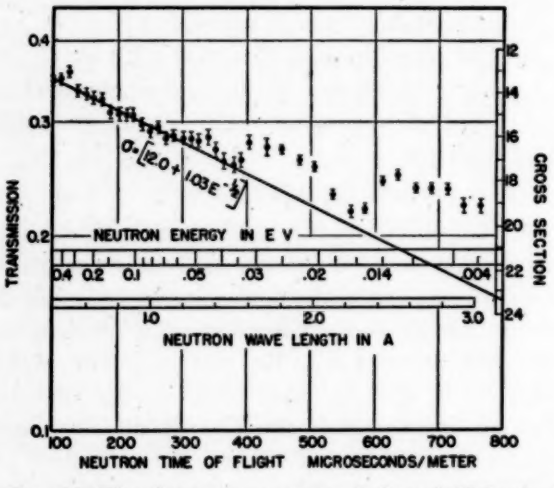

FIG. 11. The slow neutron transmission of 25.8 g/cm² of platinum in the thermal region. This curve illustrates the $1/v$ type curve in the thermal region with $\sigma=(12.0+1.03E^{-\frac{1}{2}})$ and the crystal interference effects observed at the lower energies.

[11] McMillan, Kaman, and Ruben, Phys. Rev. **52**, 375 (1937); Sherr, Bainbridge, and Anderson, Phys. Rev. **60**, 473 (1941); Pool, Cork, and Thornton, Phys. Rev. **52**, 239 (1937); McLennan, Grimmet, and Read, Nature **135**, 147 (1935).

ZIRCONIUM

A sample consisting of 6.45 g/cm² of ZrO_2 was used to investigate the slow neutron transmission of zirconium. A spectrographic analysis of the sample showed less than 5 percent Ca; 0.5 percent Zn, Si, Sr; 0.05 percent Mg, Ti, Mn, Fe, Cu, Al; 0.005 percent Be, B; traces of Sc, Y, V, Cr, Mo, Ni, Sn, Pb, Sb. For all other metals the prominent lines were not apparent. In all cases a constant cross section of 4.1 has been deducted for the oxygen.[5]

The results of measurements with wide resolution over the entire energy region are shown in Fig. 12. This shows that levels are present above 1 ev and that the results for lower energies are well matched by the $1/v$ curve $\sigma=(6.8+0.74E^{-\frac{1}{2}})$.

The region above 0.6 ev was investigated with better resolution as shown in Fig. 13. The dips indicated that there were single levels at 1.09 ev and 2.3 ev and perhaps a double level near 7 ev. The region 4 to 10 ev was then investigated with highest resolution as shown, and the dip seems to be resolved into two dips at 7.6 ev and 4.7 ev. There are no indications of other resonances.

Zirconium has 5 stable isotopes of which Zr^{91}

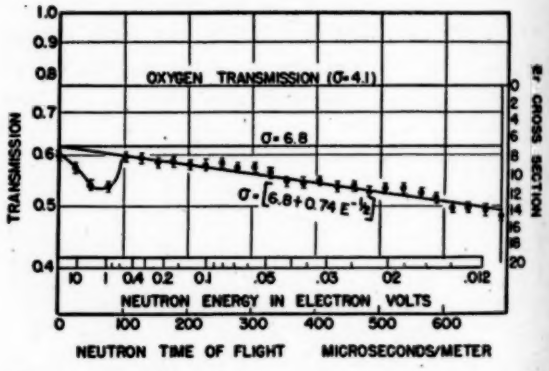

FIG. 12. The slow neutron transmission of 6.45 g/cm² of ZrO_2. This curve shows the $1/v$ type cross section for Zr in the thermal region with $\sigma=(6.8+0.74E^{-\frac{1}{2}})$ after 4.1 has been deducted for the oxygen cross section.

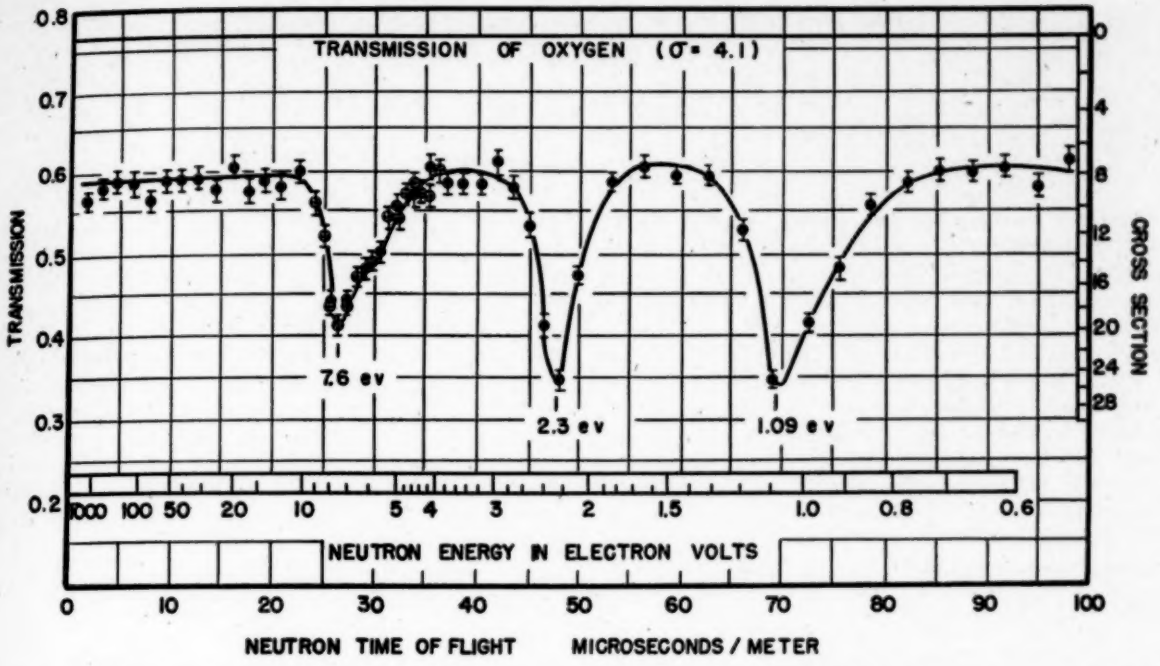

FIG. 13. The slow neutron cross section of 6.45 g/cm² of ZrO_2. This curve shows the transmission dips at 1.09 ev and 2.3 ev and the odd shaped dip in the vicinity of 7 ev which might be the sum of two dips at 5.7 ev and another at 7.6 ev.

(11.5 percent abundance) is the only odd isotope and, therefore, should be responsible for the stronger levels.[8] The weakness of the levels suggests that one or more may be owing to slight impurities in the sample. The induced activities in zirconium by (n, γ) reactions are not yet definitely assigned.

The results for Zr may be summarized as follows:

1. Below 0.6 ev the results are well matched by the $1/v$ curve
   $\sigma = [(6.8 \pm 0.3) + (0.74 \pm 0.10) E^{-\frac{1}{2}}]$.
2. There is a partially resolved level at $E_0 = (1.09 \pm 0.03)$ ev
   $\sigma_0 \Gamma \sim 5$.
3. The second level is at $E_0 = (2.30 \pm 0.07)$ ev
   $\sigma_0 \Gamma \sim 8$.
4. There is bulge on the next dip indicating a level at $E_0 = (5.7 \pm 0.5)$ ev with $\sigma_0 \Gamma \sim 10$ (uncertain).
5. The next level is at $E_0 = (7.6 \pm 0.4)$ ev
   $\sigma_0 \Gamma \sim 40$.

We take pleasure in acknowledging our indebtedness to Professor J. R. Dunning for his valuable suggestions and stimulating discussions. We wish to thank Miss Miriam Levin, who assisted with the numerous calculations involved in this paper, and the other members of the cyclotron staff who aided with these measurements.

Slow Neutron Velocity Spectrometer Studies. III. I, Os, Co, Tl, Cb, Ge*

C. S. Wu, L. J. Rainwater, and W. W. Havens, Jr.
Columbia University, Pupin Physics Laboratories, New York, New York

(Received November 8, 1946)

The $1/v$ thermal line for iodine is $\sigma=[(3.8\pm0.2)+(1.12\pm0.05)E^{-\frac{1}{2}}]$. Crystal interference effects are apparent at low energies. There is a resonance at (20.6 ± 0.4) ev with $\sigma_0\Gamma^2\sim4$. A flat-bottomed dip at 37 ev suggests two levels at (32 ± 2) ev and (42 ± 2) ev with approximately equal values of $\sigma_0\Gamma^2\sim135$. The $1/v$ thermal line for osmium is $\sigma=[(15\pm0.4)+(2.7\pm0.1)E^{-\frac{1}{2}}]$ with crystal interference effects at low energies. There are levels at (6.5 ± 0.3) ev with $\sigma_0\Gamma^2\sim10$, at (8.8 ± 0.3) ev with $\sigma_0\Gamma^2\sim35$, at (20 ± 1) ev with $\sigma_0\Gamma^2\sim25$, probable levels at (28 ± 1.5) ev with $\sigma_0\Gamma^2\sim8$, at (42 ± 2) ev with $\sigma_0\Gamma^2\sim10$, at 84 ev and several unresolved levels above 84 ev. The $1/v$ thermal line for cobalt is $\sigma=[(6.7\pm0.3)+(6.4\pm0.15)E^{-\frac{1}{2}}]$. There is an unusually strong dip at (115 ± 5) ev with $\sigma_0\Gamma^2\sim200{,}000$ (if single) and indications of other strong unresolved levels in the region of 1000 to 10,000 ev. The $1/v$ thermal line for thallium is probably $[\sigma=(9.7\pm0.2)+(0.6\pm0.2)E^{-\frac{1}{2}}]$. There are strong crystal interference effects at low energies. There is a strong dip in the transmission curve at 270 ev and another broad dip near 1100 ev. Columbium shows only a slight $1/v$ effect $\sigma=[(6.4\pm0.2)+(0.10\pm0.04)E^{-\frac{1}{2}}]$ with strong crystal interference effects at lower energies. Only a slight dip at 4.1 ev attributed to a slight Ta impurity was found in the higher energy region. Germanium shows no $1/v$ thermal slope because of the strong crystal interference effects. There is a (perhaps multiple) level at 95 ev with $\sigma_0\Gamma^2\sim800$.

INTRODUCTION

THIS is the third of a series of papers in which the results of investigations using the Columbia University Slow Neutron Velocity Spectrometer are presented. A detailed analysis of the factors involved in the operation of the instrument and the interpretation of the data is given in previous papers.[1-4] In presenting the results of the measurements for I, Os, Co, Tl, Cb, and Ge the conventions previously adopted[3,4] are used.

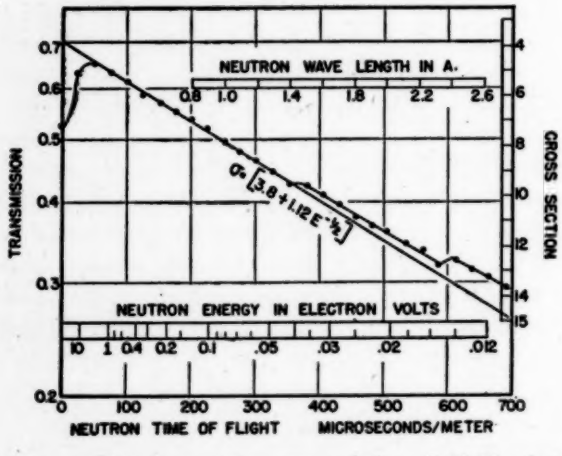
NEUTRON WAVE LENGTH IN A.
0.8 1.0 1.4 1.8 2.2 2.6
TRANSMISSION
GROSS SECTION
$\sigma=[3.8+1.12E^{-\frac{1}{2}}]$
NEUTRON ENERGY IN ELECTRON VOLTS
10 1 0.4 0.2 0.1 .05 .03 .02 .012
0 100 200 300 400 500 600 700
NEUTRON TIME OF FLIGHT MICROSECONDS/METER

FIG. 1. The slow neutron transmission of 18.86 g/cm² of iodine. This curve indicates the presence of one or more resonance levels at high energies. From 0.04 to 3 ev the results are well matched by the relation $\sigma=(3.8+1.12E^{-\frac{1}{2}})$.

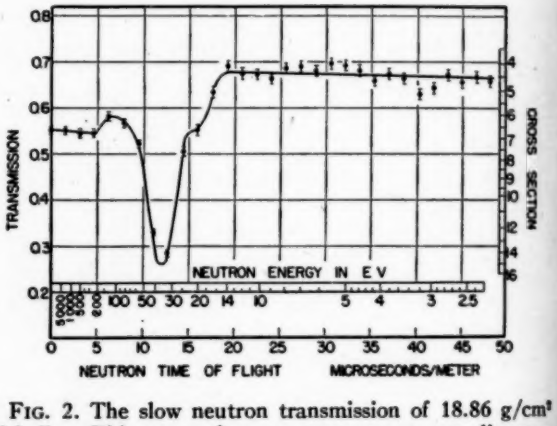
TRANSMISSION
GROSS SECTION
NEUTRON ENERGY IN E V
1000 100 50 30 20 14 10 5 4 3 2.5
0 5 10 15 20 25 30 35 40 45 50
NEUTRON TIME OF FLIGHT MICROSECONDS/METER

FIG. 2. The slow neutron transmission of 18.86 g/cm² of iodine. This curve shows a strong resonance dip near 37 ev with indication of another unresolved level near 20 ev.

* This document is based on work performed under Contract W-7405-Eng-50 with the Manhattan Project and Columbia University. It will also be published in the Manhattan Project Technical Series, Book III, Division VIII, as part of the contribution of the Physics Department, Columbia University. Publication assisted by the Ernest Kempton Adams Fund for Physical Research of Columbia University.

[1] L. J. Rainwater and W. W. Havens, Jr., Phys. Rev. **70**, 136 (1946).
[2] W. W. Havens, Jr. and L. J. Rainwater, Phys. Rev. **70**, 136 (1946).
[3] L. J. Rainwater, W. W. Havens, Jr., C. S. Wu, and J. R. Dunning, Phys. Rev. **71**, 65 (1947).
[4] W. W. Havens, C. S. Wu, L. J. Rainwater, and C. L. Meaker, Phys. Rev. **71**, 165 (1947).

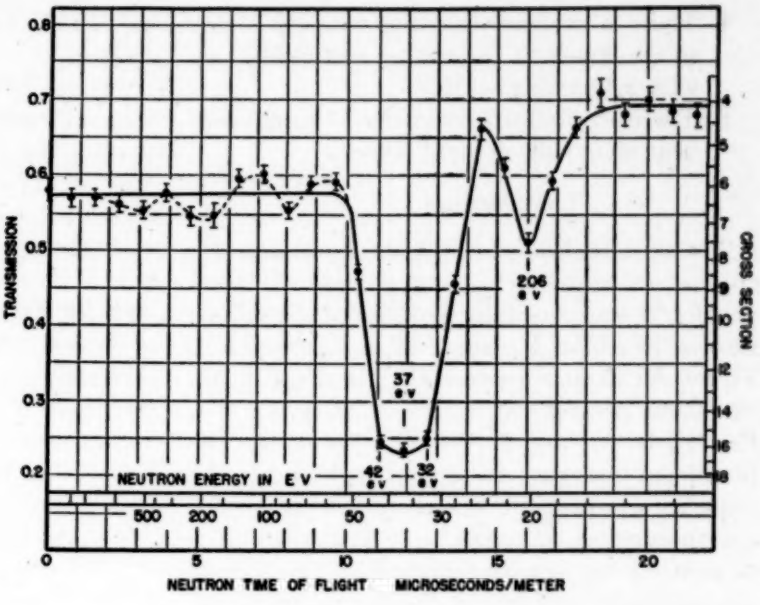

FIG. 3. The slow neutron transmission of 18.86 g/cm² of iodine. This curve was taken with the highest resolution of the spectrometer. The resonance at 20.6 ev is now clearly separated from the higher energy dip. The shape of the resonance dip at 37 ev suggests the presence of at least two levels probably at 32 ev and 42 ev.

RESULTS

Iodine

The slow neutron transmission of iodine was studied using an 18.86 g/cm² sample of analytical grade iodine packed in a thin-walled aluminum container. This sample was prepared by the Metallurgical Laboratory of the University of Chicago.

The results of the measurements using broad resolution are shown in Fig. 1. There is a dip at high energies indicating the presence of onethe more resonance levels. From 0.04 to 3 ev or results are well matched by the relation $\sigma = [(3.8+1.12)E^{-\frac{1}{2}}]$. Below 0.04 ev there is evidence of crystal interference effects with discontinuities in the transmission occurring at neutron wave-lengths of about 1.46A and 2.37A.

The energy region above 2.2 ev was next investigated with higher resolution as shown in Fig. 2. The main resonance dip is seen to occur near 37 ev with indication of another unresolved level near 20 ev. The lower transmission above 200 ev may indicate the presence of many unresolved levels.

To obtain more reliable information concerning the resonances, the region above 10 ev was investigated using the highest resolution possible with the results shown in Fig. 3. The resonance at 20.6 ev is now clearly separated from the higher energy dip. The dip at 37 ev now appears flat on the bottom where the transmission is considerably above zero. The shape of this resonance absorption curve would not be obtained if only a single resonance were present; therefore the presence of at least two levels, probably at 32 ev and 42 ev, seems reasonable. In the analysis equal $\sigma_0\Gamma^2$ values have been assumed for levels at 32 and 42 ev. The curve above 50 ev shows small irregularities that may represent weak levels near 80 ev, 200 ev, and 600 ev, but these are very uncertain. A straight line is also shown to indicate that these levels may be due to spurious effects.

Since iodine has only one isotope I^{127} all the neutron absorption effects can be assigned to this one isotope. The slow neutron induced activity in iodine is from I^{128} [5,6] which has a half-life of 24.99 min. The results for iodine may be summarized as follows:

1. The $1/v$ thermal line is given by $\sigma = [(3.8\pm0.2)+(1.12\pm0.05)E^{-\frac{1}{2}}]$.
2. There are crystal interference effects below 0.04 ev with discontinuities in the transmission curve for neutron wave-lengths of about 1.46 and 2.37A.
3. The first resonance is at $E_0 = (20.6\pm0.4)$ ev $\sigma_0\Gamma^2 \sim 4$.

---

[5] Amaldi, D'Agostino, Fermi, Ponticorvo, Rasetti, and Segrè, Proc. Roy. Soc. London A149, 522 (1935).
[6] Tape and Cork, Phys. Rev. 53, 676 (1938).

4. There is evidence that the next dip is due to two levels at (32±2) ev and (42±2) ev with $\sigma_0\Gamma^2$ values~135.
5. There are doubtful indication of weak levels near 80 ev, 200 ev, and 600 ev.

Osmium

The slow neutron transmission of osmium was studied using a 17.3 g/cm² sample of metal powder. A spectrographic analysis of the sample showed less than 1 percent Si; 0.5 percent Ca, Ti, Fe, Al, Bi; 0.05 percent Cr, Mn, Pt, Cu, Au, Pb; 0.005 percent Ag; traces of Zr, V, Co, Ni, Pa, Pd, Ir, Sn, and P. For all other metals the prominent lines were not apparent; therefore the impurity was probably less than 0.05 percent for arc insensitive materials and less than 10^{-5} percent for arc sensitive materials. The sample was originally prepared at the Bureau of Standards where it was heated in purified helium for two hours at 800°C. It was then compressed into a cell under a load of 20 tons. The sample was later opened, reduced at 120°C and recapsuled. The transmission of this sample was investigated using low resolution over the full timing range as shown in Fig. 4. The best $1/v$ line (0.1 ev to 5 ev) is $\sigma=(15+2.7E^{-\frac{1}{2}})$. Below 0.1 ev there are evidences of crystal interference effects particularly near 0.028 ev and 0.015 ev corresponding to neutron wave-lengths of 1.75 and 2.36A. In addition there is a dip at higher energies.

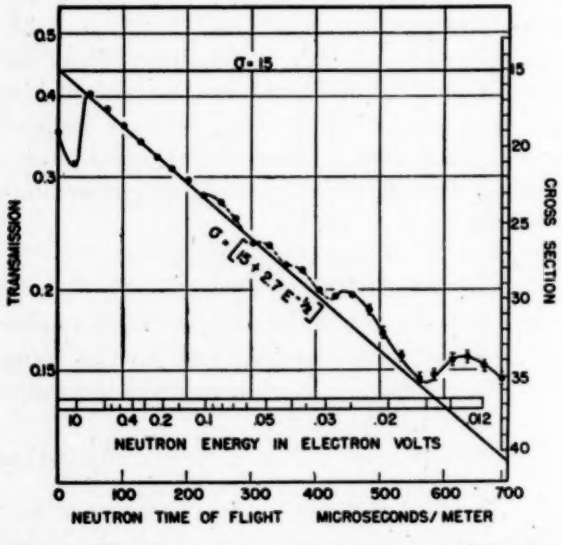

FIG. 4. The slow neutron transmission of 17.3 g/cm² of osmium. The best $1/v$ line (0.1 ev to 5 ev) is $\sigma=(15+2.7E^{-\frac{1}{2}})$. Crystal interference effects show below 0.1 ev.

The sample was next investigated using a 6.4 μsec./meter resolution width which indicated a strong dip at 8 ev and a smaller one near 80 ev. The region above 4 ev was then investigated with a 3.2 μsec./meter resolution width. The dip near 8 ev was partially resolved into two levels near 9 ev and 6 ev as in the case of the 20 ev level for iodine in Fig. 2. The results of this set of measurements showed that it would be profitable to use better resolution. Therefore the region above 4 ev was remeasured using the highest resolution with the results shown in Fig. 5. The peaks at 6.5 ev and 8.8 ev are here clearly resolved, and the peak at 20 ev is evident. The curve above 20 ev stays well below the line $\sigma=15$ representing the constant term in Fig. 4.

The dips at 84 ev and 42 ev are small, but the fact that they are probably real is indicated by the fact that they repeated on the several separate portions of the data which were combined for Fig. 5. The dip at 28 ev is less certain although it is also repeated in separate portions of the data.

Using the line $\sigma=15$ (from Fig. 4) as the value of the transmission due to scattering alone, the shape of the curve suggests that one or more levels are present at 28 ev, 42 ev, and 84 ev and that there are unresolved levels above 84 ev. The rise in transmission near zero time of flight is probably because of a decrease in the scattering cross section at higher energies.

Osmium has 7 stable isotopes to which the levels may be ascribed. Os^{189} is the most abundant (16.1 percent) odd isotope and thus may be responsible for the strong levels.[7] The activities assigned to the (n, γ) reactions in osmium are the 32-hr. Os^{191} and the 17-day Os^{193}.[8]

The results for Os may be summarized as follows:

1. The $1/v$ line in the thermal region is well represented by the equation: $\sigma=[(15\pm0.4)+(2.7\pm0.1)E^{-\frac{1}{2}}]$.
2. There is evidence of crystal interference effects at lower energies particularly for

[7] H. A. Bethe, Phys. Rev. **332**, 50 (1936).
[8] Kurtchatow, Latychew, Nemenow, and Selinow, Physik. Zeits. Sowjetunion **8**, 589 (1935); Seaborg and Friedlander, Phys. Rev. **59**, 400 (1941); Zingg, Helv. Phys. Acta **13**, 219 (1940).

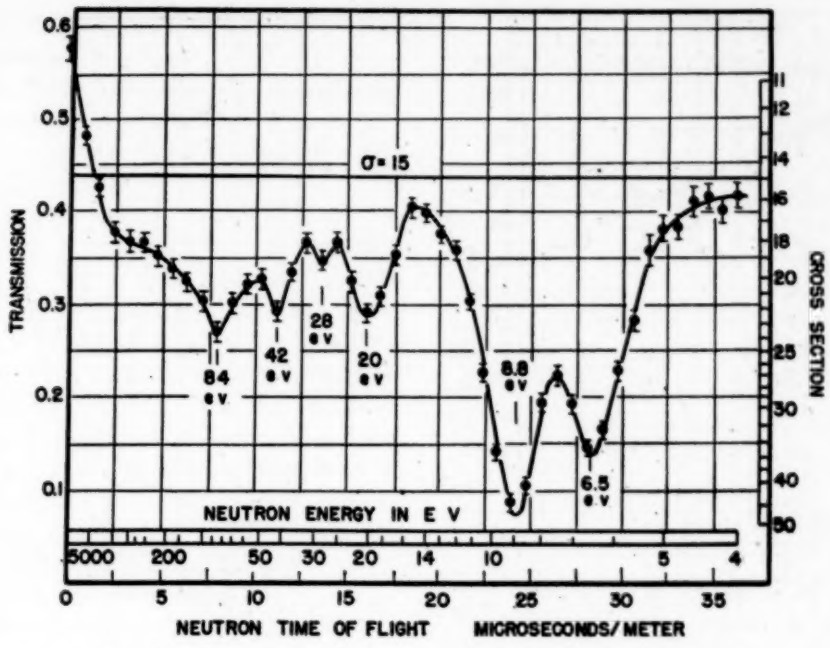

FIG. 5. The slow neutron transmission of 17.3 g/cm² of osmium. This curve was taken with the highest resolution of the spectrometer.

neutron wave-lengths of about 1.75 and 2.36A.

3. There is a level at $E_0=(6.5\pm0.3)$ ev $\sigma_0\Gamma^2\sim10$.
4. There is a level at $E_0=(8.8\pm0.3)$ ev $\sigma_0\Gamma^2\sim35$.
5. There is a level at $E_0=(20\pm1)$ ev $\sigma_0\Gamma^2\sim25$.
6. There is probably a level at (28 ± 1.5) ev $\sigma_0\Gamma^2\sim8$ (to within a factor of 10).
7. There is a level at $E_0=(42\pm2)$ ev $\sigma_0\Gamma^2\sim10$ (to within a factor of 5).
8. There is a level at $E_0=(84\pm6)$ ev with other unresolved levels above this value.

Cobalt

The slow neutron transmission of cobalt was investigated using a 12.4 g/cm² sample of cobalt metal powder. Since this was too thick for the resonance region measurements, a thinner sample of 1.06 g/cm² was also employed. A spectrographic analysis of the sample showed less than 0.5 percent P, Si, Mn; 0.05 percent Mg, Ca, Fe, Cu, B, Al; 0.005 percent Ni, As; traces of Be, Cr, Mo, Ag, In, Ge, Sn, and Pb. For all other metals the prominent lines were not apparent.

The results of the measurements using broad resolution are shown in Fig. 6. Because of the sample thickness the region below 0.15 ev was not studied. The results below 5 ev are well matched by the $1/v$ line. $\sigma=(6.7+6.4E^{-\frac{1}{2}})$, and a dip is seen at higher energies.

The sample was next measured with good resolution above 0.5 ev as shown in Fig. 7. The same $1/v$ line (determined from Fig. 6) is used

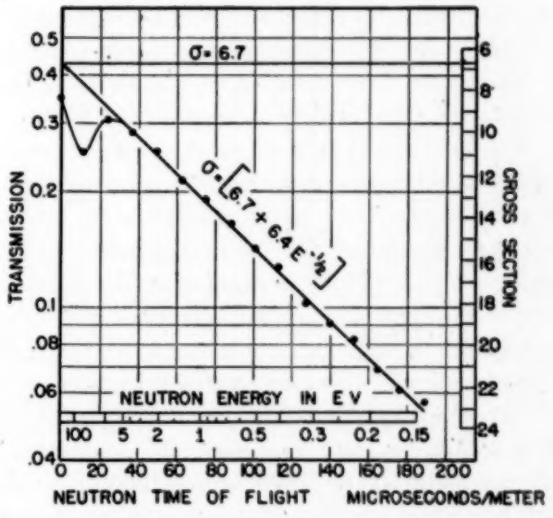

FIG. 6. The slow neutron transmission of 12.4 g/cm² of cobalt. The results below 5 ev are well matched by the $1/v$ line $\sigma=(6.7+6.4E^{-\frac{1}{2}})$. A dip is seen at higher energies.

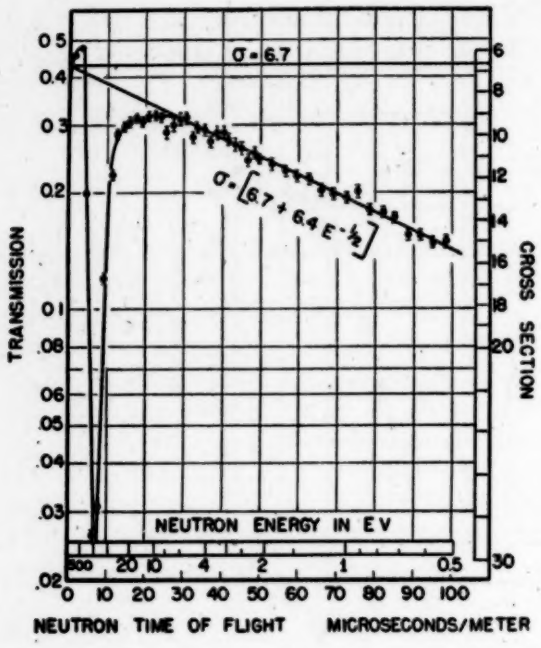

FIG. 7. The slow neutron transmission of 12.4 g/cm² of cobalt. This figure shows a strong dip near 100 ev and another small dip at zero time of flight.

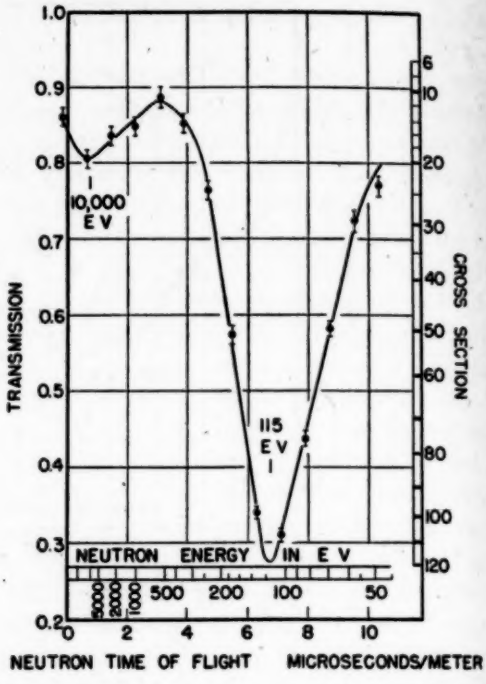

FIG. 8. The slow neutron transmission of 1.06 g/cm² of cobalt. This curve was taken by using a thinner sample and maximum resolution.

with excellent agreement. This figure shows a strong dip near 100 ev and another small dip at zero time of flight.

The region above 50 ev was measured using the thinner sample with maximum resolution as shown in Fig. 8. The shape of the dip at 115 ev is approximately the shape that would be expected for a single strong level at this point although this dip may be due to multiple unresolved levels. The cross section indicates that in the region from 1000 to 10,000 ev there are probably several strong unresolved levels.

The level at 115 ev if single, is an exceptionally strong level with $\sigma_0\Gamma^2 \sim 200{,}000$ as determined from the magnitude of the resonance dip. If the $1/v$ slope is assumed to be entirely attributed to a single level at 115 ev a value of $\sigma_0\Gamma^2 \sim 30{,}000$ is obtained. This is much smaller than the other value but is still extremely large for a single resonance level. The lower value calculated from the $1/v$ slope may indicate that the dip at 115 ev is multiple or may represent the interference effects of the strong levels above 1000 ev on the thermal cross section. Because of the observed strength of levels in cobalt they are all probably caused by the main Co^{59} isotope of 99.83 percent abundance. Co^{60} [9] induced by the (n, γ) reaction has two isomeric states with half-lives of 5.3 yr. and 10.7 min.

The results for cobalt may be summarized as follows:

1. The results below 5 ev are well matched by the $1/v$ relation $\sigma = [(6.7 \pm 0.3) + (6.4 \pm 0.15) E^{-\frac{1}{2}}]$.
2. There is a strong dip indicating a resonance at $E_0 = (115 \pm 5)$ ev $\sigma_0\Gamma^2 \sim 200{,}000$ if the dip is because of a single strong resonance. If the $1/v$ slope is attributed to a single level at 115 ev then $\sigma_0\Gamma^2 \sim 30{,}000$. The dip may be owing to several unresolved strong levels.
3. There is evidence of other strong unresolved levels in the region of 1000 to 10,000 ev.

Thallium

The slow neutron transmission of thallium was studied using a sample containing 52.09 g/cm² of the material. A spectrographic analysis of the sample showed less than 0.05 percent Ca, Pb; 0.005 percent Fe, Cu, Al; traces of Mg, Cr, Mn,

[9] Livingood and Seaborg, Phys. Rev. 60, 913 (1941); Deutsch and Elliott, Phys. Rev. 62, 558 (1942).

Cd, Si. For all other metals the prominent lines were not apparent.

The region above 0.015 ev was investigated using broad resolution as shown in Fig. 9. This shows that crystal interference effects are strong enough to make the determination of the $1/v$ slope difficult. The region above 0.5 ev was remeasured using better resolution as shown in Fig. 10. From this the $1/v$ line may be expressed as $\sigma=[(9.7\pm0.2)+(0.6\pm0.2)E^{-\frac{1}{2}}]$. This curve also shows the presence of a strong dip at several hundred volts energy with a rise in transmission well above the line $\sigma=9.7$. This rise in transmission near zero time of flight probably represents a decrease in the scattering cross section at still higher energies (>50,000 ev for example).

The high energy region above 50 ev was next investigated with maximum resolution as shown in Fig. 11. The shape of the curve suggests that there is a strong level at 270 ev and another strong level near 1100 ev although a number of unresolved levels may be present to give the observed curve. A rough analysis of the strength of the level at 270 ev, if single, indicates that $\sigma_0\Gamma^2\sim20{,}000$, a very strong level. If the $1/v$ slope is attributed entirely to a single level at 270 ev, the value $\sigma_0\Gamma^2\sim11{,}000$ is indicated. Thallium has two isotopes of about 30 percent and 70 percent abundance to which the levels must be ascribed. The two slow neutron induced activities in thallium[10] have half-lives of 4.23 min. and 3.5 yr.

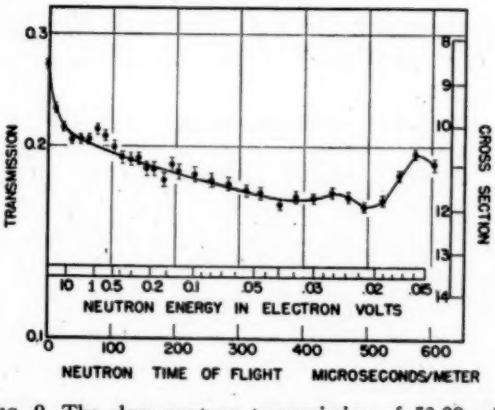

FIG. 9. The slow neutron transmission of 52.09 g/cm² of thallium. This curve was obtained by using broad resolution. The crystal interference effects are prominent.

[10] Pool, Cork, and Thornton, Phys. Rev. **52**, 239 (1937); Heyn, Nature **139**, 842 (1937); Fajans and Voigt, Phys. Rev. **60**, 619 (1941).

Columbium

The slow neutron transmission of Cb was studied using a 19.37 g/cm² disk of Cb metal. A spectrographic analysis of the sample showed less than 1 percent Ta; 0.5 percent Zr; 0.05 percent Ca, Y, Zn; 0.005 percent Be, Sc, Ti, Ni, Rh, Pd, Si; traces of V, Cr, W, Mn, Fe, Ca, Au, Al, Ga, Sn, Bi. For all other metals the prominent lines were not apparent. The results of the measurements using broad resolution over a large energy range are shown in Fig. 12. This shows the presence of a slight dip near 4 ev, a slight $1/v$ slope above 0.05 ev and pronounced crystal interference effects at lower energies. In

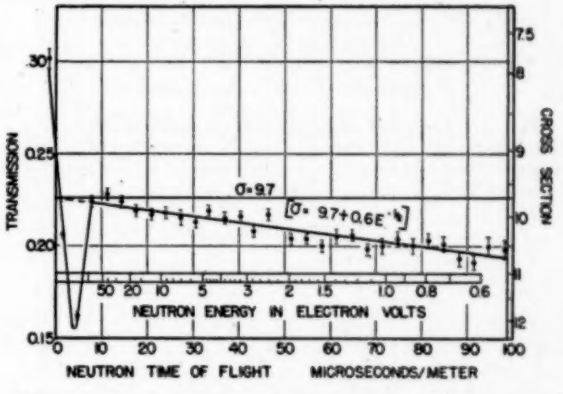

FIG. 10. The slow neutron transmission of 52.09 g/cm² of thallium. This curve represents the region above 0.5 ev as measured with better resolution. The $1/v$ line may be expressed as $\sigma=[(9.7\pm0.2)+(0.6\pm0.2)E^{-\frac{1}{2}}]$. There is also a strong dip at several hundred volts.

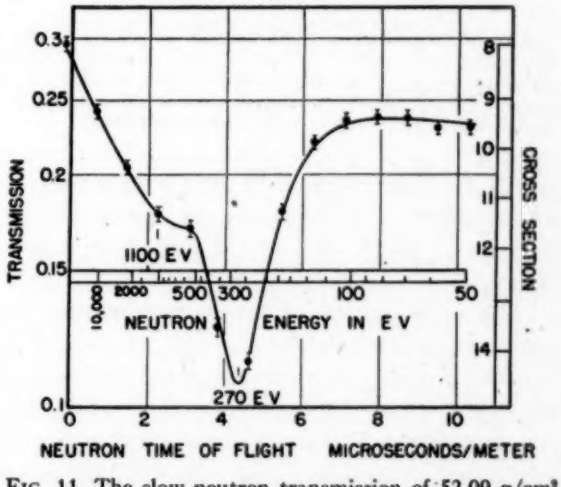

FIG. 11. The slow neutron transmission of 52.09 g/cm² of thallium using the maximum resolution of the spectrometer. The curve shows a strong main level at 270 ev and another strong level near 1100 ev. Both dips may be owing to several levels.

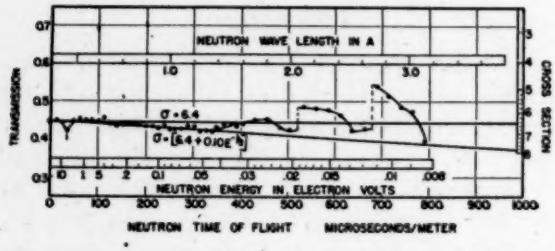

FIG. 12. The slow neutron transmission of 19.37 g/cm² of columbium. Pronounced crystal interference effects are evident at lower energies. The best $1/v$ line is $\sigma=(6.4\pm0.2)+(0.10\pm0.04)E^{-\frac{1}{2}}$].

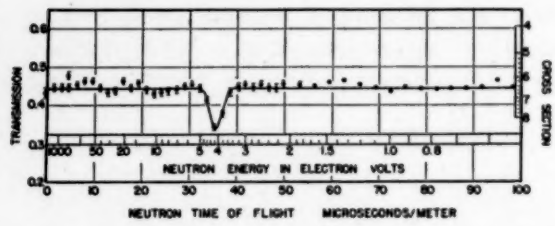

FIG. 13. The slow neutron transmission of 19.37 g/cm² of columbium. The transmission of neutrons above 0.5 ev is quite constant except the weak dip at 4.1 ev which can be attributed to an 0.4 percent Ta impurity.

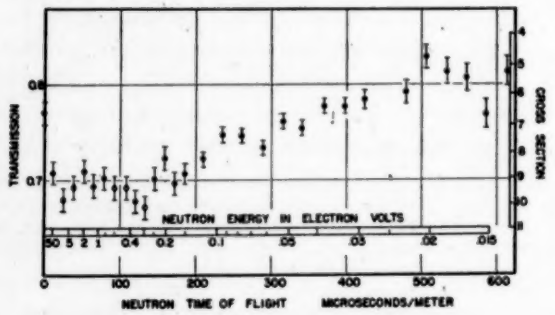

FIG. 14. The slow neutron transmission of 4.70 g/cm² of germanium. This represents the measurements as obtained by using broad resolution over a wide energy range. The presence of the crystal interference effects makes the determination of $1/v$ line impossible.

particular there are sharp discontinuities in the transmission corresponding to neutron wavelengths of about 2.05 and 2.67A. The best $1/v$ line is $\sigma=[(6.4\pm0.2)+(0.10\pm0.04)E^{-\frac{1}{2}}]$.

The region above 0.5 ev was then studied with good resolution as shown in Fig. 13. The transmission is quite constant except for the weak dip at 4.1 ev. This dip has been attributed to a slight Ta impurity.[4] From the area of the dip this could be accounted for by an 0.4 percent Ta impurity which is not unreasonable. Thus no levels have been found which can be attributed to Cb itself. Cb has only the single isotope Cb^{93}.

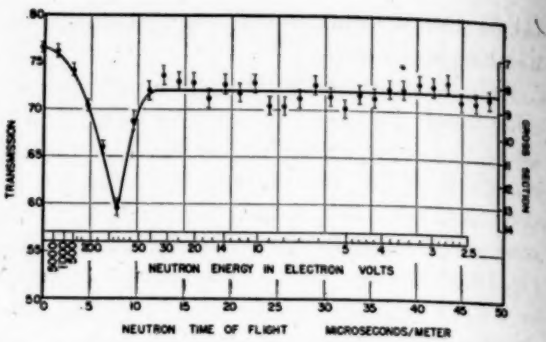

FIG. 15. The slow neutron transmission of 4.70 g/cm² of germanium. This represents the region above 2.2 ev as studied with good resolution.

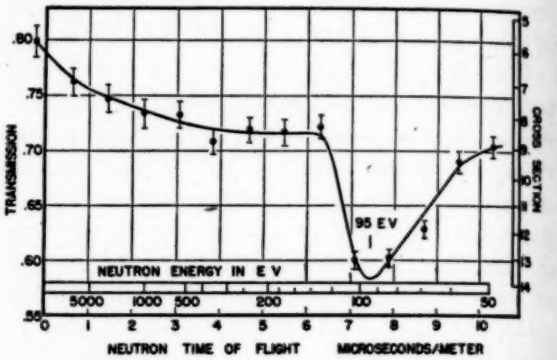

FIG. 16. The slow neutron transmission of 4.70 g/cm² of germanium. This region is explored using maximum resolution. The dip near 95 ev may be multiple in view of its peculiar shape.

The Cb^{94} nucleus would be of the unstable odd Z even A type, and this probably accounts for the absence of observable levels.[7,8] Nevertheless, an induced activity in Cb by an (n, γ) reaction has been identified.[11] It has a half-life of 6.6 min.

Germanium

The slow neutron transmission of Ge was studied using a 4.70 g/cm² disk of Ge metal. A spectrographic analysis of the sample showed less than 0.1 percent of Fe; 0.05 percent Ca, Cr, Si; 0.005 percent of W; traces of Mg, Mo, Mn, and Cu. For all other metals the prominent lines were not apparent. The results of the measurements using broad resolution over a wide energy range are shown in Fig. 14. Crystal interference

[11] Pool, Cork, and Thornton, Phys. Rev. **52**, 239 (1937); Sagane, Kojima, Miyamoto, and Ikawa, Proc. Phys. Math. Soc. Japan **22**, 174 (1940).

effects in the thermal region makes the determination of the $1/v$ slope impractical. The region above 2.2 ev was next studied using good resolution as shown in Fig. 15. This shows a small dip near 90 ev. The region above 50 ev was then studied using maximum resolution as shown in Fig. 16. This shows a dip near 95 ev which may be multiple in view of the shape of the dip. If it is because of a single level at 95 ev then $\sigma_0\Gamma^2 \sim 800$. The rise in transmission above 10,000 ev probably indicates a decrease in the scattering cross section at higher energies. There are five stable isotopes in germanium. The three well established activities[12] induced in germanium by (n, γ) reactions are 40 hr. Ge^{71}, 89 min. Ge^{75}, and 12 hr. Ge^{77}.

We take pleasure in acknowledging our indebtedness to Professor J. R. Dunning for his valuable suggestions and stimulating discussions. We wish to thank Miss Miriam Levin, who assisted with the numerous calculations involved in this paper, and the other members of the cyclotron staff who aided with these measurements.

[12] Sagane, Phys. Rev. **55**, 31 (1939); Sagane, Miyamoto, and Ikawa, Phys. Rev. **59**, 904 (1941).

PHYSICAL REVIEW VOLUME 71, NUMBER 3 FEBRUARY 1, 1947

The Electrical Charge on Precipitation at Various Altitudes and Its Relation to Thunderstorms

Ross Gunn
Army-Navy Atmospheric Electricity Project, Naval Research Laboratory, Washington, D. C.
(Received November 7, 1946)

The free electrical charges on individual precipitation particles were measured at various altitudes up to 26,000 feet by an induction method that avoided touching them. In a weak cold front exhibiting no thunderstorm activity, and having the freezing level at 11,000 feet, positive charges averaging 0.033 e.s.u. were observed from 10,000 to 26,000 feet. Negative charges averaging 0.04 e.s.u. were measured from the surface up to 20,000 feet. Positive charges were not observed below 10,000 feet and negative ones were not detected above 20,000 feet. Between these levels a mixture existed. The free charge on a large number of the particles was so great that the electric field at their surface was an appreciable fraction of the breakdown field for air, showing that powerful electrifying agencies exist even under rather quiet frontal conditions. Electric field measurements on the airplane showed that the particle charges were largely neutralized by nearby charges, presumably on the air or on the tiny cloud droplets. It is shown that the removal of this neutralizing charge will immediately produce thunderstorm electric fields and potentials. A time plot of the electric field on the surface of a flying airplane during the interval of a lightning strike is given.

ALTHOUGH it has been two centuries since Benjamin Franklin flew his kite to demonstrate the electrical character of lightning, little real progress has been made in the fundamental understanding of the electrical charge generating and transferring processes in thunderclouds. Because every lightning discharge in a cloud profoundly changes the electrical state within it, surveys of the cloud capable of detailed interpretation must be completed in a time short compared to the charging time. This means that an active thunderhead must be explored in something less than 10 seconds or, if a longer time is necessary, a steady state cloud must be chosen in which the convective activity is so low that disruptive electrical discharge does not take place. The Army-Navy Atmospheric Electricity Research Project has had assigned to it a Flying Fortress that has been instrumented to investigate the electrical state of the lower atmosphere. This airplane has flown through almost every conceivable type of weather during the past two years to determine the character and magnitude of the electrical effects associated with cloud and storm formations.[1]

[1] Gunn, Hall, and Kinzer, "The Precipitation-Static Interference Problem and Methods for its Investigation," Proc. Inst. Rad. Eng. **34**, 156P April (1946).

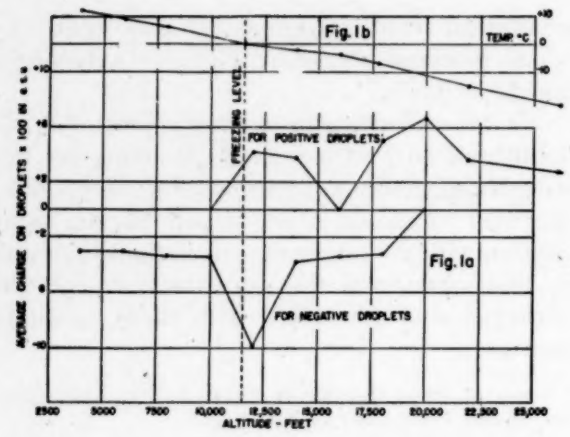

FIG. 1. (a) Average electrostatic charge on precipitation particles at various altitudes: (b) Corrected temperature as measured with MI313 aircraft psychrometer.

The present paper is concerned with the electrical characteristics of precipitation falling within a weak cold front. The observed changes in altitude and speed of the airplane flying through and at right angles to this front showed that there was negligible convective activity. Further, the electrical fields resulting from such activity were measured and found to be small. The observations showed, too, that measurable electrical charges were carried by the precipitation and that these charges, through appropriate mechanical separation, were sufficiently large to produce high electrical potentials and lightning. Measurements taken in active thunderstorm areas show that the charge per droplet (or flake) may be as much as an order of magnitude greater than those encountered in a mild cold front. Because of the stability of the front employed in this investigation, measurements made therein are considered more significant than would be the case if lightning discharges were present that suddenly might change the whole electrical configuration of the storm area.

The weather of the present investigation was a weak occluded front of the cold type accompanied with a low pressure trough oriented North-South, that moved eastward across Minnesota on July 27, 1945. As the front progressed, it became more of a cold front in character. Steady rain appeared over northern Minnesota. The project airplane flew through the front again and again at various altitudes and at right angles to the direction of the front collecting pertinent meteorological and electrical data. In addition to the usual flight instruments and precision meteorological thermometers, the airplane was equipped with two important specialized instruments designed to measure the electric field at the surface of the airplane and the electrical charge resident on the droplets of the encountered precipitation.

The electric field meters[2,3] are induction devices consisting of a highly insulated electrode exposed outside the airplane to the electric field and connected to the grid of a vacuum tube. The exposed electrode is arranged to be alternately exposed and shielded by a grounded metallic rotor driven by a small motor. In the presence of an electric field, an alternating voltage is produced on the grid of the vacuum tube that is proportional to the field. The output from the first vacuum tube is passed through an amplifier and thence to a direct current meter by way of a mechanical rectifier driven in synchronism with the grounded metallic rotor. Since such a system is phase sensitive, the indicating meter reads not only the magnitude of the electric field but also its direction. The electric field meters are mounted both on the top and on the bottom of the fuselage in such a way that it is possible to determine the probable origin of any measured electric field. These devices have been invaluable in the assessment of data and in determining the electrical state of the atmosphere.[4]

Some years ago the pioneer results of Gschwend,[5] who simultaneously measured the electrical charge and size of individual raindrops, were reinvestigated by a new method. Two highly insulated inducing rings separated vertically by 75 centimeters were mounted below a suitable collimator and connected to a high gain amplifier, the output of which was connected to a recording oscillograph. Raindrops falling through the two rings induced two successive deflections of the oscillograph, the amplitude of which determined the sign and magnitude of the

[2] R. Gunn, Phys. Rev. **40**, 307 (1932).
[3] Waddel, Drutowski, and Blatt, Proc. Inst. Rad. Eng. **34**, 161P April (1946).
[4] Stimmel, Rogers, Waterfall, and Gunn, Proc. Inst. Rad. Eng. **34**, 167P April (1946).
[5] Gschwend, Jahrb. Radioakt. u. Electronik. **17**, 62, 192 (1921).

charge on the raindrop, and the time interval between the two deflections measured the time it took the drop to fall the distance between the two inducing rings. Thus, the charge magnitude, sign, and the velocity of fall (or droplet size) could be simultaneously determined. This method has now been adapted for use on aircraft with considerable success.

A truncated sheet-metal cone is mounted on the airplane with the smallest circular opening of 9.62 cm² area presented face forward in such a way that precipitation coming through this opening will not touch the inner sides of the cone. Thence the particles move outward from the big end of the cone without being broken up or disturbed in any way. Inside the cone are mounted two inducing rings; the forward one is 5 centimeters in diameter and 5 centimeters long, while the aft ring is 12 centimeters in diameter and 5 centimeters long. The forward ring is highly insulated and connected through appropriate wires and shields to a pressurized cathode ray oscillograph equipped with a slow speed motion picture camera. The aft ring in the wider part of the cone acts as an electrostatic shield and is grounded to the cone and to the frame of the aircraft. The whole assembly is mounted on a streamlined strut 45 centimeters below the fuselage where it is moderately well shielded electrically from the moving propellers and from sharp points that might break into corona. It is found with such a device that very few precipitation particles ever hit the inducing ring and that it is easy to maintain the necessary high insulation even in the heaviest rain. Raindrops striking the leading edge of the cone and breaking up produce charges in which the figures of the pulses impressed on the oscillograph are notably different from a charged droplet proceeding through the inducing ring in a normal manner. Thus, it is possible to discard all traces except those caused by droplets that have traversed the apparatus without touching it. The output from the inducing ring is fed into a standard high sensitivity amplifier and then to a pressurized cathode ray oscillograph. A 35-millimeter movie camera is arranged to take pictures of each single sweep. The oscillograph in general is calibrated by employing standard a.c. voltages whose amplitudes are periodically photographed on a calibration frame. The calibrations for electrical quantity and for the capacity of the complete system were determined by using a small air gun and putting charges of various magnitudes on the shot fired therefrom. These charges on the shot were measured after traversing the inducing ring by being captured in a Faraday cage connected to an electrometer. Supplementing this information with a knowledge of the voltage sensitivity corresponding to any given setting of the amplifiers and the capacitance (which was 357 centimeters), the quantity sensitivity is easily checked in flight. The time of sweep per traverse of the oscillograph was usually 0.169 second. The scale of the measuring equipment and sweep rate were selected so that each sweep usually contained from 3 to 10 impulses whose magnitude and direction determined the charge on each individual droplet traversing the inducing ring.

Coherent sets of data were obtained using the above apparatus for the mild cold front described in an earlier paragraph and at various altitudes. It may be seen from Fig. 1a that electrical charges reside on the precipitation at all altitudes from the highest observed at 26,000 feet on down to the ground. In this investigated front, the charge on the precipitation at high altitudes is positive in character while at low altitudes the

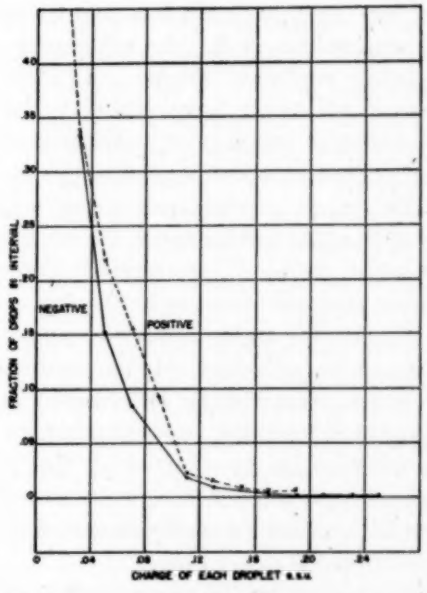

FIG. 2. Fraction of particles having observed electrostatic charge.

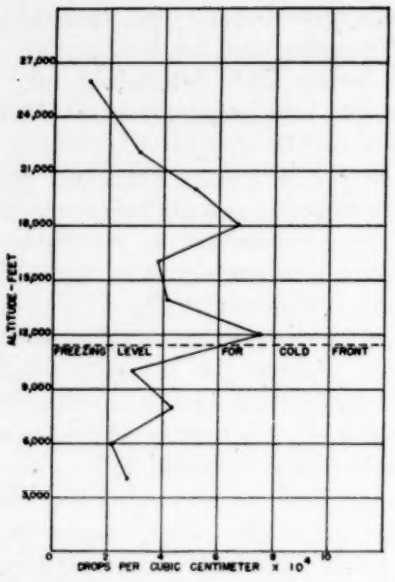

FIG. 3. Vertical distribution of the number of charged particles per unit volume.

charge on the particles was negative. However, at intermediate altitudes, for example from 20,000 feet on down to 10,000 feet, a mixture of positive and negative droplets was encountered. At 16,000 feet no positive droplets were measured, but at 14,000 feet a few and at 12,000 feet quite a number were observed. However, at lower altitudes, only negatively charged particles were encountered. The average electrical charge on some 500 positive droplets above 10,000 feet altitude approximated 0.033 electrostatic unit. The average negative charge on about 700 particles at altitudes below 20,000 feet was somewhat greater and approximated 0.04 electrostatic unit. Figure 1a shows plainly the distribution of charge on precipitation at various altitudes both for the positive and negative particles. It is thought to be of considerable theoretical importance that the freezing level is at approximately 11,000 feet and is below the general area of maximum electrification of the particles. The corrected temperatures as determined from a precision ML313 aircraft psychrometer mounted outside the fuselage are plotted in Fig. 1b. The accuracy of such temperature measurements, in common with all such measurements on aircraft, is subject to some uncertainty.

The number of droplets measured at any one altitude was hardly sufficient to permit a statistical determination of their free electrical charge, but the average over the whole storm is probably significant. In Fig. 2 the measured electrostatic charge on the intercepted droplets is plotted against the fraction of the droplets in any charge range. It may be seen that a large number of the droplets (or snow flakes) carry charges less than 0.02 e.s.u. and that the number carrying charges larger than 0.1 e.s.u. is relatively small. The difference in distribution between the positive and negative particles is not thought to be significant.

The reason why the charges on the particles seldom exceed 0.1 e.s.u. is easily understood. If a particle, for example, is assumed to be typical of "medium rain," then its radius[6] approximates 5×10^{-2} centimeter, and the electric field at its surface for a total charge of 0.1 e.s.u. is at least as great as 12,000 volts/centimeter. This value approximates the dielectric strength of air. It seems probable, therefore, that the particle electrification processes even in a quiet frontal rain area are so potent that typical droplets carry an appreciable fraction of the largest charge possible in an ordinary atmosphere. Since the dielectric strength of air is proportional to the pressure, the charge limitation imposed by corona discharge plays a relatively larger part at high altitudes than it does at the earth's surface. It is worth re-emphasizing that these charges were measured in a weak cold front that showed little evidence of important thunderstorm or electrical activity.

It has also been found possible to determine the density or the number of appreciably charged droplets per unit volume while flying through normal precipitation. It should be clear that with a known cross-sectional area exposed ahead of the inducing ring and with known values for the corrected air speed of the airplane, it is possible to determine the volume of air swept out per unit time by the opening in the cone. With values of this volume and the length of time that a given number of impulses are measured or observed on the oscillograph, it is possible to determine the number of charged drops swept up per unit volume. It is recognized that this procedure will not measure the number of tiny

[6] R. Gunn, "Electricity of Rain and Thunderstorm," Terr. Mag. Atmos. Elec. 40, 79–106 (1935).

droplets which bear very small charges, but these are of small importance in transporting water out of the cloud. In reducing the data, the number of impulses measured on the oscillograph was determined for every frame taken and the time of sweep for each frame noted. In Fig. 3 is given a plot of the number of charged precipitation particles per cubic centimeter as a function of the altitude above the ground. It should be emphasized that the number of drops per cubic centimeter is the number of drops with sufficient charge on them to produce a noticeable deflection on the oscillograph, or greater than about 0.01 e.s.u. Some drops were undoubtedly overlooked. It is interesting to notice that at 26,000 feet the number of drops per cubic meter is only about 130, and the number increases more or less irregularly as the altitude decreases to about 12,000 feet. At this level, which is near the freezing level, the number of particles per cubic meter approximates 750 and is a maximum. Below the freezing level, the density decreases rather rapidly to much smaller values. This seems to be of interest in interpreting the possible modes of formation of rain because if every raindrop in the lower atmosphere is assumed to come from a melting snow, or water and ice particle, as Bergeron has suggested,[7] it seems obvious that there should be more particles per unit volume at the freezing level than there would be raindrops below. This is because the raindrops will usually fall at a greater speed than the snow, or the water and ice particles, and

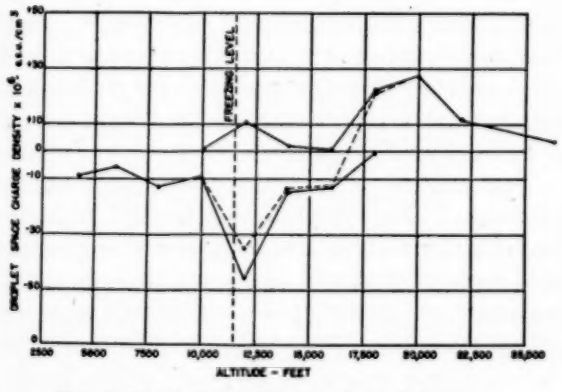

FIG. 4. Vertical distribution of particle space charge density.

[7] "On the Physics of Cloud and Precipitation," Meteor. (Union Geodesique et Geophysique Internationale, Lisbon, 1933) pp. 156–170.

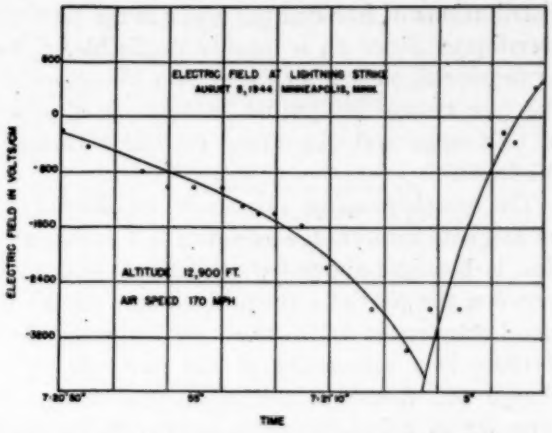

FIG. 5. Measured electric fields on B-25 before and after lightning strike, August 15, 1944, 13,000 feet.

therefore there should be a maximum in droplet density at the melting level. Our meager data suggest that this maximum may be real. A series of similar measurements in an active thunderstorm gave essentially similar results.

It should be evident from the foregoing discussion that with a knowledge of the charge on the precipitation particles and the number of particles per unit volume, one may calculate the particle space charge. Values of the particle space charge are plotted in Fig. 4 both for the positive and negative particles (solid line) and for the net particle space charge (broken line). Particle space charge must be clearly differentiated from the true space charge because neutralizing charges always surround rain droplets, and these must be counted in evaluating the true space charge. That neutralizing charges exist somewhere outside of each droplet in the cold front was well demonstrated by the fact that the measured electric fields throughout the area were, in every case, orders of magnitude smaller than one would calculate from the free charges actually resident on the precipitation. In this connection it is well to remind the reader that if the region of the free charge distribution is large compared to the vertical height above the ground, then the vertical electric field E is given nearly enough by

$$E = 4\pi \int \rho dz + E_0 \qquad (1)$$

where ρ is the true space charge density; E_0 is the originally existing field produced by surface

distributions of free charge; and z is the vertical coordinate. Since E_0 is usually negligible, $E/4\pi$ as measured on the airplane gives the value of the free charge integrated throughout a prism of unit area and extending vertically through the front.

The particle space charge is considered to be of great importance because, if relative motion is brought about by any means whatever between the particles themselves and the air or cloud droplets in which they are immersed, and if there is a separation of the two, then free charge will appear in the adjacent area. In the presence of adequate air currents, this surplus charge may obviously be some appreciable fraction of the space charge appearing on the particles alone. If the free space charge distribution is known, then the electric field and the potential distribution may be immediately calculated by standard electrostatic procedures. If it is assumed that the free space charge is equal to the space charge on the precipitation and that no compensating charge exists on the air outside the droplets, it is easy to calculate, using the observed particle space charge density shown in Fig. 4, that in a cloud area in which vertical convection takes place, that electric fields up to 20,000 volts per centimeter and potentials up to 10^{10} volts may immediately be produced. A calculation of this nature has been given in an earlier paper.[6] These calculated electric fields and potentials are an order of magnitude greater than those required for a lightning discharge and thus show that a partial separation of the charge is adequate to produce observed thunderstorm electrical effects. For example, in our B-25 experimental airplane, on August 15, 1944, we flew through an active thundercloud and were struck by lightning. An electric field indicator mounted on the belly of the plane[3] near the trailing edge of the main wing provided values of the electric field both before and after the strike even though some of our other measuring equipment was destroyed by the bolt. The strike occurred at about 13,000 feet. The electric field increased as shown in Fig. 5 to a value of about 3400 volts per centimeter in about ten seconds and recovered in three seconds. These measured values of electric field must be corrected for distortion due to the presence of the airplane in the thunder cloud. Other measurements show that if the electric field at the time of the strike was approximately vertical, then the correction for distortion was such that the electric field existing in areas away from the plane and at 13,000 feet, closely approximated 1600 volts per centimeter just prior to the stroke. Thus, making a reasonable estimate of the dimensions of the cloud, one is led to the conclusion that the measured values of electric field and potential are smaller by perhaps an order of magnitude than the values which would be produced if all the charge on the precipitation and that outside of it were suddenly separated by a distance equal to the dimensions of a typical cloud.

The significance of these results in relation to thunderstorm electricity is obvious. The measures show that in a mild cold front, there is a definite tendency for positive electricity to reside on the precipitation at high altitudes; whereas, at relatively low altitudes, there is a marked tendency for a negative charge to exist on the precipitation. Further, simultaneous measures of the electric field show that the integrated true space charge at all levels is small and neutralizing charges outside the precipitation usually exist. Clearly therefore, if vertical air currents separate the associated neutralizing positive and negative charges to any appreciable extent, large electric fields and voltages sufficiently high to cause lightning will be produced. That a redistribution of electric charge will be produced in the event of active vertical air currents can hardly be doubted.

Our data lead to the conclusion that even rain clouds are intrinsically able to produce lightning, and only mechanical effects are needed in an ordinary rainstorm to separate the already existing charge in the cloud from that on the associated precipitation.

The reasons why positive electrical charge predominates on precipitation at high altitudes and negative at relatively lower altitudes are still controversial. We are continuing our measurements on the charges measured in flight on precipitation, and it is believed that as further data become available, we may have, finally, a first-class clue as to the origin of this charging.

The author is glad to acknowledge the assistance of Franklin E. Waterfall in securing much of the presented data.

Nuclear Excitation Functions.* II. $Al^{27}(d; p, \alpha)Na^{24}$

E. T. CLARKE
Department of Physics, Massachusetts Institute of Technology, Cambridge, Massachusetts
(Received October 24, 1946)

Hitherto unknown in light elements, a new reaction involving the emission of a proton and an alpha-particle has been observed by bombarding aluminum with 14-Mev deuterons. By an analysis of its excitation function, it is shown that the activity is not generated by the well-known (n, α) reaction, but is the result of the multiple disintegration of the compound nucleus $(Al^{27}+d)$.

INTRODUCTION

IN the course of the investigation of excitation functions of reactions induced in magnesium by deuterons, two important radioactive isotopes were produced and studied: the 3.0-year isotope Na^{22} produced from Mg^{24}, and 14.8-hour Na^{24} from Mg^{26}, both by the (d, α) reaction on these stable isotopes of magnesium. The excitation functions were found by use of the stacked foil technique[1] in which a series of aluminum foils coated with evaporated magnesium was bombarded with 14-Mev deuterons. The reaction $Mg^{24}(d, \alpha)Na^{22}$ yielded the expected curve,[2] but the curve of Na^{24} *vs.* deuteron energy was anomalous in that it showed a sudden rise at high bombarding energies. Further investigation of this excitation function showed that the increased activity at the high energy end was being generated in the aluminum foils.

The only manner in which Na^{24} has been reported produced from Al^{27} is through the (n, α) reaction, and this would not be expected to show a sharp decrease in excitation through a stack of foils only $\frac{1}{2}$ mm in thickness. The new excitation curve, therefore, was studied in some detail in an effort to ascertain the reaction actually taking place.

EXPERIMENTAL PROCEDURE

A number of aluminum foils were first stacked up and bombarded with the full deuteron beam of the M.I.T. cyclotron. Half-life measurements and a chemical analysis of the activity induced in the first few foils were carried out, the results of which confirmed the assumption that the isotope being produced from the aluminum was 14.8-hour Na^{24}. A stack of fifty foils, each 4.55 mg/cm² thick, was then prepared from sections of aluminum sheet of known area and weight. Variations in thickness of the foils were found by this means to be less than 1 percent. After the deuteron beam energy had been determined,[1] the stack of foils was given a deuteron exposure of 0.81 microampere hour and allowed to decay for two days to remove the shorter lived components.

Activities in the fifty foils were measured on a bell-type mica-window beta-ray counter[3] and a scale-of-128 circuit. An aluminum absorber of 80 mg/cm² was used to bring the counting rate to a few thousand counts per minute, and each foil was placed on the absorber to minimize changes in geometry from sample to sample; the distance between counter and absorber was increased to handle the higher intensities in the first few foils. Readings were corrected for background, about 5 percent of the lowest observation, and for decay of the Na^{24} during measurement. Finally the stack of foils as a whole was compared with a 10-microgram radium standard on a calibrated platinum screen wall gamma-ray counter,[4] and was found to contain[5] 3.30 rd of Na^{24} at the time of bombardment; this quantity was used to determine the absolute cross section of the reaction.

The activities induced in the foils were then plotted as a function of deuteron bombarding

* The research described in this article was supported in part by Contract N5ori-78, U. S. Navy Department.
[1] E. T. Clarke and J. W. Irvine, Jr., Phys. Rev. 66, 231 (1944).
[2] E. T. Clarke and J. W. Irvine, Jr., Phys. Rev. 69, 680 (1946).
[3] W. Good, A. Kip, and S. Brown, Rev. Sci. Inst. 17, 262 (1946).
[4] A. Roberts, L. G. Elliott, J. R. Downing, W. C. Peacock, and M. Deutsch, Phys. Rev. 64, 268 (1943).
[5] 1 rutherford (rd) = 10^6 disintegrations per second; E. U. Condon and L. F. Curtiss, Phys. Rev. 69, 672 (1946).

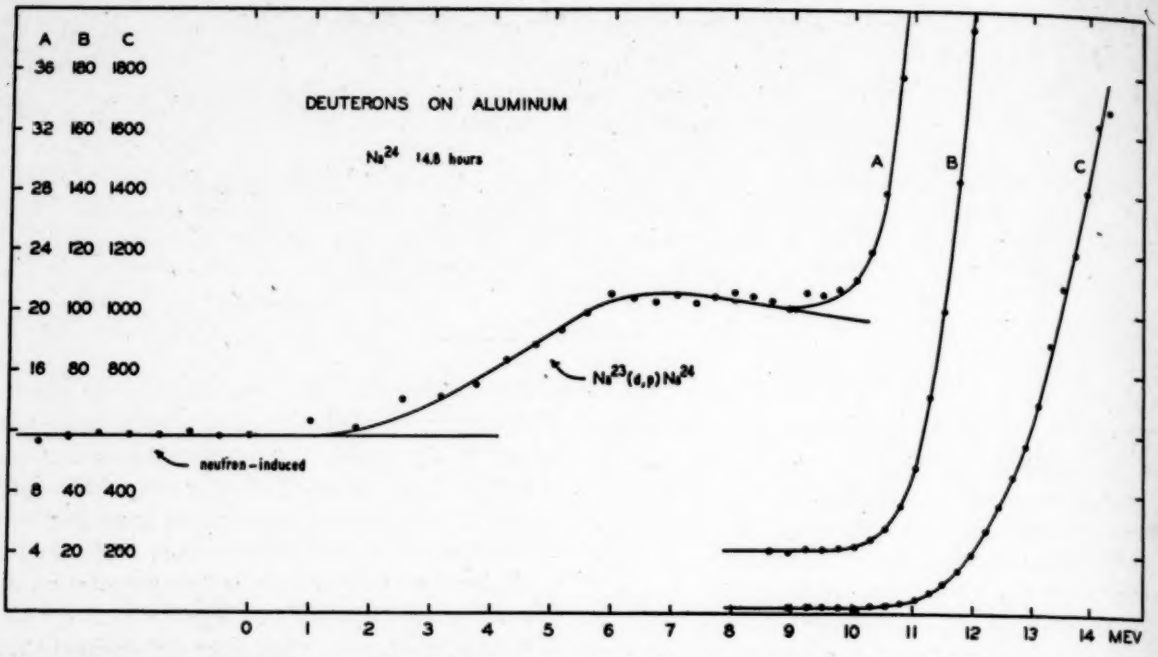

FIG. 1. Experimental excitation function of Na^{24} obtained by bombardment of aluminum foils. The ordinates, given for three ranges, are absolute, though in arbitrary units such that $1000 = 1.74 \times 10^7$ disintegrations/minute at bombardment time. Activation beyond the deuteron range is neutron induced. The $Na^{23}(d, p)Na^{24}$ activity is caused by the presence of 0.02 percent sodium contamination.

energy, the result of which is presented in Fig. 1. The curve can be divided into three distinct sections: the initial part, beyond the range of the deuterons, showing a constant excitation due to neutron activation, probably both by $Al^{27}(n, \alpha)Na^{24}$ and by $Na^{23}(n, \gamma)Na^{24}$; a region from 1 to 9 Mev in which activation first rises and then levels off with increase in bombarding energy, ascribable to sodium contamination in the aluminum metal since the curve corresponds to 0.02 percent Na producing $Na^{23}(d, p)Na^{24}$; and the interval from 9 to 14.5 Mev in which the new reaction sets in with a rapidly increasing cross section with rise in energy.

INTERPRETATION OF DATA

From the appearance of the experimental excitation function it seemed apparent that the rapid rise in production of Na^{24} with deuteron energy could not reasonably be ascribed to neutron (n, α) activation, since practically all of the product was generated in the first 0.3 mm of the aluminum target. The constant amount of Na^{24} generated in each foil beyond the range of the deuterons further bore out the hypothesis that targets of thicknesses of the order of deuteron ranges are thin for neutrons, and that no appreciable variation in neutron excitation, at least in light elements, can be expected in them.

It remained, therefore, to consider the possible deuteron reactions which might be responsible for the observed results. In disintegrating from ${}_{13}Al^{27} + {}_1H^2 \rightarrow {}_{11}Na^{24}$, 5 units of mass and 3 of charge must be emitted. Table I shows the four possible ways, together with the calculated threshold energies, in which the transition can result in emission of known elementary particles. It is evident that the only possible reaction is that of emission of a proton and an alpha-particle, all other modes requiring considerably more energy than can be imparted by 14-Mev deuterons.

Assuming that the reaction $Al^{27}(d; p, \alpha)Na^{24}$ takes place through the formation and disintegration of a compound nucleus (the Oppenheimer-Phillips mechanism has no meaning at deuteron energies high compared to that of the barrier, since in this region the deuteron break-up occurs inside the target nucleus), the shape of the excitation curve should, by analogy with

(n, p) and (n, α) excitation functions, be governed by the penetrabilities of the proton and the alpha-particle outward through the nuclear barrier. In the case of proton emission followed by loss of an alpha-particle, the total average penetrability can be expressed:

$$\bar{P}_{p,\alpha}(E_1)=\frac{1}{E_1}\int^{E_1} P_p(E_p)P_\alpha(E_\alpha)dE_p, \quad (1)$$

where E_1 represents the total available energy for the two particles, E_p and E_α the energies (including recoil), and P_p and P_α the individual penetrabilities of the proton and of the alpha-particle, respectively. The energies are related by the equation $E_1=E_p+E_\alpha$. A similar integral can be formed for the case of alpha-emission followed by proton loss; it will be slightly different because of differences in the masses and charges of the emitting nuclei.

In order to predict the absolute cross section for the $(d; p, \alpha)$ reaction, it is assumed that in the process of decay of the compound nucleus, any particle or set of particles energetically possible will emerge, and that the relative proportions of the various products are determined mainly by the probability of formation k_x of the emergent particles in the nucleus and by their penetrability P_x through the nuclear barrier. The cross section $\sigma_{d,x}$, then, may be written

$$\sigma_{d,x}=Q_c k_x P_x/\Sigma k_x P_x,$$

where Q_c is the probability of formation of a compound nucleus, and the summation extends over all possible products, including multiple disintegrations. In the assumed decay mechanism, the factor $k_x=1$ for elementary particles, less than unity for combinations such as alpha-particles.

Accordingly,

$$\sigma_{d,\alpha}=Q_c k_\alpha P_\alpha/\Sigma k_x P_x \quad (2)$$

and

$$\sigma_{d;\,p,\alpha}=Q_c k_p k_\alpha \bar{P}_{p,\alpha}/\Sigma k_x P_x;$$
$$\sigma_{d;\,\alpha,p}=Q_c k_\alpha k_p \bar{P}_{\alpha,p}/\Sigma k_x P_x. \quad (3)$$

The observed cross section should equal the sum of $\sigma_{d;p,\alpha}+\sigma_{d;\alpha,p}$. Adding Eqs. (3) and substituting $Q_c k_\alpha/\Sigma k_x P_x=\sigma_{d,\alpha}/P_\alpha$ obtained by rearrangement of Eq. (2), we find

$$\sigma_{\text{obs}}=k_p\frac{\sigma_{d,\alpha}}{P_\alpha}\bar{P}_{p,\alpha}+k_p\frac{\sigma_{d,\alpha}}{P_\alpha}\bar{P}_{\alpha,p}=\sigma_{d,\alpha}(\bar{P}_{p,\alpha}+\bar{P}_{\alpha,p}) \quad (4)$$

since $P_\alpha=1$ because the energy region in question is considerably above the barrier energy for the (d, α) reaction (6.5 Mev).

The deuteron energy E_d is corrected for recoil of the $(Al^{27}+d)$ compound nucleus and related to the total available energy E_1 by the formula

$$E_d=\frac{M+m}{M}(E_1-Q), \quad (5)$$

where M is the mass of Al^{27}, m the deuteron mass, and Q the reaction energy of the reaction $Al^{27}(d; p, \alpha)Na^{24}$.

In the determination of the quantities $\bar{P}_{p,\alpha}(E_1)$ and $P_{\alpha,p}(E_1)$, the only arbitrary factor is that of the nuclear radius. The value used here was that reported both by Grahame and Seaborg[6] and by Sherr,[7] who found $R=5.43\times10^{-13}$ cm for aluminum by measuring both elastic and inelastic scattering of fast neutrons from various targets. This radius was divided by $A^{\frac{1}{3}}=3.00$ to obtain the standard nuclear radius $r_0=1.81\times10^{-13}$ cm which was then applied to the penetrability formulae given by Bethe.[8] These penetrabilities were inserted in Eq. (1) and integrated graphically.

Since the (d, α) cross section for aluminum has not as yet been measured, the previously determined excitation function[2] for the reaction $Mg^{26}(d, \alpha)Na^{24}$ was used as an approximation. The general trend of these reactions at high energies is a decrease inversely proportional to the deuteron energy, and therefore the cross section can be expressed as a function of E_d

TABLE I. Threshold energies for possible reactions.

Particles emitted $(Al^{27}+d)-Na^{24}$	Deuteron threshold energy, Mev
$\alpha+p$	5.3
He^3+d	25.2
$2d+p$	30.8
$3p+2n$	35.5

[6] D. C. Grahame and G. T. Seaborg, Phys. Rev. **53**, 795 (1938).
[7] R. Sherr, Phys. Rev. **68**, 240 (1945).
[8] H. A. Bethe, Rev. Mod. Phys. **9**, 161 (1937).

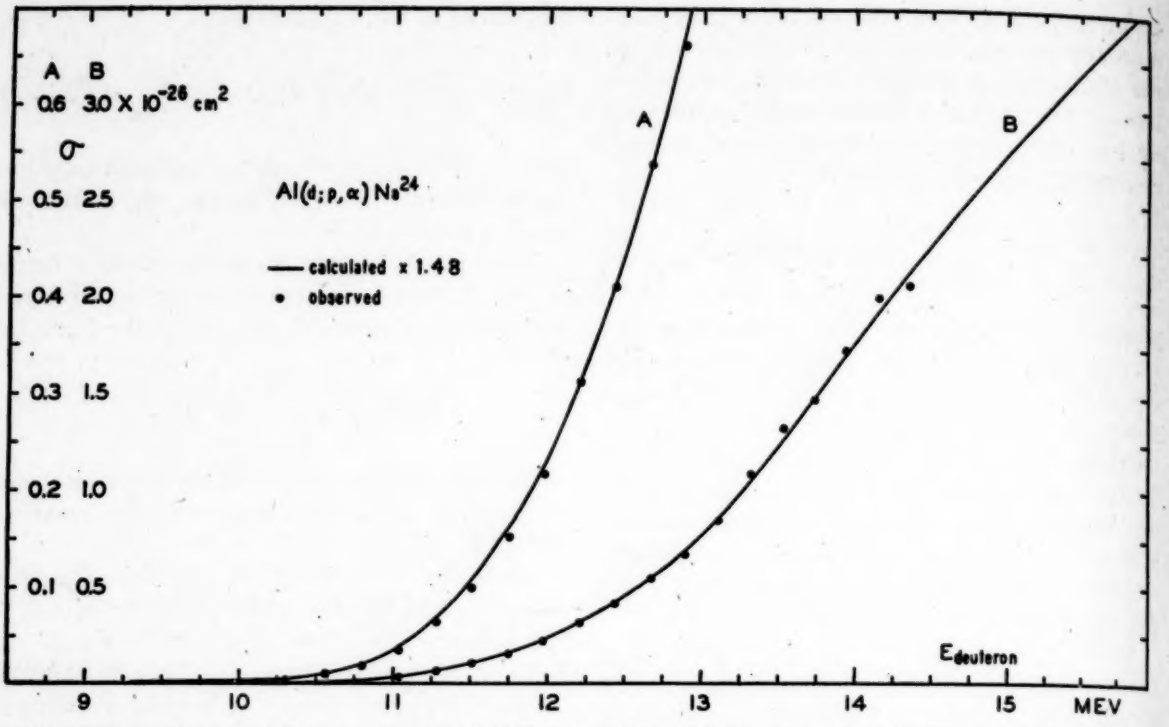

FIG. 2. Comparison of predicted excitation of $Al^{27}(d; p, \alpha)Na^{24}$ with the observed data. The calculated absolute values are within a factor of two of those found experimentally. Two ordinate scales are used to show the correspondence at lower energies.

(in Mev):

$$\sigma_{d,\alpha} = (7.0/E_d) \times 10^{-25} \text{ cm}^2. \quad (6)$$

Using Mattauch's[9] values for the neutral masses of Al^{27}(26.98980) and Na^{24}(23.99779), the reaction energy Q was found to be -4.90 ± 0.30 Mev. However, since only the difference in masses between Al^{27} and Na^{24} was needed, an independent calculation for Q was carried out, using the reaction[10] $Mg^{24} + {}_2He^4 \rightarrow Al^{27} + {}_1H^1 - 1.82$ Mev and the recently determined[11] beta-ray disintegration $Na^{24} \rightarrow Mg^{24} + 5.51$ Mev; this yielded $Q = -5.10$ Mev. An average value of $Q = -5.0$ Mev was used here since Mattauch had employed an erroneous figure (5.3 Mev) for the Na^{24} disintegration energy in checking his mass determinations.

The results of these calculations, compared with the experimental cross sections, are given in Fig. 2, where the predicted curve, multiplied by 1.48, is seen to fit the observed points. The effects of different assumed values for the quantities r_0 and Q were tested; it was found that these could be changed only by very small factors and still retain the shape of the experimental curve. With r_0 held constant, Q is determined to 0.1 Mev by this criterion, while r_0 could be varied only by about 0.1×10^{-13} cm with Q held within the limits of its probable error (0.3 Mev). The absolute cross section can be changed by about a factor of two by adjusting the variables within the limits given above, showing that the observed agreement is well within the probable error.

From the foregoing analysis there can be little doubt that the observed reaction is indeed $Al^{27}(d; p, \alpha)Na^{24}$, and that it proceeds by means of a compound nuclear mechanism. The existence of this reaction, and the success of the assumption regarding the competition for decay of the compound nucleus, also suggest an explanation for the decrease above the nuclear barrier with

[9] S. Flügge and J. Mattauch, Physik. Zeits. 44, 181 (1943).
[10] Observed by Duncanson and Miller, Proc. Roy. Soc. 146, 396 (1934); and Q values recalculated by M. S. Livingston and H. A. Bethe, Rev. Mod. Phys. 9, 300 (1937).
[11] L. G. Elliott, M. Deutsch, and A. Roberts, Phys. Rev. 63, 386 (1943).

increasing energy, observed in experimental deuteron-induced excitation curves: competition from reactions involving the emission of a second particle. The familiar $(d, 2n)$ is a special case of such reactions, in that the outgoing particles are not limited by the necessity of penetrating the Coulomb barrier and can therefore be produced with deuterons of moderate energies. The $(d; p, n)$ and $(d; n, p)$ reactions which must compete with the (d, p) and (d, n) would be difficult to observe, since they lead back to the target isotope and could be found by these techniques only where excited states of these isotopes exist. For light elements in general, where barriers are low for deuterons, the $(d; n, \alpha)$ and $(d; \alpha, n)$ reactions usually lead to stable isotopes. With the higher deuteron energies now becoming available, many more of these multiple disintegrations should be found.

The author wishes to thank Professor John W. Irvine, Jr., who kindly carried out the chemical analysis, and Professors V. F. Weisskopf, M. Deutsch, and R. D. Evans, with whom he discussed the theoretical aspects of the problem.

PHYSICAL REVIEW VOLUME 71, NUMBER 3 FEBRUARY 1, 1947

Thermal Ionization of Impurity Levels in Semi-Conductors†

B. GOODMAN,* A. W. LAWSON,** AND L. I. SCHIFF
Randal Morgan Laboratory of Physics, University of Pennsylvania, Philadelphia, Pennsylvania
(Received November 6, 1946)

The probability of ionization of an impurity level by thermal agitation in a semi-conductor is estimated by the use of a simple Debye model. It is found that the probability of ionization by one phonon decreases exponentially with the depth of the impurity level below the conduction band, approaching zero as the energy separation becomes equal to $k\theta_D$. The probability of ionization by more than one quantum is also estimated by the use of an Einstein model. It appears that the probabilities so calculated may play an important role in determining the frequency dependence of the rectification efficiency in crystal rectifiers.

INTRODUCTION

THE electrical properties of many semi-conductors are determined primarily by the presence of impurities that introduce discrete electronic energy levels which lie between the empty conduction band of the semi-conductor and the next lowest lying filled electronic band. These discrete energy levels may act either as acceptor levels or as donator levels. In the first case, they lie near the top of the filled band, are empty at zero temperature, and can accept electrons from the filled band, thus producing "hole conduction." In the second case, the levels lie near the bottom of the empty band, are full at zero temperature, and can donate electrons to the empty band, thus augmenting the intrinsic electronic conduction. The two situations are represented schematically in Fig. 1 and Fig. 2, respectively. In the following discussion we shall consider only donator levels, which produce the so-called N-type semi-conductors, with the understanding that our conclusions are also applicable to acceptor levels forming P-type semi-conductors.

When a semi-conductor is placed in contact with a metal, a rectifying junction may be formed if the relative work functions of metal and semi-conductor are suitable. In the case of an N-type semi-conductor, the effective work function of the metal must be larger than that of the semi-conductor. Then the equilibrium situation near the junction is as represented schematically by the potential diagram of Fig. 3.[1] Practi-

† This work was carried out on contract OEMsr-388 between the National Defense Research Committee and the University of Pennsylvania and was originally described in a monthly report submitted July 7, 1943.
* Now Jewett Fellow, University of California, Berkeley.
** Now at the Institute for the Study of Metals, University of Chicago.

[1] F. Seitz and S. Pasternack, "The Principles of Crystal Rectifiers," NDRC Report No. 01-102, June 10, 1942.

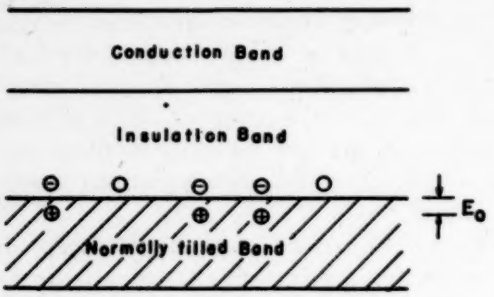

FIG. 1. Energy level diagram showing schematically the excitation of electrons from a normally filled band to acceptor levels producing hole conduction. E_0 represents the height of the acceptor levels above the normally filled band.

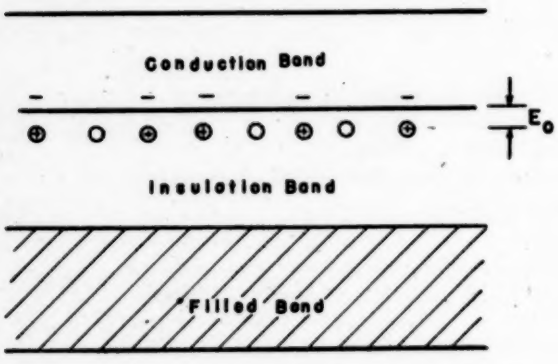

FIG. 2. Energy level diagram showing schematically the ionization of donator impurity levels to produce free electrons in the conduction band of a semi-conductor. E_0 represents the depth of the levels below the conduction band.

cally all of the donators lying more than thermal energy (kT) above the thermodynamic potential far from the junction (which is about midway between the donator levels and the bottom of the conduction band) will be ionized. This produces a net positive charge in the semi-conductor near the metal, and consequently a net negative charge in the metal on the other side of the potential barrier. Because of this double layer or potential step, the electron flow from semi-conductor to metal when the metal is made anodic by a given potential is greater than the reverse flow when the metal is made cathodic by the same amount. This results in a rectifying characteristic of the type shown in Fig. 4.

In addition to causing a net current through the junction, an applied voltage also changes the bound charge in the semi-conductor near the interface. Thus the amount of stored charge depends on the voltage, and the contact has some capacitative properties. The over-all electrical behavior of the rectifier may be represented approximately by the simple circuit of Fig. 5. It is evident that the capacity associated with the bound charge in the barrier layer will tend to short out the back resistance when the frequency becomes high enough that the impedance of C is comparable with R_b.[2] For high frequencies, this should cause the rectification efficiency to fall off as the inverse square of the frequency. Experimentally, however, in many rectifiers, the efficiency drops off much more slowly than this with increasing frequency. One possible explanation of this discrepancy lies in assuming that the circuit parameters of Fig. 5 are themselves functions of the frequency. The capacity C will be expected to decrease with increasing frequency if there is a time lag in ionization (and deionization) of the donator levels that is of the order of the period of the applied field. Such a lag can occur owing to the finite probability of ionization by thermal agitation of the lattice; an estimate of this probability is made in the following section.

THEORY

The transition probability per unit time for the excitation of electrons from donator levels is given by

$$w=(2\pi/\hbar)\,|\,V_{0K}\,|^2\rho_K, \tag{1}$$

where ρ_K, the energy density of states in the conduction band, is given by

$$\rho_K=4\pi\Omega mp/h^3. \tag{2}$$

m and p are the mass and momentum of the

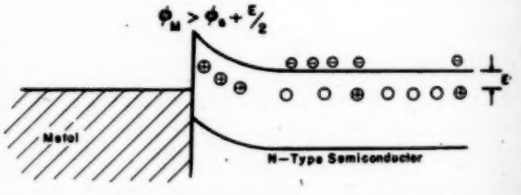

FIG. 3. Schematic diagram showing the relative energy levels in a metal and N-type semi-conductor. With no external applied field, the top of the Fermi distribution lies approximately half-way between the impurity levels and the conduction band of the semi-conductor.

[2] H. A. Bethe, "Theory of High Frequency Rectification by Silicon Crystals," NDRC Report No. 43-11, October 29, 1942.

electron, respectively, and Ω is the volume of the crystal. V_{0K} is the matrix element

$$V_{0K}=\int \psi_0 V \psi_K^* d\tau \qquad (3)$$

calculated in terms of normalized initial and final wave functions

$$\psi_0=(1/(\pi a^3)^{\frac{1}{2}})e^{-r/a},$$
$$\psi_K=(1/\Omega^{\frac{1}{2}})\exp(i\mathbf{K}\cdot\mathbf{r}). \qquad (4)$$

ψ_0 is taken for simplicity to be of hydrogenic form.

The perturbation V may be approximated as

$$V(\mathbf{r})=-\mathbf{R}_\sigma(\mathbf{r})\cdot\nabla V_0(\mathbf{r}), \qquad (5)$$

where

$$V_0(\mathbf{r})=-Ze^2\mathbf{r}/r^2,$$
$$\mathbf{R}_\sigma=\boldsymbol{\epsilon}_\sigma\exp(i\boldsymbol{\sigma}\cdot\mathbf{r}). \qquad (6)$$

Equations (5) and (6) may be interpreted as follows. The thermal agitation may be resolved into acoustic Debye waves which strain the lattice and alter the separation of electron and donator ion. The total strain will then involve a sum over the propagation vectors $\boldsymbol{\sigma}$ of the Debye waves. However, energy must be conserved between the phonons (Debye wave quanta) and the electrons, so that

$$h\nu_\sigma=\hbar^2K^2/2m+|E_0|, \quad E_0<0, \qquad (7)$$

where ν_σ is the frequency of the Debye wave and E_0 the energy of the bound electron state.

Equations (4)–(6) may be substituted into

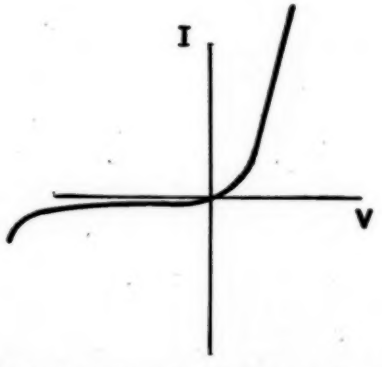

FIG. 4. Typical characteristic curve of a rectifying junction showing the dependence of current I on applied voltage V.

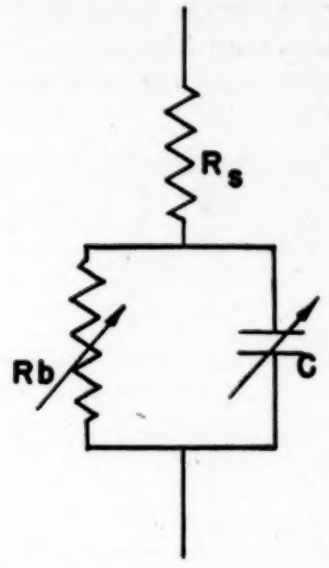

FIG. 5. Simple equivalent circuit of a rectifying contact. R_b and C, which are both functions of applied voltage, represent the resistance and capacitance of the barrier layer respectively, R_s is the bulk resistance of the semiconductor.

Eq. (3) and the integrals carried out to give

$$V_{0K}=4iaZe^2\left(\frac{\pi}{\Omega a^3}\right)^{\frac{1}{2}}\epsilon_\sigma\cos\theta_\sigma\left(\frac{\tan^{-1}aQ_\sigma-aQ_\sigma}{a^2Q_\sigma^2}\right), \qquad (8)$$

where θ_σ is the angle between $\boldsymbol{\epsilon}_\sigma$ and $\mathbf{Q}_\sigma\equiv\boldsymbol{\sigma}-\mathbf{k}$. For the situations of practical interest, σ, K, and $1/a$ are all of the same order of magnitude ($\sim 10^7$ cm^{-1}). The quantity aQ_σ will be of the order of or less than unity, and a good enough approximation to Eq. (8) may be obtained by expanding the inverse tangent and keeping the first two terms, and replacing aQ_σ by aK. This gives for the square of the matrix element

$$|V_{0K}|^2\approx\frac{16\pi Z^2e^4aK^2}{9\Omega}\epsilon_\sigma^2\cos^2\theta_\sigma. \qquad (9)$$

The amplitude of the Debye wave may be written

$$\epsilon_\sigma^2=\frac{h\nu_\sigma}{2\pi^2M\nu_\sigma^2(e^{h\nu_\sigma/kT}-1)} \qquad (10)$$

where M is the mass of the donator atom. Since we have to integrate over the Debye spectrum, we need the number of modes between ν_σ and $\nu_\sigma+d\nu_\sigma$

$$f(\nu_\sigma)d\nu_\sigma=(3h^3\nu_\sigma^2/k^3\theta_D^3)d\nu_\sigma \qquad (11)$$

where θ_D is the Debye temperature. Since the range of integration is small ($|E_0|$ is close to $k\theta_D$), the result for the total transition probability may be estimated as

$$w \approx \frac{114\pi^4 Z^2 e^4 a m^2 (2mkT)^{\frac{1}{2}}}{Mh^4} \frac{(\theta_D/T - C)}{(e^C - 1)C^{\frac{1}{2}}}, \qquad C = \frac{|E_0|}{kT}. \tag{12}$$

Typical numerical values for substitution in Eq. (12) are as follows: $\theta_D/T \cong 2$, $C \cong 3/2$, $Z \cong 0.1$, $a \cong 10^{-7}$ cm, $M = 27$ for aluminum impurity in a silicon semi-conductor. The small value of Z includes the effect of the dielectric constant (about 10) in reducing the single unbalanced charge of the aluminum ion; similarly a is larger than would be expected for a hydrogen atom by about a factor of 10. These values indicate that w is about 10^{10} sec.$^{-1}$, provided that $|E_0| < k\theta_D$.[3]

If $|E_0|$ exceeds $k\theta_D$, which seems unlikely on the basis of present information, then ionization involves the absorption of more than one phonon from the lattice vibrations. The order of magnitude of two or three phonon effects may be estimated by using the simpler Einstein model for the oscillations of the crystal lattice as follows. We assume that the atoms undergo a harmonic displacement from fixed lattice points given by

$$\mathbf{R} = \mathbf{R}_0 \sin\omega t, \tag{13}$$

which introduces a perturbation of the electron energy given by

$$V = \frac{Ze^2}{|\mathbf{r}-\mathbf{R}|} - \frac{Ze^2}{|\mathbf{r}|} = \frac{Ze^2}{r} \sum_{n=1}^{\infty} (R/r)^n P_n(\cos\theta'), \tag{14}$$

where θ' is the angle between $\mathbf{r}$ and $\mathbf{R}$, and $|R| \leqslant |r|$. Using the fact that $(Ka)^2 \ll 1$, one finds for the matrix element

$$V_{0K} = \frac{4\pi a^2 Ze^2}{(\pi a^3\Omega)^{\frac{1}{2}}} \sum_{n=1}^{\infty} (iR_0K)^n \frac{2^n n!}{(2n+1)!} \times P_n(\cos\theta')(\sin\omega t)^n. \tag{15}$$

If we expand V_{0K} in a Fourier series, the first harmonic will be the matrix element for transitions from levels lying between 0 and $k\theta_E$, the second will correspond to transitions from levels lying between $k\theta_E$ and $2k\theta_E$, i.e., two phonon transitions, etc. Using the fact that $R_0K \ll 1$, one finds

$$^1V_{0K} = \frac{4\pi a^2 Ze^2}{3(\pi a^3\Omega)^{\frac{1}{2}}} (iR_0K) P_1(\cos\theta'), \qquad ^2V_{0K} = \frac{4\pi a^2 Ze^2}{30(\pi a^3\Omega)^{\frac{1}{2}}} (iR_0K)^2 P_2(\cos\theta'). \tag{16}$$

etc.

From the foregoing equations, using the numerical value suggested above, one may show that each additional phonon absorbed reduces the transition probability by approximately a factor of 10^6.

It may readily be shown that the transition probability due to thermal radiation is of the order of 10^6 sec.$^{-1}$, and hence may be neglected in comparison with the probability of single phonon transitions.

[3] We are indebted to Professor F. Seitz for informing us of the results of an independent estimate of the transition probability that is based on the Born-Oppenheimer molecular approximation. He obtained a numerical result of the same order of magnitude.

On a General Condition of Heisenberg for the S Matrix

S. T. MA
Institute for Advanced Study, Princeton, New Jersey
(Received October 18, 1946)

It is shown that the S matrix for an attractive exponential potential, which possesses redundant zeros, does not satisfy a general condition of Heisenberg. To insure the validity of Heisenberg's condition, we introduce the supplementary condition that the interaction potential should vanish for large distances from the scattering center. It is shown that the S matrices for the attractive exponential and the Coulomb potential cut off at a large distance R give correctly both the eigenvalues of energy and the asymptotic behavior of the wave functions for the s states in the limit $R\to\infty$.

1. INTRODUCTION

RECENTLY Heisenberg[1] has proposed a new formulation of the quantum theory which deals exclusively with such physical quantities as are directly observable, namely, the discrete energy values of stationary states of closed systems, and the asymptotic behavior of wave functions at infinity in collision processes. These physical quantities are determined by Heisenberg's S matrix, which plays the same fundamental role in Heisenberg's new scheme as the Hamiltonian and wave equation in the current scheme of quantum theory. It is possible to derive from the current scheme of quantum theory certain general properties of the S matrix, such as the unitary property[2] and the relativistic invariance,[3] which can be taken over into the new formulation of the quantum theory.

The determination of closed stationary states from the S matrix has been investigated by Heisenberg and Møller. For the following investigation it is sufficient to state Heisenberg's result for the s states of a particle under the action of a central force. Let $u_n(r)$ and $u_k(r)$ be, respectively, the radial wave functions of the discrete and the continuous energy states, normalized according to the equations

$$\int_0^\infty |u_n(r)|^2 dr = 1, \quad \int_0^\infty u_k^*(r) u_{k'}(r) dr = \delta(k-k').$$

These wave functions satisfy the completeness relation

$$\sum_n u_n^*(r) u_n(r') + \int_0^\infty u_k^*(r) u_k(r') dk = \delta(r-r'). \quad (1)$$

The asymptotic expressions of these wave functions for large distances are

$$u_n(r) \sim c_n (2\pi)^{-\frac{1}{2}} \exp(-|k_n| r), \quad (2)$$

$$u_k(r) \sim (2/\pi)^{\frac{1}{2}} \sin[kr + \delta(k)], \quad (3)$$

where c_n is a constant and $\delta(k)$ is the phase of u_k. Making use of the general relations

$$S(k) = \exp[2i\delta(k)] \quad (4)$$

and

$$S^*(k) S(k) = 1, \quad (5)$$

Heisenberg obtained from (1)–(3) the following general relation for a large value of r:

$$\int_{-\infty}^{\infty} S(k) \exp(ikr) dk = \sum_n |c_n|^2 \exp(-|k_n| r). \quad (6)$$

The closed discrete states can be determined by analytic continuation from the real to the complex values of k. If $S(k)$ decreases sufficiently rapidly for large values of $|k|$, the left-hand side of (6) is equal to $2\pi i$ times the sum of the residues of $S(k) \exp(ikr)$ at the poles of $S(k)$ in the upper half of the complex plane. Identifying the discrete states with these poles, Heisenberg obtained

$$|c_n|^2 = 2\pi i [Res S(k)]_{k_n}. \quad (7)$$

For the S matrices such that the relation

$$S(k) S(-k) = 1 \quad (8)$$

in the complex plane can be derived by analytic

[1] W. Heisenberg, Zeits. f. Physik **120**, 513 and 673 (1943) Heisenberg's third and fourth papers on the S matrix have not yet been published. I am indebted to Professor Pauli for communicating to me some results in the fourth paper.
[2] W. Pauli, *Meson Theory of Nuclear Forces* (Interscience Publishers, Inc., New York, 1946), p. 49.
[3] C. Møller, Danske Vid. Sels. Math.-fys. Medd. **23**, No. 1 (1945); **22**, No. 19 (1946).

continuation of the unitary condition (5) for real values of k, the poles of $S(k)$ in the upper half-plane have corresponding zeros in the lower half-plane. Hence, when the poles and zeros are on the imaginary axis,

$$|c_n|^2=-2\pi[(dS/d|k|)_{-i|k_n|}]^{-1}. \quad (9)$$

This relation expressing the absolute magnitude of c_n in terms of $S(k)$ can also be directly derived by a method of Kramers[4] without using (6). We shall see below that there are cases in which (9) is satisfied but (6) is not satisfied.

2. REDUNDANT ZEROS

As recently reported,[5] the S matrix for an attractive exponential field presents a new feature in the eigenvalue problem. For the s states of a particle of mass m in the potential field

$$V(r)=-V_0\exp(-r/a), \quad (10)$$

where V_0 and a are positive constants, the wave equation takes the form

$$-(\hbar^2/2m)(d^2u/dr^2+k^2u)+V(r)u=0. \quad (11)$$

The solutions of Eq. (11) for a positive value of energy are the Bessel functions

$$J_{\pm i\rho}[\alpha\exp(-r/2a)],$$

where

$$\rho=2ak, \quad \alpha=2a(2mV_0)^{\frac{1}{2}}/\hbar.$$

The wave function which vanishes at the origin is

$$u_k(r)=i(2\pi)^{-\frac{1}{2}}|\Gamma(i\rho+1)/J_{i\rho}(\alpha)| \times\{J_{-i\rho}(\alpha)J_{i\rho}[\alpha\exp(-r/2a)] -J_{i\rho}(\alpha)J_{-i\rho}[\alpha\exp(-r/2a)]\}, \quad (12)$$

the normalization constant being chosen such that the asymptotic expression of Eq. (12) for large r, namely,

$$u_k(r)\sim i(2\pi)^{-\frac{1}{2}}|\Gamma(i\rho+1)/J_{i\rho}(\alpha)| \times\left\{\frac{J_{-i\rho}(\alpha)(\alpha/2)^{i\rho}}{\Gamma(i\rho+1)}\exp(-ikr) -\frac{J_{i\rho}(\alpha)(\alpha/2)^{-i\rho}}{\Gamma(-i\rho+1)}\exp(ikr)\right\} \quad (13)$$

is of the form of Eq. (3). Comparing Eq. (12) with Eq. (3) and making use of Eq. (4), we see that

$$S(k)=\frac{J_{i\rho}(\alpha)\Gamma(i\rho+1)}{J_{-i\rho}(\alpha)\Gamma(-i\rho+1)}\left(\frac{\alpha}{2}\right)^{-2i\rho}. \quad (14)$$

$S(k)$ vanishes when $J_{i\rho}(\alpha)$ vanishes or $\Gamma(-i\rho+1)$ is infinitely large. Now $J_{i\rho}(\alpha)$ has no zeros in the lower half-plane of k except those on the imaginary axis.[6] Hence the first condition is equivalent to

$$J_{|\rho|}(\alpha)=0. \quad (15)$$

The wave function corresponding to a zero k_n of Eq. (15) is[7]

$$u_n(r)=c_n(2\pi)^{-\frac{1}{2}}\Gamma(|\rho_n|+1)(2/\alpha)^{|\rho_n|} \times J_{|\rho_n|}[\alpha\exp(-r/2a)]. \quad (16)$$

The absolute magnitude of the constant c_n is given by Eq. (9) with S given by Eq. (14), as can be directly verified from the normalization condition.

The second condition

$$\Gamma(-ip\rho+1)=\infty \quad (17)$$

is satisfied by values of ρ such that

$$i\rho=|\rho|=1, 2, 3\cdots. \quad (18)$$

The wave functions Eq. (12) corresponding to the eigenvalues of Eq. (18) vanish identically. The zeros given by Eq. (18) can be regarded as redundant. We shall denote in the following the values of ρ and k corresponding to the redundant zeros by ρ_r and k_r, respectively.

3. VALIDITY OF HEISENBERG'S GENERAL RELATION

Let us now study Heisenberg's general relation, Eq. (6), as it applies to the S matrix for the exponential potential. The integral

$$\int_{-\infty}^{\infty}S(k)\exp(ikr)dk$$

in (6) can be evaluated by contour integration.

[4] H. A. Kramers, Hand- und Jahrbuch d. Chem. Physik 1, 312 (1938).
[5] S. T. Ma, Phys. Rev. 69, 668 (1946).
[6] Gray, Mathews and MacRobert, *Bessel Functions* (The Macmillan Company, New York, 1931), p. 88.
[7] H. Bethe and R. F. Bacher, Rev. Mod. Phys. 8, 111 (1936).

We have

$$\int_{-\infty}^{\infty} S(k)\exp(ikr)dk=\lim_{K\to\infty}\int_C S(k)\exp(ikr)dk +2\pi i\sum Res[S(k)\exp(ikr)], \quad (19)$$

where C denotes a semi-circle of radius K above the real axis, having its center at the origin, and the summation extends over all the poles in the upper half-plane. Equation (14) can be written in the form

$$S(k)=\Lambda_{i\rho}(\alpha)/\Lambda_{-i\rho}(\alpha)$$

if we put

$$J_p(\alpha)=(\alpha/2)^p\Lambda_p(\alpha)/\Gamma(p+1).$$

Now $\Lambda_p(\alpha)$ approaches the value 1 as p tends to infinity through a sequence of numbers not consisting of negative integers. Hence if K tends to infinity through a sequence such that $|\rho|$ is not integral

$$\lim_{K\to\infty}\int_C S(k)\exp(ikr)dk=\lim_{K\to\infty}\int_C \exp(ikr)dk =\int_{-\infty}^{\infty}\exp(ikr)dk=2\pi\delta(r)=0$$

since $r\neq 0$. Therefore

$$\int_{-\infty}^{\infty} S(k)\exp(ikr)dk=2\pi i\sum Res[S(k)\exp(ikr)] =\sum_n|c_n|^2\exp(-|k_n|r) -2\pi\sum_r\left(\frac{dS}{d|k|}\right)^{-1}_{-i|kr|}\exp(-|k_r|r). \quad (20)$$

It can be easily shown from (14) that

$$(dS/d|k|)_{-i|kr|}>0, \quad (21)$$

so that the second sum over the redundant eigenvalues is smaller than zero. Comparing Eq. (20) with Eq. (6) we see that Heisenberg's general condition is not satisfied by Eq. (14). It has recently been proposed by D. ter Haar[8] to make use of Eq. (21) for discarding the redundant zeros.

This example raises a question of the validity of Heisenberg's relation, Eq. (6). Heisenberg's derivation outlined in Section 1 holds good only if the difference between the exact wave function $u_k(r)$ and its asymptotic expression Eq. (3) is small in comparison with the wave function $u_n(r)$. This is not the case with the exponential potential, however, as can be seen from Eqs. (12), (3), and (2).

We can see how the difficulty of redundant eigenvalues arises from the approximate treatment by evaluating the integral

$$\int_0^{\infty} u_k^*(r)u_k(r')dk$$

for the exact wave function (12). From Eq. (12) we have

$$\int_0^{\infty} u_k^*(r)u_k(r')dk=\int_{-\infty}^{\infty} f(k;r,r')dk, \quad (22)$$

where

$$f(k;r,r')=(2\pi)^{-1}\{\Gamma(i\rho+1)\Gamma(-i\rho+1)/J_{i\rho}(\alpha)J_{-i\rho}(\alpha)\}\{J_{-i\rho}(\alpha)J_{i\rho}(\alpha)J_{i\rho}[\alpha\exp(-r/2a)] \times J_{-i\rho}[\alpha\exp(-r'/2a)]-J_{i\rho}(\alpha)^2J_{-i\rho}[\alpha\exp(-r/2a)]J_{-i\rho}[\alpha\exp(-r'/2a)]\}. \quad (23)$$

Now the integral of $f(k;r,r')$ taken round the semicircle C referred to above has the limit

$$\lim_{K\to\infty}\int_C f(k;r,r')dk=(2\pi)^{-1}\int_{-\infty}^{\infty}\{\exp[ik(r'-r)]-\exp[ik(r'+r)]\}dk =\delta(r'-r)-\delta(r'+r)=\delta(r'-r). \quad (24)$$

Hence

$$\int_{-\infty}^{\infty} f(k;r,r')dk=\delta(r'-r)+2\pi i\sum Resf(k;r,r'). \quad (25)$$

But at the poles where $\Gamma(i\rho+1)=\infty$ the residue vanishes. Hence

$$2\pi i\sum Resf(k;r,r')=-i\sum[ResJ_{-i\rho}(\alpha)^{-1}]\Gamma(i\rho+1)\Gamma(-i\rho+1)J_{i\rho}(\alpha) \times J_{-i\rho}[\alpha\exp(-r/2a)]J_{-i\rho}[\alpha\exp(-r'/2a)]$$

$$=-\sum_n u_n^*(r)u_n(r')$$

[8] D. ter Haar, Physica, in the press.

so that

$$\int_0^\infty u_k^*(r)u_k(r')dk=\delta(r'-r)-\sum_n u_n^*(r)u_n(r'),$$

which is just Eq. (1). In spite of the factor $\Gamma(i\rho+1)$ in the integrand of Eq. (22) the summation in the final result extends only over the true eigenvalues. The above calculation may be taken to be a direct verification of the completeness relation. For large distances r and r', we have, by Eq. (2)

$$\int_0^\infty u_k^*(r)u_k(r')dk=\delta(r'-r)-(2\pi)^{-1}\sum_n|c_n|^2\exp[-|k_n|(r+r')]. \tag{26}$$

In the approximate treatment, however, we have

$$\int_0^\infty u_k^*(r)u_k(r')dk=\delta(r'-r)-(2\pi)^{-1}\int_{-\infty}^\infty S(k)\exp[ik(r+r')]dk$$

$$=\delta(r'-r)-(2\pi)^{-1}\sum_n|c_n|^2\exp[-|k_n|(r+r')]$$

$$-i\sum_r Res\{S(k)\exp[ik(r+r')]\}_{i|k_r|},$$

which has an additional term corresponding to the redundant zeros.

This discussion shows the necessity of introducing a supplementary condition for the validity of Heisenberg's general relation. We can take for the supplementary condition the condition that the potential $V(r)$ should vanish for large distances from the scattering center, because under such a condition the wave function $u_k(r)$ is equal exactly to the expression (3) for large distances and therefore Eq. (6) holds with certainty.

4. POTENTIALS CUT OFF AT A LARGE DISTANCE

Møller has investigated the exponential potential (10) cut off at a large distance R, i.e., the potential

$$\begin{aligned} V(r)&=-V_0\exp(-r/a) && (0<r<R)\\ &=0 && (\quad r>R). \end{aligned} \tag{27}$$

The wave function $u_k(r)$ is now given exactly by (3) when $r>R$, and, except for a constant factor, given by (12) when $r<R$. The requirement of continuity of $u_k(r)$ and its derivative at $r=R$ gives

$$S(k)=-\exp(-2ikR)\frac{J_{-i\rho}(\alpha)J_{i\rho+1}[\alpha\exp(-R/2a)]+J_{i\rho}(\alpha)J_{-i\rho-1}[\alpha\exp(-R/2a)]}{J_{-i\rho}(\alpha)J_{i\rho-1}[\alpha\exp(-R/2a)]+J_{i\rho}(\alpha)J_{-i\rho+1}[\alpha\exp(-R/2a)]}. \tag{28}$$

For large values of $|k|$ in the upper half-plane of k such that $2a|k|$ is not an integer,

$$S(k)\exp(ikr)\sim-\exp[ik(r-2R)]\frac{J_{i\rho+1}[\alpha\exp(-R/2a)]}{J_{i\rho-1}[\alpha\exp(-R/2a)]}\sim-\frac{\Gamma(i\rho)}{\Gamma(i\rho+2)}\left(\frac{\alpha}{2}\right)^2$$

$$\times\exp(-R/a)\exp[ik(r-2R)],$$

and so

$$\lim_{K\to\infty}\int_C S(k)\exp(ikr)dk$$

vanishes for $r>2R$.[9] In accordance with the general discussion of Section 1 the eigenvalues of k are the values of k in the lower half-plane satisfying the equation $S(k)=0$ or by Eq. (28)

$$J_{-i\rho}(\alpha)J_{i\rho+1}[\alpha\exp(-R/2a)]+J_{i\rho}(\alpha)J_{-i\rho-1}[\alpha\exp(-R/2a)]=0, \tag{29}$$

[9] Whittaker and Watson, *Modern Analysis* (Cambridge University Press, New York, 1927), p. 115.

an equation first obtained by ter Haar. Equation (29) reduces to Eq. (15) when $R\to\infty$. Thus the redundant zeros no longer appear if we cut off the potential at a large distance R and subsequently make R tend to infinity after the eigenvalues have been determined from the S matrix.

Though the potential (27) becomes the potential (10) when R becomes infinitely large, the expression (28) goes over to (14) only when the imaginary part of k lies between $\pm 1/2a$. Above this region $S(k)\to\infty$ and below this region $S(k)\to 0$.

This is not the case, however, with the derivative of S with respect to $|k|$ at a point where (29) is satisfied. At such a point

$$\frac{dS}{d|k|}=-\exp(-2ikR)\frac{\dfrac{d\rho}{d|k|}\dfrac{d}{d\rho}\{J_{-i\rho}(\alpha)J_{i\rho+1}[\alpha\exp(-R/2a)]+J_{i\rho}(\alpha)J_{-i\rho-1}[\alpha\exp(-R/2a)]\}}{J_{-i\rho}(\alpha)J_{i\rho-1}[\alpha\exp(-R/2a)]+J_{i\rho}(\alpha)J_{-i\rho+1}[\alpha\exp(-R/2a)]}.$$

But for large values R

$$\frac{d}{d\rho}\{J_{-i\rho}(\alpha)J_{i\rho+1}[\alpha\exp(-R/2a)]\}\sim 0,$$

$$\frac{d}{d\rho}\{J_{i\rho}(\alpha)J_{-i\rho-1}[\alpha\exp(-R/2a)]\}\sim\frac{dJ_{i\rho}(\alpha)}{d\rho}J_{-i\rho-1}[\alpha\exp(-R/2a)],$$

$$J_{-i\rho}(\alpha)J_{i\rho-1}[\alpha\exp(-R/2a)]+J_{i\rho}(\alpha)J_{-i\rho+1}[\alpha\exp(-R/2a)]\sim J_{-i\rho}(\alpha)J_{i\rho-1}[\alpha\exp(-R/2a)],$$

so that

$$\frac{dS}{d|k|}\sim-\exp(-2ikR)\frac{dJ_{i\rho}(\alpha)}{d|k|}\frac{J_{-i\rho-1}[\alpha\exp(-R/2a)]}{J_{-i\rho}(\alpha)J_{i\rho-1}[\alpha\exp(-R/2a)]}\to-\left(\frac{\alpha}{2}\right)^{-2i\rho}\frac{\Gamma(i\rho)}{\Gamma(-i\rho)}\frac{dJ_{i\rho}(\alpha)}{d|k|}\Big/J_{-i\rho}(\alpha),$$

which is just the derivative of Eq. (14) with respect to $|k|$, whether the imaginary part of k is smaller or larger than $-1/2a$. From Eq. (9) we see that the expression $c_n\exp(-|k_n|r)$ represents the correct asymptotic behavior of the wave function for all the discrete states as $R\to\infty$. Now we have seen above that Eq. (28) tends to Eq. (14) as $R\to\infty$ for real values of k corresponding to positive energy states. It follows therefore that the S matrix for the cut-off exponential potential gives the correct asymptotic expression of the wave function for all the s states in the limit $R\to\infty$.

It is of interest to observe that for large values of R Eq. (28) differs very little from the expression

$$S(k)=-\exp(-2ikR)\times\frac{J_{i\rho}(\alpha)J_{-i\rho-1}[\alpha\exp(-R/2a)]}{J_{-i\rho}(\alpha)J_{i\rho-1}[\alpha\exp(-R/2a)]},\quad(30)$$

when k is real; but the behavior of Eq. (30) is quite different from that of Eq. (28) when k is complex. This example shows that the analytic continuation in the eigenvalue problem has to be carried out with great caution.

A somewhat different situation occurs in the case of the Coulomb potential cut off at a large distance R. As shown by Møller, we have for the s states

$$S(k)=(2kR)^{-2i/ka}\frac{\Gamma(1+i/ak)}{\Gamma(1-i/ak)},\quad(31)$$

where a is a negative constant for an attractive field. The eigenvalues are determined by the poles where

$$\Gamma(1+i/ak)=\infty,$$

from which we have

$$i/ak=-n\quad(n=1,2,3\cdots).$$

In the vicinity of the point $k=1/ian$,

$$S(k)\sim(-1)^{n+1}(2kR)^{2n}[\Gamma(n+1)]^{-2}k/(k-1/ani).$$

Hence by Eq. (7)

$$|c_n|^2=2\pi|k_n|(2R|k_n|)^{2n}[\Gamma(n+1)]^{-2}. \quad (32)$$

As $R\to\infty$, $S(k)$ tends to ∞ or 0 according as k is above or below the real axis, and $|c_n|\to\infty$. The expression

$$|c_n|\exp(-|k_n|R)=(2\pi|k_n|)^{\frac{1}{2}}(2R|k_n|)^n \times\Gamma(n+1)^{-1}\exp(-|k_n|R), \quad (33)$$

however, gives just the asymptotic value of $u_n(r)$ at $r=R$, as can be seen from the well-known expression for the radial wave function of the s states

$$u_n(r)=N_n r\exp(-|k_n|r)L_n^1(2|k_n|r),$$

where

$$N_n=[(2|k_n|)^3(n-1)!/2n(n!)^3]^{\frac{1}{2}}$$

and L_n^1 is an associated Laguerre polynomial.*

I wish to express my sincere gratitude to Professor Pauli for his advice on this work.

* *Note added in proof.*

The eigenvalues given by Eq. (18) are redundant because they are not given by the current scheme of quantum theory. They appear only when we determine the eigenvalues from the expression of $S(k)$ given by Eq. (14) without considering the behavior of the wave function in Eq. (12). Dr. D. ter Haar has recently informed me that according to a recent investigation of R. Jost, it is not sufficient to discard the redundant zeros in all cases on the basis of the inequality (21). It should be noted that the conclusion of the present paper, namely that Heisenberg's general condition given by Eq. (6) is not satisfied by the expression of $S(k)$ given by Eq. (14), is independent of the sign of inequality (21), and therefore holds even when the sign of (21) is changed.

PHYSICAL REVIEW VOLUME 71, NUMBER 3 FEBRUARY 1, 1947

The Invariant Form of Quantum Equations and the Schroedinger-Heisenberg Parallelism

E. M. CORSON
The Institute for Advanced Study, Princeton, New Jersey

(Received October 30, 1946)

Some years have passed since the appearance of Dirac's striking interpretation of the Heisenberg-Schroedinger parallelism in the equations of motion, and yet it appears that there still remain obscure points which have led to misunderstanding. Although the Schroedinger method suffices to deal with many practical problems, the flexibility of the Dirac-Jordan representation theory, aside from its intrinsic unity and beauty, recommends it to general theoretical investigation. The present paper considers the invariant form of the equations of motion in relation to the Schroedinger-Heisenberg pictures of quantum mechanics insofar as the latter refer to the "pictured" intrinsic motion of states (vectors) and observables (Hermitian operators). The discussion is divided roughly into 5-sections: Operator and Vector Transforms, Contact Transformations, Heisenberg-Schroedinger Operators, Equations of Motion and Invariant Properties, and the Density Operator and Operator Spur. Where possible, quasi-geometrical diagrams are given to illustrate the relation and transition between the several "pictures of the motion."

Notation:†

$\boldsymbol{\alpha}$, $\boldsymbol{\beta}$, $\mathbf{q}$, etc. (boldface type) = operators.
$|\rangle$ = state or coordinate vector in Hilbert space.
$\langle|=|\rangle^*$ = adjoint vector.
$|\rangle_r$ = transformed vector.
$\langle|\boldsymbol{\alpha}|\rangle=\langle|\cdot\boldsymbol{\alpha}\cdot|\rangle$ = general matrix element.
$|\alpha'\rangle$, α' = prototype eigenvector and eigenvalue belonging to operator $\boldsymbol{\alpha}$.

A. OPERATOR AND VECTOR TRANSFORMS

WHEN two dynamical variables $\boldsymbol{\alpha}_r$ and $\boldsymbol{\alpha}$ are related by an equation of the form

$$\boldsymbol{\alpha}_r=\mathbf{U}\boldsymbol{\alpha}\mathbf{U}^{-1}, \quad (1)$$

then we say that $\boldsymbol{\alpha}_r$ is the transform of $\boldsymbol{\alpha}$ under the similarity or collineatory transformation

† The notation here is that used in the author's forthcoming book on *Perturbation Calculus and Representation Theory.*

generated by the operator $\mathbf{U}$. Furthermore, if $\mathbf{U}$ is unitary, i.e., $\mathbf{U}^*=\mathbf{U}^{-1}$, then the transformation is termed unitary or conjunctive. Similarity transformations in general have the important property that two operators so related have the same eigenvalue spectrum, with the transformed eigenvectors given by

$$|\rangle_\tau=|\alpha_\tau'\rangle=\mathbf{U}|\alpha'\rangle. \tag{2}$$

Thus

$$\begin{aligned}&\boldsymbol{\alpha}|\alpha'\rangle=\alpha'|\alpha'\rangle,\\ &\boldsymbol{\alpha}_\tau\mathbf{U}|\alpha'\rangle=\mathbf{U}\boldsymbol{\alpha}\mathbf{U}^{-1}\mathbf{U}|\alpha'\rangle=\alpha'\mathbf{U}|\alpha'\rangle,\end{aligned} \tag{3}$$

showing that $\mathbf{U}|\alpha'\rangle$ is an eigen-$|\rangle$ of $\boldsymbol{\alpha}_\tau$ belonging to the eigenvalue $\alpha_\tau'=\alpha'$,[1] and conversely we can show that any eigenvalue of $\boldsymbol{\alpha}_\tau$ is also an eigenvalue of $\boldsymbol{\alpha}$. The unitary transformations have the additional important property that real observables (Hermitian operators) are transformed into real observables, and again all algebraic relations between operators and vectors are invariant. To verify these properties we note, first, that for $\boldsymbol{\alpha}$ and $\boldsymbol{\alpha}_\tau$ real,

$$\boldsymbol{\alpha}_\tau{}^*=\mathbf{U}^{-1*}\boldsymbol{\alpha}\mathbf{U}^*=\boldsymbol{\alpha}_\tau=\mathbf{U}\boldsymbol{\alpha}\mathbf{U}^{-1}, \tag{4a}$$

hence

$$\boldsymbol{\alpha}\mathbf{U}^*\mathbf{U}-\mathbf{U}^*\mathbf{U}\boldsymbol{\alpha}=[\boldsymbol{\alpha},\,\mathbf{U}^*\mathbf{U}]_-=0 \tag{4b}$$

which shows that $\mathbf{U}^*\mathbf{U}$ commutes with any linear operator,[2] and it follows that $\mathbf{U}^*\mathbf{U}$ is at most a scalar multiple of the identity operator. Without loss of generality we may take $\mathbf{U}^*\mathbf{U}=\mathbf{I}$, which condition characterizes unitary operators.

Similarly,

$$\begin{aligned}&(\boldsymbol{\alpha}+\boldsymbol{\beta})_\tau=\mathbf{U}(\boldsymbol{\alpha}+\boldsymbol{\beta})\mathbf{U}^*=\boldsymbol{\alpha}_\tau+\boldsymbol{\beta}_\tau,\\ &(\boldsymbol{\alpha}\boldsymbol{\beta})_\tau=\mathbf{U}(\boldsymbol{\alpha}\boldsymbol{\beta})\mathbf{U}^*=\mathbf{U}\boldsymbol{\alpha}\mathbf{U}^*\mathbf{U}\boldsymbol{\beta}\mathbf{U}^*=\boldsymbol{\alpha}_\tau\boldsymbol{\beta}_\tau,\end{aligned} \tag{5}$$

and, in particular, for

$$\boldsymbol{\xi}=\boldsymbol{\xi}(\boldsymbol{\alpha},\,\boldsymbol{\beta});\quad \boldsymbol{\xi}_\tau=\mathbf{U}\boldsymbol{\xi}\mathbf{U}^*=\boldsymbol{\xi}(\boldsymbol{\alpha}_\tau,\,\boldsymbol{\beta}_\tau)$$

which may be readily verified using the general definition of well-ordered functions of observables.

[1] With the convention that $\boldsymbol{\alpha}$ and $\boldsymbol{\alpha}_\tau$ with the same number of primes denote the same number, e.g., $\alpha_\tau'=\alpha'$, but it is necessary to retain both symbols for this common eigenvalue to preserve the properties and meaning of symbols such as $\langle\alpha'|\alpha_\tau'\rangle$, $\langle\alpha'|\boldsymbol{\beta}|\alpha_\tau'\rangle$, etc.

[2] Decomposing any linear operator into the sum of a Hermitian and anti-Hermitian operator.

B. CONTACT TRANSFORMATIONS

A contact transformation in quantum as well as in classical mechanics is defined as a transformation from one set of canonical coordinates and momenta, $\mathbf{q}_r$, $\mathbf{p}_r$ say, to another $\mathbf{q}_{rr}$, $\mathbf{p}_{rr}$. The quantal condition for a set of variables to be canonical is the commutator $[\mathbf{q}_r,\,\mathbf{p}_r]_-=i\hbar$, and being algebraic is much simpler than its classical counterpart, though more restrictive.[3] The quantal contact transformations are in fact simply a special case of the unitary transformations mentioned above, as is intrinsically evident from the required invariance of the commutator. To show this explicitly we investigate the transformation from the canonical variables $\mathbf{q}_r$, $\mathbf{p}_r$ to $\mathbf{q}_{rr}$, $\mathbf{p}_{rr}$, and to this end we first introduce the two representations in which the $\mathbf{q}$'s and $\mathbf{q}_r$'s, respectively, are diagonal; the phases being so chosen that the correspondence $\langle'q|\mathbf{p}|''q\rangle=-i\hbar\delta'('q-''q)$[4] holds for both in their respective variables.

The linear operator $\mathbf{U}$ is defined by its mixed representative

$$\langle'q_r|\mathbf{U}|''q\rangle=\delta('q_r-''q),^5 \tag{6}$$

and is readily seen to be unitary since

$$\begin{aligned}\langle'q|\mathbf{U}|''q\rangle&=\int\langle'q|'''q_r\rangle d'''q_r\langle'''q_r|\mathbf{U}|''q\rangle\\ &=\langle'q|''q_r\rangle\end{aligned} \tag{7}$$

so that

$$\begin{aligned}\langle'q|\mathbf{U}\mathbf{U}^*|'''q\rangle&=\int\langle'q|\mathbf{U}|''q\rangle d''q\langle''q|\mathbf{U}^*|'''q\rangle\\ &=\int\langle'q|''q_r\rangle d''q_r\langle''q_r|'''q\rangle\\ &=\delta('q-'''q)=\langle'q|\mathbf{I}|'''q\rangle.\end{aligned} \tag{8}$$

[3] True canonical quantum variables must have continuous eigenspectra, and hence the class of such variables in quantum theory is strictly limited. See P. A. M. Dirac, *Quantum Mechanics* (Oxford University Press, New York, 1935). E. M. Corson, Phys. Rev. 70, 728 (1946).

[4] The primes slanted to the left indicate the complete representation, i.e., the complete set of commuting observables, e.g.,

$$\begin{aligned}\langle'q|\mathbf{p}_r|''q\rangle=-i\hbar&\delta(q_1'-q_1'')\cdots\delta(q_{r-1}'-q_{r-1}'')\\ &\times\delta'(q_r'-q_r'')\delta(q_{r+1}'-q_{r+1}'')\cdots\delta(q_n'-q_n'').\end{aligned}$$

[5] The δ function here is meaningful because of the fact that the eigenvalues of $\mathbf{q}_r$ and $\mathbf{q}$ range over the same infinite spectrum, from $-\infty$ to ∞.

Further

$$\langle {}'q_\tau | \mathbf{q}_{\tau\tau}\mathbf{U} | {}''q\rangle = q_{\tau\tau}'\delta({}'q_\tau - {}''q),$$
$$\langle {}'q_\tau | \mathbf{U}\mathbf{q}_\tau | {}''q\rangle = \delta({}'q_\tau - {}''q)q_\tau'', \tag{9}$$

and the equality of these expressions gives

$$\mathbf{q}_{\tau\tau} = \mathbf{U}\mathbf{q}_\tau\mathbf{U}^{-1} = \mathbf{U}\mathbf{q}_\tau\mathbf{U}^*. \tag{10}$$

Similarly,

$$\langle {}'q_\tau | \mathbf{p}_{\tau\tau}\mathbf{U} | {}''q\rangle = -i\hbar\partial/\partial q_{\tau\tau}'\delta({}'q_\tau - {}''q),$$
$$\langle {}'q_\tau | \mathbf{U}\mathbf{p}_\tau | {}''q\rangle = i\hbar\partial/\partial q_\tau''\delta({}'q_\tau - {}''q), \tag{11}$$

from which it follows that

$$\mathbf{p}_{\tau\tau} = \mathbf{U}\mathbf{p}_\tau\mathbf{U}^*. \tag{12}$$

The concept of contact transformations in quantum mechanics can be extended to include dynamical systems for which no canonical coordinates and momenta exist in the strict sense, by defining such transformations as simply unitary. This generalization corresponds to the fact that the invariant properties associated with unitary transformations give them importance in their own right, whereas true contact transformations are an important but special case.

C. SCHROEDINGER-HEISENBERG OPERATORS

We consider the special contact transformation generated by the unitary operator $\mathbf{U} = \exp(i\mathbf{H}t/\hbar)$ where t is the time and $\mathbf{H}$ is the Hamiltonian operator of the dynamical system of interest, which at present is assumed not to depend explicitly on t.

Then if the $\mathbf{q}$'s and their eigenvectors $|{}'q\rangle$ are constant,[6] satisfying the equations

$$\frac{d}{dt}|{}'q\rangle = 0, \quad \frac{d}{dt}\mathbf{q} = 0, \tag{13}$$

their transforms $\mathbf{q}_\tau = \mathbf{U}\mathbf{q}\mathbf{U}^*$ and $|{}'q_\tau\rangle = \mathbf{U}|{}'q\rangle$ must satisfy the equations

$$\left.\begin{aligned} i\hbar\frac{d}{dt}|{}'q_\tau\rangle &= -\mathbf{H}|{}'q_\tau\rangle, \\ i\hbar\frac{d}{dt}\mathbf{q}_\tau &= \mathbf{q}_\tau\mathbf{H} - \mathbf{H}\mathbf{q}_\tau = [\mathbf{q}_\tau, \mathbf{H}]_- \end{aligned}\right\} \tag{14}$$

since

$$\frac{d}{dt}\mathbf{U} = \frac{i}{\hbar}\mathbf{H}\mathbf{U} \quad \text{and} \quad \frac{d}{dt}\mathbf{U}^* = -\frac{i}{\hbar}\mathbf{U}^*\mathbf{H}. \tag{15}$$

For algebraic functions[7] of non-commuting observables we can readily verify that $\xi(\mathbf{q}_\tau, \mathbf{p}_\tau) = \xi_\tau = \mathbf{U}\xi\mathbf{U}^*$, and if ξ does not explicitly depend on the time it follows that ξ_τ satisfies the equation[8]

$$i\hbar\frac{d\xi_\tau}{dt} = \xi_\tau\mathbf{H} - \mathbf{H}\xi_\tau. \tag{16}$$

This result, which is Heisenberg's equation of motion for functions of observables, may also be derived (as shown by Dirac) by noting that if the *basic* vectors obey the relation

$$i\hbar\frac{d}{dt}|\rangle = -\mathbf{H}|\rangle \tag{17}$$

then an observable attached to this "moving" system of coordinates may be characterized by the equation

$$\xi_\tau|a\rangle = |b\rangle \tag{18}$$

where $|a\rangle$ are $|b\rangle$ are vectors embedded in the moving representation. From (18) we obtain

$$i\hbar\frac{d}{dt}\xi_\tau|a\rangle - \xi_\tau\mathbf{H}|a\rangle = -\mathbf{H}|b\rangle = -\mathbf{H}\xi_\tau|a\rangle, \tag{19}$$

from which (16) follows since $|a\rangle$ is arbitrary. Both systems (13) and (14) form proper repre-

[6] In the following discussion it will be seen that the index τ for "transformed" can in many cases be read as "time dependent" with equal meaning. However, zero subscripts corresponding to initial values are by custom usually omitted as the sense will always be clear from the equations and context. Obviously, an eigenvalue per se, with index merely identifies the observables in question in accord with the convention of footnote 1, and does not imply time dependence.

[7] Thus far it has been possible to define only algebraic, well-ordered functions unambiguously in quantum theory, and this limitation has greatly hampered further development of theory. See, however, P. A. M. Dirac, Rev. Mod. Phys. 17, 195 (1945).

[8] When ξ involves t explicitly, as for example the density operator ρ (Section E), the above equation must be generalized to

$$i\hbar\frac{d}{dt}\xi_\tau = i\hbar\frac{\partial}{\partial t}\xi_\tau + [\xi_\tau, \mathbf{H}]_-$$

which again exactly parallels the classical Hamiltonian equations of motion.

sentations (actually a single infinity of bases) and it is convenient to refer to these coordinate systems and attached operators as "fixed" and "moving," respectively.[9] We may note that **H** has at any time the same functional form in terms of the dynamical variables of either system (13) or (14), but in the latter, as in (16)–(19), these dynamical variables are represented by moving linear operators. However, for the operator **H**, this distinction is in general of a trivial nature owing to the special form of the generator **U**.

In the previous discussion we introduced an ordinary time variable in an indirect and somewhat incidental way as a parameter in a particular unitary transformation, and it thus appears that the time plays a rather subsidiary parametric role in quantum theory. This is in fact broadly speaking the case, in the sense that it is not possible to introduce an observable (operator) which would represent the time.[10]

In particular the frequently met statement that "the time and the negative of the Hamiltonian are canonically conjugate in analogy with classical mechanics" is quite incorrect, and particularly surprising in view of the well-known quantum condition for canonical conjugacy and its corollary requirement of continuous eigenvalue spectra which so sharply restrict this class of dynamical variables.

The final point which we must consider to round out the essential structure of the theory is the relation between states, or equivalently, the vectors which represent them, at successive instants in time. In classical theory the equations of motion are relations between dynamical variables at different times, while in quantum theory they must be expected ultimately to be relations between the *average* values of the variables at different times, since the symbolic scheme is given physical content by virtue of the basic postulate that the number $\langle\xi\rangle=\langle|\xi|\rangle$ is the expectation or average value of the observable ξ for the physical state $|\rangle$ provided the latter is suitably normalized.

Of course we cannot derive the equations of motion on purely epistemological grounds, but we can show that the invariance of our symbolic equations under unitary transformations leads to several equivalent and equally fundamental formulations. In particular, we observe that states and dynamical variables are not prescribed by uniquely determined vectors and operators since we may pass from any original set to the transforms $|\rangle\rightarrow\mathbf{U}|\rangle$, $\xi\rightarrow\mathbf{U}\xi\mathbf{U}^*$, etc., obtaining the same physical results. Hence what we must ultimately determine is the value of the expression

$$d/dt\langle\xi\rangle, \tag{20}$$

and we must not impute any absolute significance to the equations of motion insofar as this term usually refers to the "pictured" intrinsic motion of states and observables.

D. CHANGE OF STATES IN TIME. EQUATIONS OF MOTION

We extend the usual 3-dimensional sense of superposition of states by the assumption that the principle also holds in 4 dimensions, which from the former point of view simply means that states, that are linear combinations of other states at one instant of time, remain so at all times. This implies that all states of a system vary with time, if at all, according to a law of the form

$$|\,;t+\delta t\rangle=\mathbf{G}(t+\delta t,\,t)\,|\,;t\rangle,^{11} \tag{21}$$

where **G** is an infinitesimal linear operator which is assumed to be of the form $\exp(-i\mathbf{H}\delta t/\hbar)$, so that $i\hbar(d/dt)\,|\,;t\rangle=\mathbf{H}\,|\,;t\rangle$ and its conjugate

$$i\hbar\frac{d}{dt}\langle\,;t|=-\langle\,;t|\,\mathbf{H}. \tag{22}$$

Either of these equations may be called Schroedinger's wave equation, although this term is more familiar in reference to their representative forms. If we apply the unitary transformation generated by **U**, again assuming **H** to be constant in time, we obtain an alternative (Heisenberg) law for the time dependence of physical states,

[9] As we shall explain later, they are representations in what are called the Schroedinger and Heisenberg pictures of quantum mechanics.

[10] This remains true in the relativistic formulation even though the space-time variables are essentially on a mathematically equal footing.

[11] In this equation, which might be termed the Schroedinger postulate, the time dependence is indicated by the time variable after the semi-colon, to separate it from the quantum variables.

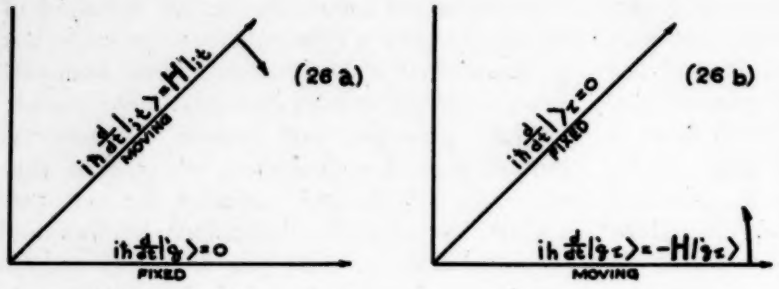

FIG. 1. Geometrical picture of different formulations of the wave equation.

namely $ih(d/dt)|\rangle_\tau=0$ where

$$|\rangle_\tau=\mathbf{U}|\,;t\rangle=|\,;0\rangle. \tag{23}$$

The laws (22) and (23), combined with the results of Section C, define equivalent quantum-mechanical equations which are termed the Schroedinger and Heisenberg pictures.

In tabular form

	S-picture	*H*-picture
States as vectors:	*I*A. moving: $ih(d/dt)|\,;t\rangle=\mathbf{H}|\,;t\rangle$	*II*A. fixed: $ih(d/dt)|\rangle_\tau=0$
Dynamical variables as linear operators:	*I*B. fixed: $ih(d/dt)\xi=0$	*II*B. moving: $ih(d/dt)\xi_\tau=[\xi_\tau,\mathbf{H}]_-$

To these we might properly add the corresponding equations governing representation in these pictures, namely (13) and (14), but it is usual to find only *I*A. and *II*B. mentioned as equations of motion. We may quite literally say that quantities fixed in the *S*-picture are moving in the *H*-picture, and conversely. The correspondence being such that if $|1\rangle$, $|2\rangle$ denote states[12] satisfying the equations of motion (in either picture) and ξ denotes any dynamical variable (in the corresponding picture) not explicitly dependent on t, then

$$ih\frac{d}{dt}\langle 1|\xi|2\rangle=\langle 1|\xi\mathbf{H}-\mathbf{H}\xi|2\rangle \tag{24}$$

and in particular

$$ih\frac{d}{dt}\langle\xi\rangle=\langle[\xi,\mathbf{H}]_-\rangle \tag{25}$$

which is the invariant form of the equations of motion, being independent of the picture used. To these one might add the invariant form of the wave equation (27) below.

[12] Here we might have written $|1;t\rangle$, ξ_τ etc., the meaning of the indices depending on the picture, but as in most discussions, no distinguishing subscripts are used since strictly speaking ξ and ξ_τ represent the same observable and similarly for the state vectors $|\rangle$. The spirit of quantum theory permits no rigid distinction, and it is not uncommon to use ξ (without index) with both meanings in a single equation, the distinction being clear from the context.

Equations (24)–(25) simply express the fact that in consequence of the linear and invariant properties of equations in quantum mechanics, the development or behavior of a system in time may be described as a development of the states themselves, the observables remaining constant equal to the value of the dynamical variables corresponding to the initial time, or conversely.

The practical way of writing Eqs. (22) and (23) is in terms of representations, and as we have shown they must lead to identical physical results. If, for example, we take a representation in which the coordinate observables are diagonal,[13] which means that we take the representation (13) together with the equations of motion (22), or (14) with (23), then these lead to the familiar form of Schroedinger's wave equation.

S-picture:

$$ih\frac{d}{dt}\langle'q|\,;t\rangle=\int\langle'q|\mathbf{H}|''q\rangle d''q\langle''q|\,;t\rangle$$
$$=H_{op}\langle'q|\,;t\rangle. \tag{26a}$$

H-picture:

$$ih\frac{d}{dt}\langle'q_\tau|\rangle_\tau=\int\langle'q_\tau|\mathbf{H}|''q_\tau\rangle d''q_\tau\langle''q_\tau|\rangle_\tau$$
$$=H_{op}\langle'q_\tau|\rangle_\tau. \tag{26b}$$

[13] Logically this may be called Schroedinger's representation in either picture, but it is customary to reserve this term for the former fixed representation (13).

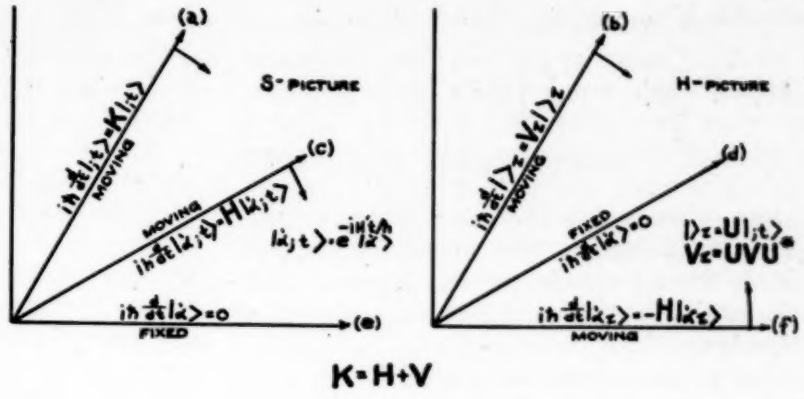

FIG. 2. Geometrical picture of possible representations when the basic states are all eigenstates of the Hamiltonian.

The invariant form would then be

$$i\hbar\frac{d}{dt}\langle'q|\rangle=\langle'q|\mathbf{H}|\rangle. \tag{27}$$

The difference is viewpoint in the above formulations of the wave equation is perhaps best seen in a geometrical picture,[14] Fig. 1.

It is thus permissible to speak of the wave equation in the *S*- and *H*-pictures, which are of course identical, as differing geometrically in the sense that the time dependence enters the generalized direction cosine (probability amplitude) from the right and left, respectively; i.e., in the former it is introduced through the dependence of the states themselves, while in the latter the time dependence is put into the representation. It is important to understand that the **q**-diagonal Schroedinger representation is only a special case, though unquestionably the most important, of a whole class of representations which have the common property of being fixed, and lead to wave equations of the form (26a). Whether or not the right-hand side of the wave equation involves a sum, or integral, or both, depends on the eigenvalue spectrum of the observables defining the representation.

The Schroedinger equation (26a) is perfectly general, and we now wish to specialize to the case of a dynamical system for which **H** is constant, i.e., in which there are no exterior forces varying with time. Then there are solutions of the form[15]

$$\langle'q|'\alpha;t\rangle=\langle'q|'\alpha\rangle e^{-iH't/\hbar} \tag{27a}$$

with

$$\int\langle'q|\mathbf{H}|''q\rangle d''q\langle''q|'\alpha\rangle=H'\langle'q|'\alpha\rangle. \tag{27b}$$

Here $\boldsymbol{\alpha}$ indicates **H** and such other observables which combine with **H** to form a complete commuting set of which $|\alpha'\rangle$ is a typical eigenvector. According to footnote 8, a function of the dynamical variables not explicitly dependent on the time is a constant if it commutes with **H**. Such variables are the "constants of the motion," and since they must commute with **H** at all times, this usually requires that **H** be a constant (in time). The constancy of **H** in the Heisenberg picture means that $\partial\mathbf{H}/\partial t=0$, or that **H** itself does not involve t explicitly and hence is a constant in the *S*-picture too. Since the constants of the motion satisfy the condition $(d/dt)\boldsymbol{\alpha}=0$ in either picture ($\boldsymbol{\alpha}_\tau=\mathbf{U}\boldsymbol{\alpha}\mathbf{U}^*=\boldsymbol{\alpha}$), there is a certain inherent redundancy in the notation in this case. We retain the "transform" subscript, etc., in the present discussion, however, to conform with the general scheme of presentation.

Equation (27b) is the standard equation for determining the eigenvalues of **H**, and hence when **H** does not involve t explicitly there exist solutions, periodic in time of the above form with H' an eigenvalue of **H**. This special kind of state is such that the average value of an ob-

[14] The moving vectors in the diagram are indicated as though rotating, although this is admittedly a somewhat loose description.

[15] We consider only (26a) to avoid needless repetition, since (26b) leads to the same conclusions with but slight change in notation.

servable is independent of time, since

$$\langle \xi \rangle = \langle `\alpha; t | \xi | `\alpha; t \rangle = \int\int \langle `\alpha; t | `q \rangle \times d`q \langle `q | \xi | ``q \rangle d``q \langle ``q | `\alpha; t \rangle,^{16} \quad (28)$$

which according to (27a) is independent of t. Thus the probability of obtaining any particular result when we make an observation is independent of the time, and such states are termed "stationary."

Let us now consider the representation we get when we take the stationary states to be the *basic* states. From the respective equations of motion we obtain the geometrical picture (Fig. 2) of the various possible representations when the basic states are all *eigenstates of the Hamiltonian.*[17]

Representation (c) with the constants of the motion $\boldsymbol{\alpha}$ diagonal is moving in the S-picture and is therefore fixed in the H-picture (d). Alternatively, we can introduce a representation with the $\boldsymbol{\alpha}$'s diagonal which is fixed in the S-picture (e) and is thus moving in the H-picture (f). In this special case there is as indicated above a duplicity of motation since (c) is related to (e) and (d) by the same phase factor, and likewise (f) to (e) and (d). We would prefer to keep the notation consistent within each picture, but this should cause no difficulty. The fixed representations in the two pictures, namely (e) and (d), differ only in that the basic vectors of the Heisenberg representation (d) satisfy the equations of motion *II*A. Nevertheless, in the equation

$$\langle `\alpha | ; t \rangle = \langle `\alpha | \rangle_\tau e^{-iH't/\hbar}$$

the left- and right-hand representatives are sometimes referred to as the Schroedinger and Heisenberg representatives of the "same" state. Actually the two representations do not differ in phase, except as a figure of speech, since the phase difference in the representatives arises from the fact that $|;t\rangle$ and $|\rangle_\tau = \mathbf{U}|;t\rangle$ (referring now, as in the Fig. 2, to states specified by the Hamiltonian $\mathbf{K}$) represent the same state, but in different pictures.

It should be noted that the representative of an observable ξ [12] in the representations (c) and (d) varies according to the Heisenberg law . . . constant $\exp i(H'-H'')t/\hbar$, the constant being the representative of ξ in (e) and (f), respectively. The above diagram also illustrates the exception to the fixed-moving parallelism between the two pictures, which arises when we compare systems with different Hamiltonians, e.g., $\mathbf{H}$ amd $\mathbf{K}=\mathbf{H}+\mathbf{V}$ above. The equation of motion of state (a) when expressed in the fixed Schroedinger type representation (e) leads to the Schroedinger wave equation.

$$i\hbar \frac{d}{dt}\langle `\alpha | ; t \rangle = \sum_{``\alpha} \langle `\alpha | \mathbf{K} | ``\alpha \rangle \langle ``\alpha | ; t \rangle = H' \langle `\alpha | ; t \rangle + \sum_{``\alpha} \langle `\alpha | \mathbf{V} | ``\alpha \rangle \langle ``\alpha | ; t \rangle. \quad (29)$$

Assuming a discrete spectrum for definiteness. The same result with appropriate change of notation is obtained for the transformed state vector $|\rangle_\tau$, i.e., (b) relative to the moving Heisenberg axes (f). This equation may be ascribed as giving the variation with time of the direction cosine between (a) and (e), or equivalently (b) and (f), due to $\mathbf{K}$. Whichever picture we adopt to obtain (29), the matrix of $\mathbf{V}$ (or $\mathbf{V}_\tau$) appearing therein is constant except insofar as $\mathbf{V}$ itself involves t explicitly. In perturbation problems, one is usually more interested in the separate effect of the perturbing potential $\mathbf{V}$ when considered from the point of view of the unperturbed system defined by $\mathbf{H}$. Or as we may say, we consider only the variation in the direction cosine between (a) and (c), or (b) and (d), due to the added potential $\mathbf{V}$.

In the H-picture we have

$$i\hbar \frac{d}{dt}\langle `\alpha | \rangle_\tau = \sum_{``\alpha} \langle `\alpha | \mathbf{V}_\tau | ``\alpha \rangle \langle ``\alpha | \rangle_\tau, \quad (30)$$

and in the S-picture

$$i\hbar \frac{d}{dt}\langle `\alpha; t | ; t \rangle = \sum_{``\alpha} \langle `\alpha; t | \mathbf{V} | ``\alpha; t \rangle \langle ``\alpha; t | ; t \rangle. \quad (31)$$

---

[16] In the H-picture

$$\tau\langle `\alpha | \xi_\tau | `\alpha \rangle_\tau = \int\int \tau\langle `\alpha | `q_\tau \rangle d`q_\tau \langle `q_\tau | \xi_\tau | ``q_\tau \rangle d``q_\tau \langle ``q_\tau | `\alpha \rangle_\tau$$

which gives the same result; indeed $\langle `q_\tau | \xi_\tau | ``q_\tau \rangle$ is constant, and this condition characterizes a moving basis in the $H$-picture, just as the constancy of $\langle `q | \xi | ``q \rangle$ characterizes a fixed basis in the S-picture.

[17] Properly, only the stationary state representation in the H-picture is called the Heisenberg representation, since it was the first discovered in quantum mechanics; Heisenberg (1925).

These equations are of course identical, and the essential point to note is that, in both, the matrix of $\mathbf{V}$ varies rapidly according to the Heisenberg law $\sim\exp i(H'-H'')t/\hbar$, aside from any explicit dependence of $\mathbf{V}$ on t.

In general theoretical work one may use one or other general picture as convenience dictates, and it is not ordinarily necessary to use distinguishing indices or subscripts as we have done here for emphasis. A note of caution may be added to the effect that although it is customary to give the laws of motion in the previously mentioned limited form (*I*A, *II*B), and we may for reasons of convenience pass back and forth from the *S*- to *H*-pictures; they do not hold simultaneously.

Thus as a final illustration

$$\langle|\xi_\tau|\rangle=\int\langle|'q_\tau\rangle d'q_\tau\langle'q_\tau|\xi_\tau|''q_\tau\rangle d''q_\tau\langle''q_\tau|\rangle$$
$$=\int\langle;t|'q\rangle d'q\langle'q|\xi|''q\rangle d''q\langle''q|;t\rangle \tag{32}$$
$$=\langle;t|\xi|;t\rangle$$

which follows immediately from the transformation theory.

E. THE DENSITY OPERATOR

Quite frequently we have to deal with dynamical systems whose specification is less complete than heretofore considered, in the sense that it may be unnecessary or even impossible to know that the dynamical system is in a specified state at a given time. Instead, the available information may be only that the system is to be found in one or another of a number of accessible states according to a given probability distribution.

The problem thus stated is essentially a statistical one, and in classical theory leads to the concepts of the Gibbs ensemble, phase space, etc., the details of which are of no great interest in the present connection. Here we need only recall the well-known fact that the concept of phase space has, strictly speaking, no meaning in quantum mechanics due to the non-commutation of canonical coordinates and momenta which precludes the simultaneous assignment of the values required to specify a phase space. Nonetheless, there exists a close quantal analogy to the classical "density in phase," and it is primarily the mathematics of this "quantum density" which we wish to consider here. We introduce the density operator here because it has in consequence of its definition certain apparently anomalous properties which can cause confusion, and seem best disposed of while we are considering the general equations of motion.

Let us suppose that it is given that P_n is the probability that a dynamical system under study is at a certain time in the nth state $|n;t\rangle$ of a certain set of states accessible to it. Here we are implicitly assuming that the set of states cover a discrete range as indicated by the ordinal parameter n; the extension to the case of a continuous or mixed range being trivial. As indicated, we are at present considering the *S*-picture (states as moving vectors) and in an arbitrary representation determined by the fixed operators ξ whose eigenspectrum may be taken as continuous for definiteness, the wave functions will appear as $\langle'\xi|n;t\rangle$, etc.

For a single state the probability that the ξ's have values in the range $d'\xi$ at ξ', is $|\langle'\xi|;t\rangle|^2$, and hence for the given distribution in the present case the corresponding probability will be

$$\sum_n|\langle'\xi|n;t\rangle|^2P_n. \tag{33}$$

This expression can be formally interpreted as a diagonal element of the quantum density operator ϱ, defined directly by the tensor or outer product

$$\varrho=\sum_n|n;t\rangle P_n\langle n;t|=\sum_n\mathbf{U}^*|n\rangle P_n\langle n|\mathbf{U}, \tag{34}$$

or by its representative which is actually more general[18]

$$\langle'\xi|\varrho|''\xi\rangle=\sum_n\langle'\xi|n;t\rangle P_n\langle n;t|''\xi\rangle. \tag{35}$$

The density operator is a rather exceptional if not hybrid construct since its representative in a fixed Schroedinger type representation as defined by (35) obviously varies with time. This is simply due to the fact that ϱ spans a set of moving physical states, and hence itself explicitly varies with time (Eq. (38)) in the *S*-picture

[18] Since in the approximate treatment of many-particle problems, ϱ can always be defined through (35) even when the form (34) cannot be written explicitly.

in contrast to the more familiar observables which do not explicitly depend on time. The transform of (34) defines the density operator ϱ_τ in the H-picture as

$$\varrho_\tau = \mathbf{U}\varrho\mathbf{U}^* = \sum_n |n\rangle P_n \langle n| \tag{36}$$

and

$$\langle {}'\xi_\tau | \varrho_\tau | {}''\xi_\tau \rangle = \sum_n \langle {}'\xi_\tau | n\rangle P_n \langle n | {}''\xi_\tau \rangle. \tag{37}$$

The Heisenberg density operator will also vary unusually with time since $\langle {}'\xi_\tau | \varrho_\tau | {}''\xi_\tau \rangle$ varies with time instead of being constant, as it would be for a simply moving observable. In fact we shall find that ϱ_τ itself is constant. The equation of motion of the density operator is most easily obtained by differentiating (34), which gives

$$ih\frac{\partial}{\partial t}\varrho = \mathbf{H}\varrho - \varrho\mathbf{H} = -[\varrho, \mathbf{H}]_-, \tag{38}$$

P_n being a constant so long as the system is undisturbed.[19]

It immediately follows that

$$ih\frac{d}{dt}\varrho_\tau = 0, \tag{39}$$

which is also quite obvious from the constancy of $|\rangle$ in the definition (35). The formal definition of the density operator is especially convenient since from (34) it is trivially evident that ϱ is Hermitian.[20] Further it is readily seen that ϱ has only positive eigenvalues, thus paralleling the non-negative character of the classical density in phase. Thus if $|\rho'\rangle$ be an eigen-$|\rangle$ of ϱ, we have

$$\sum_n |n; t\rangle P_n \langle n; t | \rho'\rangle = \rho' |\rho'\rangle \tag{40a}$$

and

$$\sum_n P_n |\langle n; t | \rho'\rangle|^2 = \rho' \langle \rho' | \rho'\rangle, \text{ i.e., } \rho' > 0.^{21} \tag{40b}$$

For a system distributed over the various states in this manner, the average value of an observable α will be

$$\begin{aligned}\langle\alpha\rangle &= \sum_n P_n \langle n; t | \alpha | n; t\rangle \\ &= \int\int \sum_n P_n \langle n; t | {}'\xi\rangle d'\xi \langle {}'\xi | \alpha | {}''\xi\rangle d''\xi \langle {}''\xi | n; t\rangle \\ &= \int\int \langle {}'\xi | \alpha | {}''\xi\rangle d''\xi \langle {}''\xi | \varrho | {}'\xi\rangle d'\xi \\ &= \int \langle {}'\xi | \alpha\varrho | {}'\xi\rangle d'\xi.\end{aligned} \tag{41}$$

The average value of an observable is given by summing or integrating the product $\alpha\varrho$ along the diagonal, over the eigenvalue spectrum of the observables defining the representation. This diagonal sum, or integral (or both) is called the spur of the operator product, and for any representation satisfies the conditions

$$Sp(\alpha\beta\gamma) = Sp(\beta\gamma\alpha) = Sp(\gamma\alpha\beta). \tag{42}$$

The spur of a product of operators is invariant under cyclic interchange, and also under unitary transformation.

Thus the physical content of the quantum equations of motion can be written most concisely in the form

$$\langle\alpha\rangle = Sp(\varrho\alpha), \tag{43}$$

$$\begin{aligned}ih\frac{d}{dt}\langle\alpha\rangle &= Sp(ih\dot{\varrho}\alpha) \\ &= Sp\{\varrho(\alpha\mathbf{H} - \mathbf{H}\alpha)\} = \langle\alpha\mathbf{H} - \mathbf{H}\alpha\rangle.\end{aligned} \tag{44}$$

ACKNOWLEDGMENT

The author takes the opportunity to express his appreciation to Professor P. A. M. Dirac for his courtesy in reading this paper, and to Professor S. T. Ma for helpful discussions of the subject matter.

[19] The same result may be obtained somewhat less directly from the definition (35), and similarly (39) from (37).

[20] Noting that $|a\rangle\langle b|^* = |b\rangle\langle a|$ and that $0 \leq P_n \leq 1$.

[21] Alternatively: $\varrho - \varrho^2 = \sum_n P_n(1 - P_n)|n; t\rangle\langle n; t|$ from which $0 \leq \rho' \leq 1$.

Letters to the Editor

PUBLICATION of brief reports of important discoveries in physics may be secured by addressing them to this department. The closing date for this department is, for the issue of the 1st of the month, the 8th of the preceding month and for the issue of the 15th, the 23rd of the preceding month. No proof will be sent to the authors. The Board of Editors does not hold itself responsible for the opinions expressed by the correspondents. Communications should not exceed 600 words in length.

On the Disintegration of Negative Mesons

M. CONVERSI, E. PANCINI, AND O. PICCIONI*
Centro di Fisica Nucleare del C. N. R. Istituto di Fisica dell'Università di Roma, Italia

December 21, 1946

IN a previous Letter to the Editor,[1] we gave a first account of an investigation of the difference in behavior between positive and negative mesons stopped in dense materials. Tomonaga and Araki[2] showed that, becuase of the Coulomb field of the nucleus, the capture probability for negative mesons at rest would be much greater than their decay probability, while for positive mesons the opposite should be the case. If this is true, then practically all the decay processes which one observes should be owing to positive mesons.

Several workers[3] have measured the ratio η between the number of the disintegration electrons and the number of mesons stopped in dense materials. Using aluminum, brass, and iron, these workers found values of η close to 0.5 which, if one assumes that the primary radiation consists of approximately equal numbers of positive and negative mesons, support the above theoretical prediction. Auger, Maze, and Chaminade,[4] on the contrary, found η to be close to 1.0, using aluminum as absorber.

Last year we succeeded in obtaining evidence of different behavior of positive and negative mesons stopped in 3 cm of iron as an absorber by using magnetized iron plates to concentrate mesons of the same sign while keeping away mesons of the opposite sign (at least for mesons of such energy that would be stopped in 3 cm of iron). We obtained results in agreement with the prediction of Tomonaga and Araki. After some improvements intended to increase the counting rate and improve our discrimination against the "mesons of the opposite sign," we continued the measurements using, successively, iron and carbon as absorbers. The recording equipment was one which two of us had previously used in a measurement of the meson's mean life.[5] It gave threefold (III) and fourfold (IV) delayed coincidences. The difference (III)−(IV) (after applying a slight correction for the lack of efficiency of the fourfold coincidences) was owing to mesons stopped in the absorber and ejecting a disintegration electron which produced a delayed coincidence. The minimum detected delay was about 1 μsec. and the maximum about 4.5 μsec. Our calculations of the focusing properties of the magnetized plates (20 cm high; $\beta = 15{,}000$ gauss) and including roughly the effects of scattering, showed that we should expect almost complete cut-off for the "mesons of the opposite sign." This is confirmed by our results, since otherwise it would be very hard to explain the almost complete dependence on the sign of the meson observed in the case of iron.

TABLE I. Results of measurements on β-decay rates for positive and negative mesons.

Sign	Absorber	III	IV	Hours	M/100 hours
(a) +	5 cm Fe	213	106	155.00′	67±6.5
(b) −	5 cm Fe	172	158	206.00′	3
(c) −	none	71	69	107.45′	−1
(d) +	4 cm C	170	101	179.20′	36±4.5
(e) −	4 cm C+5 cm Fe	218	146	243.00′	27±3.5
(f) −	6.2 cm Fe	128	120	240.00′	0

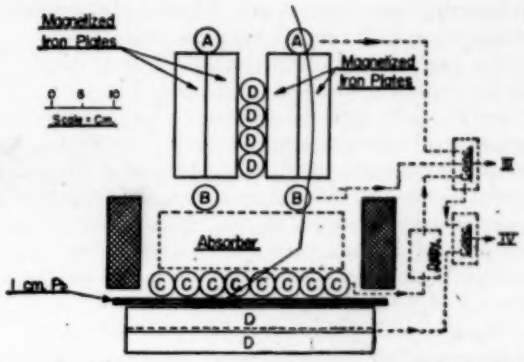

FIG. 1. Disposition of counters, absorber, and magnetized iron plates. All counters "D" are connected in parallel.

The results of our last measurements with two different absorbers are given in Table I. In this table "Sign" refers to the sign of the meson concentrated by the magnetic field. $M = (\text{III}) - (\text{IV}) - P(\text{IV})$, the number of decay electrons, is corrected for the lack of efficiency (p) in our fourfold coincidences (~ 0.046).

The value M_- (5 cm Fe) is but slightly greater than the correction for the lack of efficiency in our counting, so that we can say that perhaps no negative mesons and, at most, only a few (~ 5) percent undergo β-decay with the accepted half-life.

The results with carbon as absorber turn out to be quite inconsistent with Tomonaga and Araki's prediction. We used cylindrical graphite rods having a mean effective thickness of 4 cm because we were unable to procure a graphite plate. In addition, when concentrating negative mesons, we placed above the graphite a 5-cm thick plate of iron to guard against the scattering of very low energy mesons which might destroy the concentrating effect of our magnets. We alternated the following three measurements:

A. Negative mesons with 4 cm C and 5 cm Fe,
B. Negative mesons with 6.2 cm Fe (6.2 cm Fe is approximately equivalent to 4 cm C+5 cm Fe as far as energy loss is concerned.
C. Positive mesons with 4 cm C.

The comparison between A and B gave the difference in behavior between Fe and C, once we had established the fact that practically no disintegration electrons came from negative mesons in the 5-cm iron plate. The comparison between A and C gives the difference in behavior between negative and positive mesons in carbon. This must be considered as a qualitative comparison because of the slightly different action of the magnetic field in concentrating mesons of different ranges (4 cm C+5 cm Fe in one case and 4 cm of C in the other). We could not, of course, add 5 cm of Fe for the positive mesons too, since positive mesons do decay in Fe.

The great yield of negative decay electrons from carbon shows a marked difference between it and iron as absorbers. Tomonaga and Araki's calculation also give for carbon a much higher ratio of capture to decay probability for negative mesons, so we are forced to doubt their estimation. It is possible that a suitable dependence of the capture cross section, σ_c, on the nuclear charge, Z, might explain these results; however, if the ratio of the capture to decay probability also depends on the density as Tomonaga and Araki pointed out, then it would require a very irregular dependence on Z to also explain the cloud-chamber pictures of some authors[8] showing negative mesons stopped in the chamber without any decay electrons coming out.

Concerning the difference between M_+ and M_- in carbon, we should like to point out that it is not necessary to assume that σ_c for carbon has an appreciable value for negative mesons. A positive excess, $(H_+-H_-)/(H_++H_-)$ of 20 percent in the hard component, as it seems to be[7] is sufficient to explain our results since this gives $H_+/H_-=1.5$ which is greater than M_+/M_- for carbon. Impurities in the graphite could also explain some preference for M_+, with a suitable dependence of σ_c on Z.

Further experiments on this subject are now in progress, in an attempt to calculate the capture cross section, and to know how it depends on Z.

* Now Visiting Research Associate at Massachusetts Institute of Technology, Cambridge, Massachusetts.

[1] M. Conversi, E. Pancini, and O. Piccioni, Phys. Rev. 68, 232 (1945).
[2] S. Tomonaga and G. Araki, Phys. Rev. 58, 90 (1940).
[3] F. Rasetti, Phys. Rev. 60, 198 (1941); B. Rossi and N. Nereson, Phys. Rev. 62, 417 (1942); M. Conversi and O. Piccioni, Nuovo Cimento 2, 71 (1944); Phys. Rev. 70, 874 (1946).
[4] P. Auger, R. Maze, and Chaminade, Comptes rendus 213, 381 (1941).
[5] M. Conversi and O. Piccioni, Nuovo Cimento 2, 40 (1944); Phys. Rev. 70, 859 (1946).
[6] Y. Nishina, M. Takeuchi, and T. Ichimiya, Phys. Rev. 55, 585 (1939); H. Maier-Leibnitz, Zeits f. Physik 112, 569 (1939); T. H. Johnson and R. P. Shutt, Phys. Rev. 61, 380 (1942).
[7] H. Jones, Rev. Mod. Phys. 11, 235 (1939); D. J. Hughes, Phys. Rev. 57, 592 (1940); G. Bernardini, M. Conversi, E. Pancini, E. Scrocco, and G. C. Wick, Phys. Rev. 68, 109 (1945).

Further Remarks on the Redundant Zeros in Heisenberg's Theory of Characteristic Matrix

S. T. Ma
Institute for Advanced Study, Princeton, New Jersey
December 27, 1946

RECENTLY Dr. Opechowski[1] made a remark on my previous communication concerning the redundant zeros.[2] Reasoning in accordance with the current scheme of quantum theory, he came to the conclusion that all the eigenvalues of the closed states in the problem discussed in my note were given by the first condition, and there were no eigenvalues given by the second condition. That is of course quite correct. In fact it is a result already well known, and that is why the term "redundant zeros" was introduced for the eigenvalues given by the second condition.

Dr. Opechowski has, however, apparently overlooked the fact that I was studying the eigenvalue problem from the point of view of the theory of characteristic matrix, a new scheme of quantum theory recently proposed by Heisenberg.[3] In applying this theory to the spherically symmetrical states of a particle in a central field of force, one determines first $S(k)$, the eigenvalue of the characteristic matric for the spherically symmetrical states and *real* values of k. The quantity $S(k)$ is equal to the ratio of the amplitude of the outgoing wave to that of the incoming wave. One then performs an analytic continuation into the complex plane of k and determines the zeros of $S(k)$ in the lower half of the complex plane. Proceeding in this way, I obtained both sets of eigenvalues mentioned in my note. It is clear that my conclusion based on the new scheme of quantum theory cannot be invalidated by Dr. Opechowski's considerations based on the current scheme of quantum theory.

The question of the part played by the characteristic matrix as a fundamental concept in the future development of quantum theory need not be considered here, as that is irrelevant to the point at issue.

[1] W. Opechowski, Phys. Rev. 70, 772 (1946).
[2] S. T. Ma, Phys. Rev. 69, 668 (1946).
[3] W. Heisenberg, Zeits. f. Physik 120, 513, 673 (1943). Heisenberg's third and fourth papers on the same subject are now in press. A summary of the four papers has recently been given by Heisenberg in a paper entitled "On the Theory of Elementary Particles," now also in press. Cf. also C. Møller, Det. Kgl. Danske Vid. Sels. Fys.-Math. Medd. 23, No. 1 (1945); 24, No. 19 (1946); ter Haar, Physica (1946) in press; S. T. Ma, Phys. Rev. (1947), in press.

Production and Isotopic Assignment of a 90-Day Activity in Element 43*

E. E. Motta, G. E. Boyd, and A. R. Brosi
Clinton Engineer Works, Monsanto Chemical Company, Clinton Laboratories, Oak Ridge, Tennessee
July 31, 1946

PREVIOUS deuteron bombardments of Mo using the cyclotron have led to the production of a variety of periods associated with the chemistry to be expected from element 43.[1,2] However, the mass assignment of many of these isotopes has not been reported. Neutron bombardments of purified samples of $Ru(OH)_3$ in the Clinton self-sustaining chain reacting pile have been found to produce a number of these same activities, and, in one case at least, an isotopic assignment seems possible.

Experiments have been carried out wherein growth was observed of a daughter activity formed by K-capture decay of a previously-discovered three-day Ru^{97} isotope.[3] Extensive chemical tests in which the known six-hour 43^{99} activity was employed as a monitor have shown this daughter activity to be an isotope of element 43, thus permitting its assignment to 43^{97}. The activity has been observed to decay with a half-life of 93 ± 5 days over three months time. The radiations have been found to consist

largely of very soft electrons of 1.5 mg/cm² half-thickness in Al, along with possibly a small amount of unconverted gamma-radiation and probably x-rays. The half-period and character of the radiations possessed by this 43 isotope suggest that its activity is the same as that observed by Cacciapuoti and Segrè[1,4] from the deuteron bombardment of molybdenum.

* This paper is based on the results of research performed under contract W-35-058-eng-71 with the Manhattan Project at the Clinton Laboratories, Oak Ridge, Tennessee.

[1] B. N. Cacciapuoti and E. Segrè, Phys. Rev. **52**, 1252 (1937).
[2] G. T. Seaborg and E. Segrè, Phys. Rev. **55**, 808 (1939).
[3] W. H. Sullivan, N. R. Sleight and E. M. Gladrow, private communication (see Plutonium Project Report CC-1493, March 8, 1944).
[4] B. N. Cacciapuoti, Phys. Rev. **55**, 110 (1939).

Electrical Conductivity of Na-Ammonia Solutions at Low Temperatures

LUIGI GIULOTTO AND ALBERTO GIGLI
Istituto di Fisica "A. Volta" dell'Universita di Pavia, Pavia, Italia
January 6, 1947

R. A. OGG[1] has observed that the electrical resistance of approximately one-molar sodium solutions in liquid ammonia decreases when rapidly frozen, so that the resistance of solid solutions is very low compared with the resistance of liquid solutions. Moreover, experiments carried out with an adaptation of the classical "ring experiment" in magnetic field, induced Ogg to think that these solutions may act as superconductors up to 180°K.

With successive experiments, Boorse *et al.*,[2] and Daunt and co-workers,[3] could not confirm the existence of superconductivity. Hodgins,[4] on the contrary, reports that four trials, of the numerous ones he carried out, gave positive results.

Some experiments on superconductivity and measurements of resistance carried out by us, seem to contribute to the clarification of this phenomenon. The solutions we used were approximately of one-molar concentration and were prepared by dipping into purified ammonia, glass ampoules containing sodium which had been just broken. The rapid freezing of the solutions was obtained by the falling of a small quantity of solution into a small glass having a thin plane bottom, previously immersed in the liquid air. Immediately on the bottom of the glass a solid disk was formed which in a few seconds reached the temperature of the liquid air. This operation was performed between the pole pieces of an electromagnet capable of providing a field of about 500 gauss. Afterwards the glass was rapidly extracted and brought near a magnetometer whose sensitivity was about 10^{-4} gauss. The duration of this last operation was of the order of one second. To avoid too rapid heating of the solid disk, a plush disk was applied on the bottom of the glass which could remain saturated with the liquid air. Twenty trials gave negative results. It is to be assumed that the disk was often broken during the freezing, which evidently, however, could not entirely prevent the circulation of eventual persistent currents.

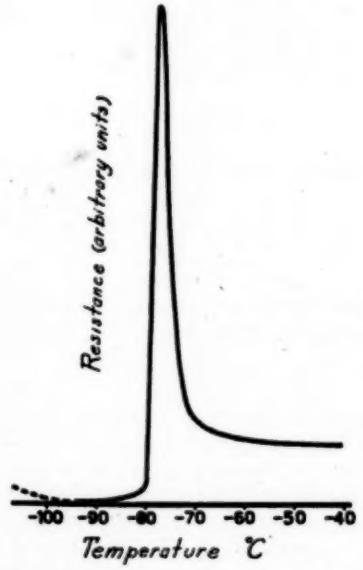

FIG. 1. Typical resistance curve of sodium-ammonia solution in the neighborhood of the solidification temperature.

Measurements of resistance of the solutions at different temperatures have been carried out, while they were progressively frozen or heated. The cell containing the solution was constructed from a small glass on whose bottom two strip platinum electrodes connected with a Wheatstone bridge, in which a resistance was continuously variable, were disposed, and the soldering of a very thin copper-constantan couple was protected from the ammonia by a little bed of white wax.

More or less rapid freezing or heating of the solution may be obtained by simple artifices. By not too rapid freezing or heating (the time necessary for the solidification or melting of the disk was of the order of one minute), it was noted that the variation of the resistance as a function of the temperature is similar to Fig. 1, which refers to one particular experiment with a 0.7 molar solution.

Evidently the resistance of the liquid solution increases very rapidly near the solidification temperature. Below this temperature a sudden decrease of resistance was observed, to a value much smaller than the one attained by the liquid solution. This phenomenon is reversible with the temperature. In the particular case shown in Fig. 1, the ratio of maximum resistance to minimum resistance is about 150, and it is to be supposed that with still slower freezing or heating this ratio might become greater. Evidently, as the solution solidifies, the resistance decreases very much. The increase of resistance which is noted immediately above this temperature is probably owing to the fact that, in the proximity of the solidification point, two liquid phases can be formed. With very rapid freezing, on the contrary, one may not note the increase of resistance which precedes the solidification, or only a very small increase may be noted. This probably occurs because solid and liquid phases are contemporaneously present but not in thermal equilibrium, and therefore it is to be assumed that the true range of this phenomenon does not depend on the velocity of freezing.

We could not measure very exactly the resistance of the solid at the temperature of the liquid air because, in the

greatest number of cases, even a little below the solidification temperature cracks were formed in the disk, thus falsifying the measurements and causing an illusory increase of resistance. In the luckiest cases the resistance at the temperature of the liquid air was found to be almost equal to that of the solid just below the solidification point.

There was still the possibility that the solid resistance was much lower than the one measured with this method, because of the resistances in the contacts. Therefore measurements with a potentiometer method were carried out. The resistance of the solid also was always found with this method and so in all our experiments the phenomenon of superconductivity was absent. On the other hand, the fact which we demonstrated, that the sudden decrease of resistance occurs just at the solidification point, induces us to think rather of a phenomenon depending just on the change of state, than of a phenomenon of superconductivity.

[1] R. A. Ogg, Phys. Rev. 69, 243 (1946).
[2] H. A. Boorse, D. B. Cook, R. B. Pontius, and M. W. Zemansky, Phys. Rev. 70, 92 (1946).
[3] J. G. Daunt, M. Desirant, K. Mendelssohn, and A. J. Birch, Phys. Rev. 70, 219 (1946).
[4] J. W. Hodgins, Phys. Rev. 70, 568 (1946).

Relative Abundance of the Copper Isotopes and the Suitability of the Photometric Method for Detecting Small Variations in Isotopic Abundance

HENRY E. DUCKWORTH AND BENJAMIN G. HOGG
Scott Laboratory, Wesleyan University, Middletown, Connecticut
January 6, 1947

USING a Dempster double-focusing mass spectrograph,[1] the abundance ratio of the two copper isotopes was determined photometrically with a view to ascertaining the value of the method in detecting small variations in isotopic abundances. Following the general method of Mattauch and Ewald,[2,3] the blackening curve of Ilford Q11 plates was obtained by using as standards the isotopes of zinc, which have been accurately measured by Nier.[4] A brass rod served as one of the electrodes in a Dempster spark source[5] and provided both zinc and copper ions. The intensities of the mass spectrum lines were measured with a microphotometer, and a blackening curve was drawn for each photographic plate. On most plates there were more than one exposure and, in these cases, the blackening curve was drawn with considerable certainty.

The values of the ratio Cu^{63}/Cu^{65} obtained by measurement of twenty-one mass spectra are listed below:

2.258	2.335	2.242	2.284	2.135
2.292	2.433	2.160	2.342	2.400
2.296	2.215	2.010	2.425	2.392
2.145	2.370	2.342	2.362	2.230
		2.142		

These data lead to a mean value of the ratio $Cu^{63}/Cu^{65}=2.277\pm0.017$, the probable error being based on the internal consistency of the experimental results. The manner in which the present blackening curves were obtained, namely, in most cases by use of two or more zinc spectra of varying intensity, tended to cancel out small errors in the presumed abundance of the zinc standard. Consequently the isotopic constitution of copper is $Cu^{63}=69.48\pm0.16$ percent and $Cu^{65}=30.52\pm0.16$ percent. Flugge and Mattauch[6] give a value for the packing fraction of $Cu^{63}=-8.13\pm0.10\times10^{-4}$, while Duckworth[7] gives $(f)_{av}$ for Cu^{63} and Cu^{65} to be $-7.92\pm0.25\times10^{-4}$. Assigning a value of $f=-8.03\pm0.10\times10^{-4}$ to both copper isotopes, and using the ratio given above, namely, 2.277 ± 0.017, one obtains a chemical atomic weight of 63.542 ± 0.006. This is not in very good agreement with the accepted chemical atomic weight[8] of 63.57 but does agree splendidly with the recent value of 63.542 obtained by Hönigschmid and Johannsen.[9] Ewald's latest value[3] for the Cu^{63}/Cu^{65} ratio is 2.330 ± 0.032.

Some remarks should be made regarding the efficacy of the method for detecting small variations from the natural abundance. If enough of the sample material is available to make, say, ten determinations of the type described above, the probable error in the ratio would be of the order of 0.020. Since there is associated with the natural ratio a probable error of 0.017, variations would "probably" (used in the probable error sense) be real if they exceeded $0.037/2.277=0.016$ of the natural ratio. As the measured ratios diverged still further from the natural value, the certainty of the variation being a real one would increase in the statistical manner. With the present accuracy the method would not be useful for variations from the natural abundance of less than about one-half percent.

These measurements were made while the authors were at the University of Manitoba. The senior author gratefully acknowledges the support of the National Research Council of Canada. The authors were ably assisted in the experiment by Miss Constance Cox, a senior student in physics at the University of Manitoba.

[1] A. J. Dempster, Proc. Am. Phil. Soc. 75, 755 (1935).
[2] J. Mattauch and H. Ewald, Zeits. f. Physik 122, 314 (1944).
[3] H. Ewald, Zeits. f. Physik 122, 487 (1944).
[4] A. O. Nier, Phys. Rev. 50, 1041 (1936).
[5] A. J. Dempster, Nature 135, 542 (1935).
[6] S. Flugge and J. Mattauch, Physik. Zeits. 44, 181 (1943).
[7] H. E. Duckworth, Phys. Rev. 62, 19 (1942).
[8] J. Am. Chem. Soc. 63, 850 (1941).
[9] O. Hönigschmid and T. Johannsen, Naturwiss. 31, 548 (1943).

Angular Distribution of the $Li^7(p, \alpha)\alpha$ Reaction

SYLVAN RUBIN, W. A. FOWLER, AND C. C. LAURITSEN
W. K. Kellogg Radiation Laboratory, California Institute of Technology, Pasadena, California
December 30, 1946

MEASUREMENTS of the angular distribution of the 8-cm alpha-particles produced in the reaction

$$Li^7+H^1\rightarrow 2\ He^4,$$

have been made for the range of proton energy from 400 to 1400 kev. Approximate agreement with previous work[1,2] up to 900 kev is observed, but there is only a gradual decrease in the asymmetry from 800 to 1400 kev.

The apparatus used was a scattering camera,[3] similar in principle to that described by Chadwick, *et al.*,[4] using photographic detection of the emitted alpha-particles. Figure 1 shows the apparatus schematically. The 2″×4″

Eastman fine-grain alpha-particle plates were located close to the target, the center of which was 15.1 mm from the plane of the surface of the emulsion. The paths of the alpha-particles which struck the emulsion along a circular arc at 50 mm from the target extended over a continuous angular range of 25° to 155° to the direction of the incident beam. The target surface was at 22° to the proton beam, which was 3/32″×1/16″ in cross section, making a target area of 3/32″×5/32″. An aluminum foil separated the target from the photographic plate to stop protons scattered from the target.

All the data were taken with a single thin target, consisting of a 20-kev thick coating of LiOH (measured parallel to proton beam), on beryllium metal. Beryllium was used in order to minimize x-ray emission from the target backing.[5] Preliminary data on a clean beryllium target showed only a very weak production of long range particles, probably caused by low energy deuteron contamination of the proton beam. The yield of these was too low to interfere with the measurements on the 8-cm Li alphas, and the occasional proton tracks could usually be recognized by their longer range and lower grain density, and ignored in counting the alpha-tracks.

The alpha-particle yield as a function of angle was obtained by counting individual tracks in the emulsion, using a microscope with a mechanical stage with micrometer screw. A total of 3000–10,000 tracks were counted on each plate, at 12–24 different angular positions, in equal plate areas (usually 0.8 mm²), along a circular arc at 50 mm from the target. The counts were corrected to equal solid angles from the target in center-of-mass coordinates, and the observed angles corrected to center-of-mass coordinates.

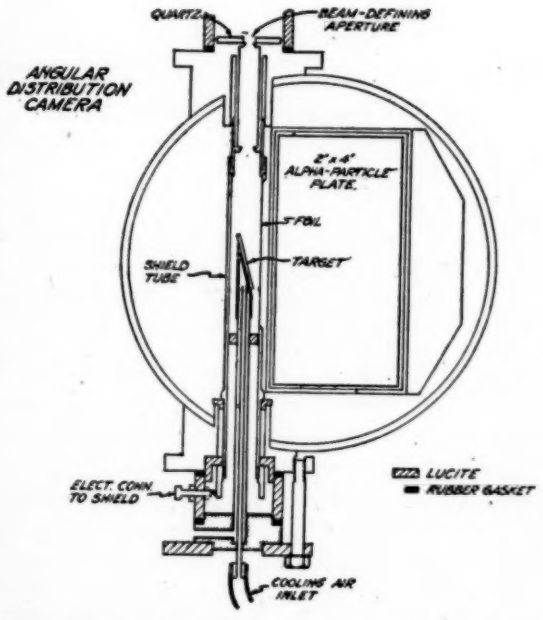

FIG. 1. Semi-schematic drawing of scattering camera. Most of the exposures were made after changing to a curved foil holder, to make the thickness more nearly the same at all angles.

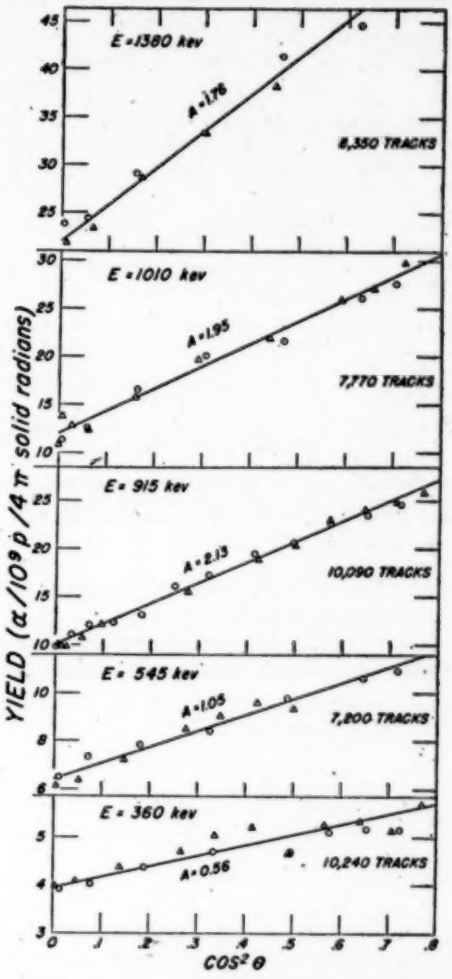

FIG. 2. Some of the observed angular distribution functions, in center-of-mass coordinates. Total number of tracks counted for each curve are given. Fractional P.E. of each point is roughly $0.7(n/N)^{\frac{1}{2}}$ where n is No. of points; N is No. of tracks.

The proton charge to the target on each run was measured, so that the yield per proton could be calculated from the track density and the geometry of the arrangement.

Angular distribution functions at several different energies are shown in Fig. 2. The distribution is of the form:

$$Y(\theta, E) = Y_0(E)[1+A(E)\cos^2\theta],$$

where $Y(\theta, E)$ is the yield per unit solid angle, at an angle θ in the center-of-mass system with respect to the direction of the incident protons, and at a proton energy, E, measured in the laboratory system. $Y_0(E)$ is the 90° yield function. The unit solid angle used for the yield data is a sphere, so that the total yield over the sphere is given by $Y_0(1+A/3)$.

Figure 3 shows the function $A(E)$, obtained from 13 such curves, at various proton energies. Although Swartz, *et al.*,[3] indicated a fairly sharp maximum in A at about 700 kev, we have found only a gradual decrease above 900 kev. The value of A reaches the same maximum

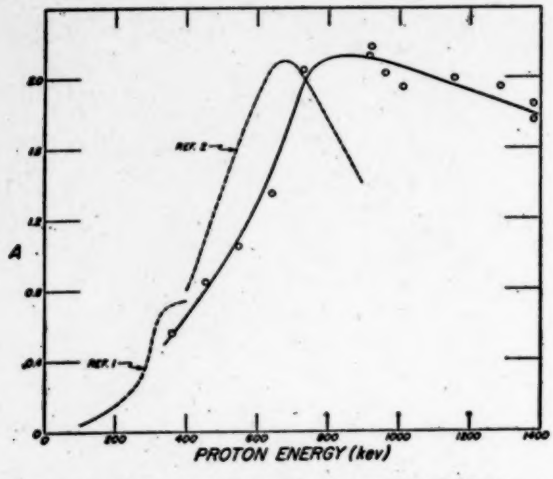

FIG. 3. Coefficient of $\cos^2\theta$ term in the angular distribution as a function of proton energy. Solid curve is fitted to our data. Dashed curves are previously published results (references 1 and 2).

observed by Swartz, *et al.*, but does not appear to change rapidly between 800–1400 kev.

The data which we obtained on yield per proton as a function of energy are not particularly accurate, but show no indication of any resonance, at 90°, 180°, or in total yield over the sphere, in the region up to 1400 kev. The 90° yield is a linearly increasing function up to 1400 kev in essential agreement with previous results[6,7] up to 1000 kev.

Dr. R. F. Christy has made some calculations to relate these data on the angular distribution with the magnitude and energy dependence of the total cross section, in terms of the dispersion theory. Although the cross section is not accurately known above 0.2 Mev, it seems to show no pronounced indication of resonance from 0 to 1.4 Mev. A reasonable fit of the data is obtained with two resonances having $\Gamma=1$ Mev at 0 and 1.8 Mev roughly. The latter is taken to have $J=2$, but the former may be $J=0$ or $J=2$. If σ is normalized by the measurement of Haworth and King,[8] the proton width agrees well with that derived from the γ-ray resonance at 0.44 Mev only if the 0 energy resonance has also $J=2$.

[1] V. J. Young, A. Ellet, and G. J. Plain, Phys. Rev. **58**, 498 (1940).
[2] C. D. Swartz, H. H. Rossi, B. Jennings, and D. R. Inglis, Phys. Rev. **65**, 80 (1943).
[3] S. Rubin, Phys. Rev. **70**, A447 (1946).
[4] J. Chadwick, A. N. May, T. G. Pickavance, and E. F. Powell, Proc. Roy. Soc. **183**, 1 (1944).
[5] M. S. Livingston, F. Genevese, and E. J. Konopinski, Phys. Rev. **51**, 835 (1937).
[6] M. Ostrofsky, G. Breit, and D. P. Johnson, Phys. Rev. **49**, 22 (1935).
[7] L. H. Rumbaugh, R. B. Roberts, and L. R. Hafstad, Phys. Rev. **54**, 657 (1938).
[8] L. J. Haworth and L. D. P. King, Phys. Rev. **54**, 38 (1938).